# Mathematical Modelling

of

# Wave-Current Interaction

in

# a Hydrodynamic Laboratory Basin

Helena Margaretha

The research described in this dissertation was undertaken at the Group of Applied Analysis and Mathematical Physics, Department of Applied Mathematics, in the Faculty EWI, Universiteit Twente, PO Box 217, 7500 AE Enschede, The Netherlands

Part of the research was executed at the Center for Mathematical Modelling and Simulation, Institut Teknologi Bandung, Indonesia

The funding of the research was provided by the Maritime Research Institute Netherlands (MARIN)



Printed by Wöhrmann Printing Service, Zutphen, The Netherlands
The summary in Dutch was done by Mirjam Aartsen

ISBN: 90-365-2230-7

This dissertation was typeset using LaTeX 2ε

# MATHEMATICAL MODELLING OF WAVE-CURRENT INTERACTION IN A HYDRODYNAMIC LABORATORY BASIN

PROEFSCHRIFT

ter verkrijging van
de graad van doctor aan de Universiteit Twente,
op gezag van de rector magnificus,
prof. dr. W.H.M. Zijm,
volgens besluit van het College voor Promoties
in het openbaar te verdedigen
op vrijdag 23 September 2005 te 15:00 uur

door

Helena Margaretha
geboren op 12 Mei 1975
te Bandung, Indonesië

Dit proefschrift is goedgekeurd door de promotor
prof. dr. E.W.C. van Groesen

en de assistent-promotor
dr. Andonowati

*Even youths grow tired and weary, and young men stumble and fall; but those who hope in the Lord will renew their strength. (Isaiah 40:30-31a)*

# Summary

This dissertation concerns the study of surface waves on a layer of fluid when a current is present in the layer. In particular we derive a model that describes the adaptation process when a given surface wave on still water meets at a certain point a current. Both wave and current will then start to interact to reach a steady state situation. For the typical task of a hydrodynamic laboratory to generate a desired wave above a given current, this model can be used to design a method to predict the properties of the waves and current before the adaptation, which is desired for the practical generation process in the laboratory.

Restricting to small amplitude waves, for any current profile a harmonic wave of given frequency will be adapted to the current if the dispersion relation is satisfied. This dispersion relation is well known in the absence of currents, but is rather cumbersome in the presence of depth-dependent nonlinear currents. To find the dispersion relation in that case, one has to solve the equation for the vertical fluid velocity in the layer, the so-called Rayleigh equation, which clearly depends on the given current. In general, analytical solutions cannot be found, and the solution has to be approximated, leading to an approximate dispersion relation. In this thesis the approximation is obtained using a variational characterization of the dispersion relation. Substituting approximate solutions of the Rayleigh equation in the governing functional then leads to the approximate dispersion relation. We show that using the WKB approximations for solutions of the Rayleigh equation leads to a good approximate dispersion relation for currents with nonlinear profiles.

Having formulated in this way the steady state situation of waves and currents, we consider the problem when a wave and current meet at a certain position. At that position the dispersion relation is not satisfied. Then an adaptation process sets in, and a model is designed that describes a quasi-homogeneous spatial evolution to an asymptotic state in which the changed wave and current are steady again.

To get a physical understanding of the adaptation process, we designed a low-dimensional model using clearly interpretable variables. The natural variables to describe the wave are the wave frequency, the wave length, the wave amplitude and the mean-free surface elevation. To describe changes in the current, we choose to use approximate parameterized profiles; changes in the current are then described by changes of the parameters. The model for the adaptation process is then found by

requiring several natural conservation properties to be satisfied. More specifically, we make sure that at each position the continuity equation and the kinematic boundary condition are satisfied exactly. Furthermore, we require that the mass, momentum, and energy density fluxes are conserved. These conditions make it possible to define the spatial changes of the parameters of the model, and predict the values of the asymptotic steady state. The derived quasi-homogeneous process is an approximate description, but we investigate a-priori estimates and show that the errors are small. To validate the model, we compared model results with laboratory experiments that can be found in the literature. Besides these, a series of tests was designed and conducted in the offshore basin of MARIN, the Maritime Research Institute Netherlands, Wageningen. Comparisons with all available flumes and basin experiments show that in all cases the model correctly predicts the qualitative results of the interaction process, and that for many experiments, including the one at MARIN, the predictions are also quantitatively correct.

# Acknowledgements

This dissertation is the result of a research project within the group of Applied Analysis and Mathematical Physics, University of Twente. Here I would like to express my sincere thanks to the following people who have directly or indirectly involved in accomplishing this dissertation.

I am enormously grateful to Prof. Brenny van Groesen, my promotor, from whom I learned the attitude of doing research in applied mathematics. His intelligence and confidence have helped me in finishing this dissertation. I thank also his patience and support during the time when I was ill. I would also like to pronounce my sincere and grateful thanks to Dr. Andonowati, my co-promotor, for her support especially in the last one and a half year of this research. I greatly enjoyed working in her laboratory at the Centre for Mathematical Modelling and Simulation (P2MS) Institut Teknologi Bandung. I also appreciate the opportunity to join the 2004 EU project of P2MS ITB, that has broaden my view on industrial work and the necessity of collaboration between universities and industries.

This research was funded by the Maritime Research Institute Netherlands (MARIN). In particular, I thank Dr. Rene Huijsmans for the opportunity to execute this research. Working with a MARIN's project was a valuable experience: learning how to design and analyze experiments and how to present results to engineers.

I would like to thank the other members of the graduation committee: Prof A.J. Mouthaan, Prof. J.A. Battjes, Prof. A.W. Heemink, Prof. H.W.M. Hoeijmakers, and Prof. S.A. van Gils.

I thank Gert Klopman for fruitful scientific discussions and his constant presence in all of the PhD committee meeting that was held approximately once every three months. I greatly appreciate his deep knowledge and careful thought. I thank also Dr. Frits van Beckum. It was nice that I could just walk to his room whenever I have question regarding numerics.

I particularly would like to thank Prof. Edy Soewono from Institut Teknologi Bandung, who has opened a door for me to go and study in the Netherlands.

My stay in the AAMP/MPCM group in the TWRC building/CS-TO library/RA building was enjoyable because of the good companion from the corridor/library mates. In particular: Lyuba (with whom I shared not only a room but also the constant presence of sweets and cookies in our room), Agus (to whom I come to have

general math discussion), Sena (from whom I got MATLAB hints and various softwares), Edy and Timco (for good jokes and mathematics puzzles), Monica and Vita and Jaqueline (for good talks, dinners, and friendship), Dr Nining Sari Ningsih for all good laughs and inspiring talks during her two months stay at the AAMP group, and my room mates in Ravelijn: Natanael, Hadi, and Henk. I thank Natanael for letting me use his personal library in the room, so that in the last year I did not have to carry a lot of books (including the big heavy LaTeX book) back and forth ID-NL. I thank Marielle, our secretary, for her support especially in the period when I was writing and finishing this dissertation.

During my stay at P2MS ITB, I enjoyed very much the friendly atmosphere there. In particular I thank the friendship and support from Bu Rini, Adri, Nur, Yudith, Bu Eulis, Icha, Lilik. I will definitely miss our lunch-time excursion that we had every day.

In both good and difficult times, I am always encouraged by good talks with (and sms + phone calls + emails from) Hanny, Mirjam, Praveen, Weidji, and Arun. Thanks for your prayer and care. You guys were also great travel buddies! ;o) Thanks also to Sheela, Mark, Silvia, Yenny, Novi, Netty, Rolien, Daniella, Stuart, and Abraham. I would like to thanks all members and former members of BS-Twente (some of them I have mentioned above) for their prayer and friendship.

My special gratitude is directed to my parents and my brother and sister, Yusak and Astrid. I am really blessed by your constant prayer, support, care, unconditional love, trust, and great understanding.

For the completion of this dissertation I thank the Almighty God, who works miraculously in my life and who is always with me wherever I go.

Bandung, 26-08-2005
Helena Margaretha

# Contents

# Notations

In the list below, the notations used throughout this dissertation are listed in alphabetic order of their first symbol. Besides a short description of the notation, the section where the notation is introduced is given for further reference.

## Notations starting with a Roman symbol

| | |
|---|---|
| $a$ | amplitude of the free surface elevation [Section 2.3] |
| $a_0$ | amplitude of the current-free wave [Section 4.3.3] |
| $a^\infty$ | the asymptotic value of $a$ [Section 4.3.1] |
| $\mathcal{A}$ | the canonical action functional for $\mathcal{L}$ [Section 3.2] |
| $\mathcal{B}$ | the dual variational formulation for $\mathcal{L}$ [Section 3.2] |
| $c$ | phase velocity $\frac{\omega}{k}$ [Section 3.1] |
| $c_g$ | group velocity $\frac{d\omega}{dk}$ [Section 3.5] |
| $\mathcal{E}$ | energy [Section 2.2] |
| $f$ | the characteristic function of the Rayleigh equation [Section 2.3] |
| $\mathcal{F}$ | energy-flux [Section 2.2] |
| $\mathcal{F}^\infty$ | the constant for the energy-density flux [Section 4.3.1] |
| $g$ | gravitational constant [Section 2.1] |
| $h$ | the constant reference depth [Section 2.1] |
| $\mathcal{I}$ | mass-flux [Section 2.2] |
| $\mathcal{I}_0$ | the constant for the mass-density flux [Section 4.3.1] |
| $k$ | wave number [Section 2.3] |
| $k_0$ | wave number of the current-free wave [Section 4.3.3] |
| $k^\infty$ | the asymptotic value of $k$ [Section 4.3.1] |
| $L$ | the distance of adaptation [Section 5.2] |
| $\mathcal{L}$ | variational formulation for the eigenvalue value problem [Section 3.2] |
| $\mathcal{M}$ | momentum-flux [Section 2.2] |
| $\mathcal{M}_0$ | the constant for the momentum-density flux [Section 4.3.1] |
| $\mathcal{O}$ | big-O notation for infinitesimal asymptotic [Section 2.3] |
| $p$ | (fluid) pressure [Section 2.1] |
| $\hat{p}$ | amplitude function of the first-order pressure [Section 2.3] |
| $\overline{p}_2$ | second-order mean pressure [Section 4.3.1] |

| | |
|---|---|
| $\mathbf{P}$ | the parameter set [Section 4.3.1] |
| $\mathbf{P}^{\infty}$ | the equilibrium point of the parameter dynamics [Section 4.3.1] |
| $P_c$ | parameter for the deformation of the current profile [Section 4.3.1] |
| $P_c^{\infty}$ | the asymptotic value of $P_c$ 4.3.1] |
| $q_i$ | interpolation function(s) in the Green-Naghdi theory for fluid sheets [Section 4.4.3] |
| $\mathcal{R}^{\text{bottom}}$ | error in the bottom boundary condition [Section 4.1] |
| $\mathcal{R}^{\text{CE}}$ | error in the continuity equation [Section 4.1] |
| $\mathcal{R}^{\text{dbc}}$ | error in the dynamic boundary condition [Section 4.1] |
| $\mathcal{R}^{\text{DR}}$ | error in the dispersion relation [Section 4.2] |
| $t$ | time [Section 2.1] |
| $\mathcal{R}^{\text{E}_1}$ | error in the Euler equation for the horizontal momentum [Section 4.1] |
| $\mathcal{R}^{\text{E}_2}$ | error in the Euler equation for the vertical momentum [Section 4.1] |
| $\mathcal{R}^{\text{kbc}}$ | error in the kinematic boundary condition [Section 4.1] |
| $\mathcal{R}^{\text{Rayleigh}}$ | error in the Rayleigh equation [Section 4.2] |
| $t$ | time [Section 2.1] |
| $u$ | horizontal velocity [Section 2.1] |
| $\hat{u}$ | amplitude function of the first-order horizontal velocity [Section 2.3] |
| $U$ | mean horizontal velocity (i.e., the current) [Section 2.1] |
| $U_c$ | profile of the initial (wave-free) current [Section 4.3.1] |
| $U_{\text{change}}$ | the deformation of the current profile [Section 4.3.1] |
| $w$ | vertical velocity [Section 2.1] |
| $\hat{w}$ | amplitude function of the first-order vertical velocity [Section 2.3] |
| $\hat{w}_{\text{a}}$ | approximation for $\hat{w}$ [Section 4.2] |
| $\hat{w}_{\text{norm}}$ | normalized (approximate) solution of the Rayleigh equation [Section 4.3.2] |
| $\hat{w}_{\text{trial}}$ | trial function that approximates $\hat{w}$ [Section 3.2] |
| $x$ | horizontal coordinate [Section 2.1] |
| $z$ | vertical coordinate [Section 2.1] |

## Notations starting with a Greek symbol

| | |
|---|---|
| $\alpha$ | the constant for the wave volume [Section 4.3.2] |
| $\beta$ | the characteristic coeficient of the dispersion relation [Section 2.3] |
| $\delta_{\hat{w}}\mathcal{L}$ | the variational derivative of $\mathcal{L}$ with respect to $\hat{w}$ [Section 3.2] |
| $\epsilon$ | perturbation parameter [Section 2.3] |
| $\eta$ | free surface elevation [Section 2.1] |
| $\eta_0$ | the mean free surface elevation [Section 2.1] |
| $\eta_0^{\infty}$ | the asymptotic value of $\eta_0$ [Section 4.3.1] |
| $\theta$ | wave phase [Section 2.3] |
| $\theta_0$ | initial wave phase [Section 2.3] |

| | |
|---|---|
| $\rho$ | fluid density [Section 2.1] |
| $\sigma$ | small parameter for the curvature of the current profile [Section 4.2] |
| $\xi_i$ | unknown function(s) for the velocities in the Green-Naghdi theory for fluid sheets [Section 4.4.3] |
| $\psi$ | a 'momentum-like' quantity for $\hat{w}$ [Section 3.2] |
| $\psi_{\text{trial}}$ | trial function that approximates $\psi$ [Section 3.2] |
| $\omega$ | wave frequency [Section 2.3] |

## Other notations

| | |
|---|---|
| $< \cdot >$ | time-average over a wave period [Section 2.2] |

# Chapter 1

# Introduction

## 1.1 A hydrodynamic laboratory

A concise definition of a hydrodynamic laboratory is given by Westhuis [76]:

> "A hydrodynamic laboratory is a complex of facilities in which maritime structures are tested on a model scale."

Before the actual construction, a maritime structure (ship, floating platform, fixed platform, etc) must be tested in a proportionally scaled version of the specific sea condition in which that structure will be operated. Hydrodynamic properties of the structure must also be precisely calculated and investigated. Tests with scaled models under realistic conditions remain invaluable as an accurate and objective way to quantify and demonstrate the behavior and performance of a ship or structure. For accurately testing various design structures, a hydrodynamic laboratory must be able to provide precise scaled-versions of various conditions of the real sea.

The research that leads to this dissertation was initiated by the Maritime Research Institute Netherlands (MARIN), which is an independent research institute working on model testing and design consultancy for ocean structures and ships. MARIN provides commercial shipbuilders, owners, propeller manufacturers, naval architects and the offshore industry with state-of-the-art performance predictions, design consultancy, testing services and simulation and training consultancy. MARIN owns seven different testing facilities: offshore (wave-current) basin, sea keeping and manoeuvring basin, high speed basin, shallow water basin, cavitation tunnel, deep water towing tank, and depressurized towing tank. Each facility is unique, and is meant to test specific resistances/performances of different components of maritime structures.

The object of this research is the new offshore (wave-current) basin at MARIN, which was opened in 2000 (Figure 1.1). The current-culverts are visible in Figure 1.2. It is equipped with advanced systems for generating waves, current and wind. It is designed for testing models of offshore structures, which are fixed, moored, or

controlled by dynamic positioning. It is also used for other tests: offloading tests in deep and shallow water, concept, installation and dredging tests, and free sailing and captive sea keeping and manoeuvring tests in wave-current combinations and on shallow water. Figure 1.3 shows a cross-section of the basin.

Figure 1.1: The new offshore (wave-current basin) of MARIN. The individually controlled flaps of the wavemaker on the longitudinal side of the basin are clearly visible on the left foreground. The other series of flaps are located at the farthest side. Source: [43]

The horizontal dimension of the basin is 36 m × 45 m. The water depth of the basin can be varied by means of an adjustable floor from 0.5 m up to a maximum of 10.5 m. In addition, a pit with a diameter of 5 m and a depth of 20 m gives the ability for deep water mooring tests up to 3000 m (prototype). The carriage can control the movement of the model in both directions of the horizontal plane at a speed up to 3.2 m / s. With an extra installed turnable arm, the system is able to perform captive manoeuvring tests in shallow and deep water. The wave generators can produce various wave types, as required in model testing. The wave generators are positioned at two adjacent sides of the basin and consist of hinged flaps. Each segment (width 40 cm) has its own driving motor, which is controlled separately. The system is equipped with compensation of wave reflection from the model and the wave absorbers. Opposite to this wave generator, passive wave absorbers are installed. Current can be generated with various profiles (uniform, hurricane, parabolic, etc). Divided over the water depth of 10.5 m, six layers of culverts, each equipped with a

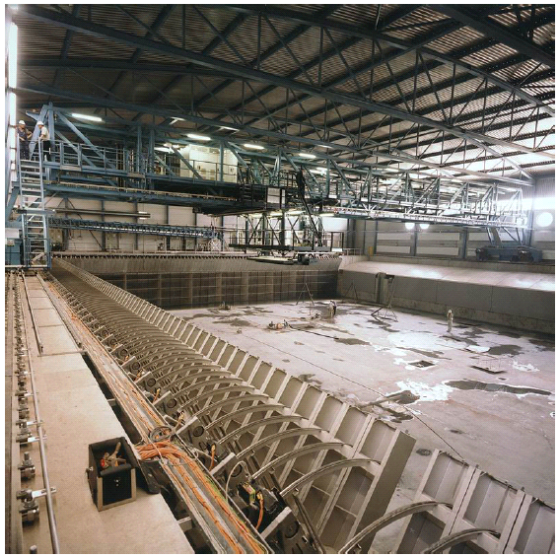

Figure 1.2: The wave-current basin of MARIN without water. The current culverts are visible at the farthest side

pump, are installed. When generating a current, water is continuously injected from one side of the basin, sucked from the opposite side, and recirculated by pipes outside the basin, with a given constant discharge for each pipe, that maintains a specific vertical profile of horizontal mass-transport in the basin. Figure 1.4 shows a picture

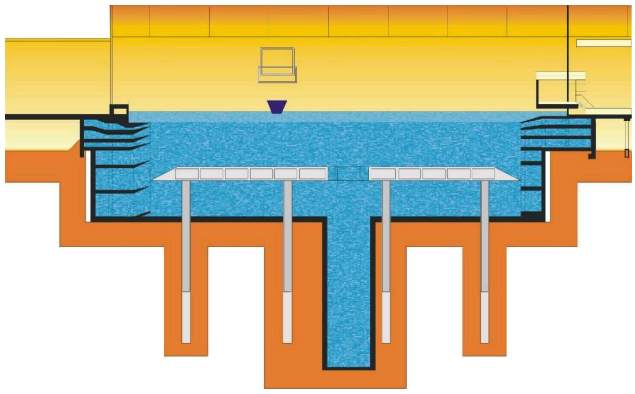

Figure 1.3: A cross-section of the new offshore basin. The six layers of culverts and the liftable bottom are shown. Source: [44]

of these culverts. The basin is also equipped with a wind generator: a free moving and positionable platform of 24 m width, equipped with electrical fans.

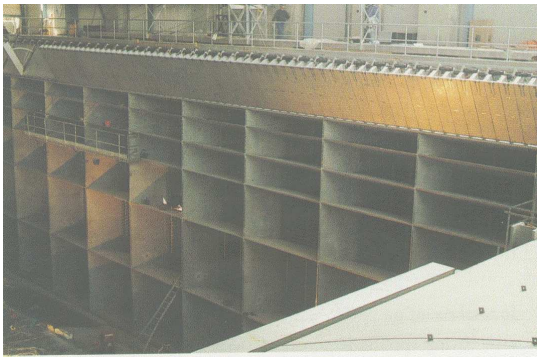

Figure 1.4: A picture of the six layers of culverts at a wavemaker side. Source: [44]

## 1.2 Aim and scope of this research

The objective of this research is to find a model that can be used for designing a method to generate waves and currents in the offshore (wave-current) basin of MARIN. The wind, which is also possible to be made in this basin, is not considered in this research. The ideal aim is to be able to predict how current and wave have to be prepared such that when the wavemaker is operated, a prescribed flow field consisting of the specified current and the requested surface waves are generated in the laboratory. Since the bottom in the new basin can be lifted, interest is specifically also in the dependence on the depth. The difficulty of getting a requested wave and current environment is due to the interaction between wave and current. In the presence of a current, the wavemaker motion will produce waves that are different from the waves produced (by the same wavemaker motion) in the absence of currents. On the other hand, the interaction also changes the current profile, especially in the region near the free surface. For the purpose of the laboratory, a model that can predict changes of both wave and current is needed.

In [69] Thomas reported that his experiment shows that the wave deforms in an interval of one wave length. It is also observed in the wave-current basin of MARIN that the most visible deformation of the surface waves takes place in a short interaction region around the position where the injected currents reach the free surface. In order to verify this, a series of measurements were made in MARIN (test no. 17710-1-OB (2002)). Explanations and quantitative analysis of these measurements are reported by Margaretha [39] and Voluer [75]. Results and analysis of this experiment will be reviewed in Chapter 6 of this dissertation. The analysis indicates that the

wavelength measured near the wavemakers (i.e. 2 m from the wavemakers) is very different than the wavelength measured in the middle of the basin (i.e. at 17 m from the wavemakers). Near the wavemaker, the measured wavelength is close to the one predicted by the wave-only dispersion relation, and in the middle of the basin it agrees with the theoretical dispersion relation of the spatially-steady wave-current interaction (i.e. the homogeneous problem). It is also observed that the change in the wavelength clearly corresponds to the observed spatial variation in the wave amplitude.

These observations motivate us to make a model which allows continuous and simultaneous changes in the wave and current properties. In the research that led to this dissertation, we developed an approach which describes the entrance effect of wave and current that possibly occurs in a laboratory basin. Assumptions used in the model are directly related to the situation in the hydrodynamic laboratory basin.

## 1.3 Literature review

The general equations of hydrodynamics were established by Daniel Bernoulli and Leonhard Euler in the eighteenth century. The interaction of wave and current is a particular subject in hydrodynamics. This problem has been studied extensively in the last decades. Many papers on this problem investigate various cases of steady interaction, i.e., when the current profile and the wave properties (e.g. wave amplitude, wave length) do not change in space and time. In this dissertation, the equilibrium condition arising from the steady wave-current interaction is defined as the homogeneous problem. Discussions on this problem are well documented by Peregrine [50], Peregrine and Jonsson [51], Jonsson [28], Thomas and Klopman [70], and Dingemans [17]. Discussions on the exact/approximate solutions of the 'wave part' of the velocities and/or their stability are given by, for example, Fenton [19], Dalrymple [12], Thompson [71], Simmen and Saffman [58], Shrira [57], Baddour and Song [4], Swan and James [66]. Numerical methods for calculating the solutions are given by Dalrymple [13], Thomas [69]. Approximations to the dispersion relation or the phase velocity are given by Skop [59], Stewart and Joy [60], Kirby and Chen [32], Miles [46], Margaretha et al. [40]. Practical applications of this knowledge are, for example, application of a surface current as a hydraulic breakwater (Brevik [10] and Taylor [68]) and separation of incident and reflected waves in wave-current flumes (Kyung [34]).

Experiments showing effects of current on the free-surface waves and/or waves on the current profile were reported by Bakker and van Doorn [5], Thomas [69], Kemp and Simons [29] [30], Klopman [33], Suastika et al. [62], Swan [65], Swan et al. [67], Margaretha [38] [39]. In the last experiment [39] an attempt was made to measure the horizontal variation of the free surface elevation and the current in the basin of MARIN. This was done by slowly moving the wave probes plus the current meter in the direction opposite to the direction of the wave. Unfortunately slow movement of the carriage induced a lot of vibration, thus the data measured during the movement

are difficult to analyze. However, from the analysis of the data obtained during steady measurements at fix places, we are able to draw conclusions on the global changes of wave and current.

From all these experiments it is observed that when a regular wave interacts with a (uniform/non uniform) following current, the wave amplitude becomes smaller and the wave length becomes longer. But when a regular wave interacts with an adverse current, the wave amplitude becomes higher and the wave length becomes shorter. The increase/decrease of the wave amplitude and wave length clearly depend on the strength and the profile of the current. On the other hand, the deformation of the current profile clearly depends on the height and the frequency of the wave.

It is observed that when a uniform current flows in the direction of the wave propagation then the current becomes weaker. But if a uniform current flows against a wave then the current becomes stronger.

For the interaction of monochromatic waves and uniform current, a number of models predicting changes on wave and/or current are found in the literature. We refer here to the model proposed by Longuet-Higgins and Stewart [36] [37], Thomas [69], Battjes [6], and Baddour and Song [3]. We also found models given by Boussinesq-type equations, e.g. the one derived by Chen et al. [11]. All these models can be classified into two classes: models that predict only the wave deformation (therefore information on the current is required), and models that predict both changes of wave and current. Each class can also be divided into two subclasses: models that predict only the steady-state of the interaction (thus no spatial or temporal variation is involved) and models that provide the slowly-varying variations of the wave-current changes. The general theory for slowly-varying irrotational flow is given in the book of Whitham [77]. Models assuming slowly-varying wave parameters are relevant for describing phenomena in the ocean/sea, where nature develops waves and currents in a large domain. But in a laboratory basin the length is limited and the wave-current environment is made by 'abruptly' entering waves into a current region, with the aim that somewhere in the middle of the basin we obtain a requested wave-current environment that is a scaled version of a specific position in the ocean. As remarked by Thomas [69], although some models assuming slowly varying waves give good prediction to experimental data, there is no exact justification on the validity of using these models when predicting wave-current environment in a basin/flume of finite length.

The interaction shows more complex patterns for currents with shearing profiles. There are two types of sheared current which are mostly asked to be generated in a hydrodynamic laboratory. Those currents are commonly called *turbulent current* (Figure 1.5A) and *hurricane current* (Figure 1.5B). A turbulent current is a sheared current which profile is almost linear near the free surface but is very curved near the bottom. Thus, this type of current induces turbulence and mixing near the bottom. This type of current was used in the experiments by Kemp and Simons [29] [30] and Klopman [33]. A hurricane current, as reflected by its name, is a sheared current

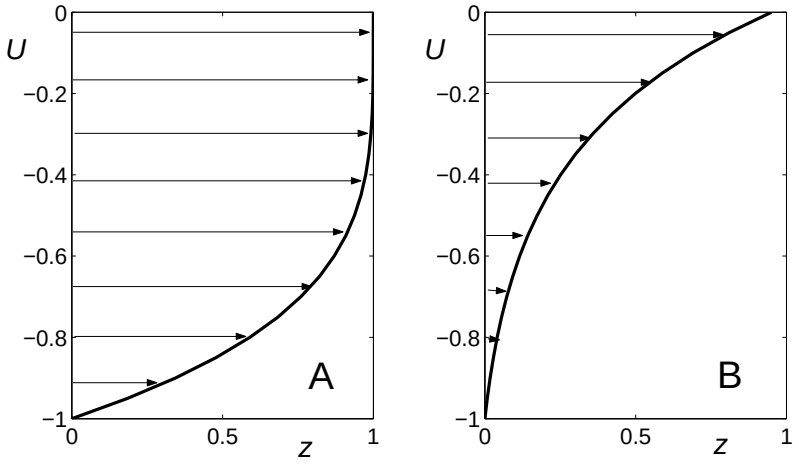


Figure 1.5: (A) a turbulent current; (B) a hurricane current

that is formed when a strong wind blows above a body of water. This current is almost uniformly zero near the bottom but has a very strong shear near the surface. Experiments on this type of current were conducted by Swan [65] and Swan et al. [67].

It is reported in the literature that if a turbulent current flows in the direction of the wave propagation then the strength of the current decreases near the surface but slightly increases near the bottom. But if a turbulent current flows against a wave then the strength of the current increases near the surface but slightly decreases near the bottom.

Swan et al. [67] report that for *favorable* hurricane currents the wave motion produces a reduction in the magnitude of both the near-surface current and the vorticity distribution. However in the *adverse* current cases the current change is markedly different: the near-surface vorticity increases but there is no general tendency for the change of the strength of the near-surface current.

For depth-dependent currents, a model for predicting deformation of the current profile is given by Groeneweg and Klopman [23]. Also, Swan et al. [67] presented a model to calculate deformation of a regular wave propagating on a depth-dependent current. In the model proposed by Swan, the change of the current profile must be known a priori. Using results from laboratory experiments, Swan et al. [67] demonstrate the prediction of the models. The predicted wave amplitude and wave length agree very well with the experiment. However, as remarked in that paper, in practice the change of the current profile is not known a priori. Therefore, for practical application Swan et al. [67] suggest to couple their model with, for example, the model explained by Groeneweg and Klopman [23]. This model follows the General-

ized Lagrangian Mean (GLM) theory described by Andrews and McIntyre [2]. This model shows qualitative and quantitative agreement with Klopman's measurement [33]. The paper by Groeneweg and Klopman is followed by the paper by Groeneweg and Battjes [24]. In the latter paper, the model based on the GLM formulation is applied to investigate the validity of two fundamentally different explanations that give a qualitative explanation of the possible physical processes that cause the deformation of the current profile: the model proposed by Nielsen and You [48] that relies on a local force balance in a plane in the streamwise direction and assumes that changes on the current profile are purely caused by phenomena in the longitudinal direction; and the model proposed by Dingemans et al. [16] that show that the secondary lateral circulations, which are the result of the so-called wave-induced Craik-Leibovich (CL) vortex force, are responsible for changes in the current profile. In their paper [24] Groeneweg and Battjes show that the longitudinal component of the wave-induced driving forces are much more dominant than the lateral components. The models based on the GLM formulation [23] [24] are good models to predict and explain the deformation of the current profile for the equilibrium condition (i.e., the homogeneous problem). However, these models do not deal with the inverse problem that we investigate because the related current-free wave is not accommodated in these models. The reason why we are interested to know the related current-free wave is because when current is absent, reliable wavemaker theories are available (see for example the book of Dean and Dalrymple [14] or the papers of Schäffer and Klopman [55] and Schäffer and Steenberg [56]). Thus, in the absence of currents it is relatively easy to get a desired wave in the basin. By generating a specific current-free wave, interaction with the current changes both the wave and the current into the desired wave-current combination.

## 1.4 Outline of the dissertation

The outline of the dissertation is as follows. Chapter 2 provides a mathematical overview of the problem. This includes the governing equations, the relationships between the governing equations and the conservation laws, description of the linear homogeneous problem and its solutions, and the role of the dispersion relation. Opening with a recapitulation of relevant background materials, the chapter ends with an overview of the model on which the dissertation is focused.

Chapter 3 deals with a model to approximate the dispersion relation of the homogeneous problem. The model is derived through variational formulations of the Rayleigh equation and the boundary conditions. The model is applicable for arbitrary depth-varying currents. The model is guaranteed to give a good approximation provided that the so-called 'trial function' is chosen carefully. The choice depends on the current profile. By taking good trial functions, we show that the model gives a better agreement to the exact dispersion relation than other models found in the literature.

Chapter 4 describes the mathematical model that is essentially the focus of the dissertation. In this chapter the model is described in detail, without prescribing any specific current profile. Analysis of the accuracy of the model is given. A discussion on the analogy and comparison with the method of Green-Naghdi [21] [22] [31], which is somewhat related to the problem that we address, is given.

Basically an extension of Chapter 4, Chapter 5 deals with case studies for uniform and linear currents. Predicted changes on both the wave properties and the current profile, as well as the 'distance' of adaptation, are reported and analyzed. Comparisons with various laboratory experiments on both uniform and depth-dependent currents found in the literature are also reported.

As a part of the research, a laboratory experiment consisting of a series of tests was designed and conducted in the Maritime Research Institute Netherlands (MARIN). Set up of the experiment and the results are reported in Chapter 6. Analysis on the results and possible applicability of the proposed model for the wave-current basin of MARIN is also discussed in this chapter.

In Chapter 7 we present a discussion on the inverse problem and recommendations for dealing with irregular waves and for extending the proposed method to get more flexibility in describing the deformation of the current profile.

# Chapter 2

# Mathematical Overview of the Problem

In this chapter, the governing equations and the basic conservation laws are presented. Then the definition and properties of linear monochromatic solutions of the homogeneous problem are given. This is followed by an overview of the model to be derived.

## 2.1 The governing equations

The problem of wave-current interaction to be studied will be restricted to two-dimensions. This means that the surface waves propagate without making an angle to the current.

First we define the coordinate system of the problem. All physical quantities depend only on one horizontal direction denoted by $x$ and the vertical direction (positive upwards) denoted by $z$. The free surface at rest (i.e. without waves and currents) is taken at the value $z = 0$.

The free-surface is the part of water that directly touches the air. It is denoted by $z = \eta(x,t)$, which gives the elevation of the free surface at point $x$ for time $t$. For periodic waves, we define the mean free-surface elevation as $z = \eta_0(x)$ given by the time-average of $\eta(x,t)$ over the wave period: $\eta_0(x) = \int_0^T \eta(x,t)\,dt/T$. The motion of the fluid is given by the components of velocity at every point of the water domain and for any time. We denote by $u(x,z,t)$ the velocity component in the (horizontal) $x-$direction and by $w(x,z,t)$ the one in the (vertical) $z-$direction. The pressure is denoted by $p(x,z,t)$.

In the dissertation all variables are made dimensionless with the constant reference depth $h$ and the gravitational acceleration $g$. This means that lengths are scaled with $h$, time is scaled with $\sqrt{h/g}$, velocities are scaled with $\sqrt{gh}$, and the pressure is scaled with $(\rho g h)$. In this work, the wavelength (or, wave number) is not used as one of the scaling factors because it will become one of the varying variables in the model to be derived. Throughout the dissertation, notations $\eta$, $u$, $w$, and $p$ denote nondimensional normalized variables. The flat bottom is given by $z = -1$.

Precise derivations and detailed descriptions of the equations for general surface waves problems are given in Dingemans [17]. Wave-current interaction is governed by the equations for inviscid-incompressible water flow with a free-surface at the top boundary:

$$\partial_t \eta + u\eta_x - w = 0 \qquad \text{at } z = \eta, \tag{2.1}$$

$$p = 0 \qquad \text{at } z = \eta, \tag{2.2}$$

$$\partial_t u + u\partial_x u + w\partial_z u + \partial_x p = 0, \qquad -1 \le z \le \eta \tag{2.3}$$

$$\partial_t w + u\partial_x w + w\partial_z w + \partial_z p + 1 = 0, \qquad -1 \le z \le \eta \tag{2.4}$$

$$\partial_x u + \partial_z w = 0, \qquad -1 \le z \le \eta \tag{2.5}$$

$$w = 0 \qquad \text{at } z = -1. \tag{2.6}$$

Equations (2.1)-(2.6) are called the kinematic and the dynamic free surface boundary conditions, the Euler equations, the continuity equation, and the bottom boundary condition, respectively. An exact solution of these governing equations is given by any steady current flowing below a flat surface (i.e. without any wave). For this case, we have $u = U(z)$, $\eta = 0$, $w$ is zero everywhere, and $p$ is given by the hydrostatic pressure $p = -z$. However, when a surface wave is present (i.e. $\eta_x \neq 0$ and $\eta_t \neq 0$), in general exact solutions are not known.

## 2.2 Basic conservation laws

In the following we will present the conservation laws for the total mass, the total momentum, and the total energy. First, we define the mass-flux $\mathcal{I}$, the momentum-flux $\mathcal{M}$, the energy-flux $\mathcal{F}$, and the energy $\mathcal{E}$ as follows:

$$\mathcal{I}(x,t) \equiv \int_{-1}^{\eta} u dz, \tag{2.7}$$

$$\mathcal{M}(x,t) \equiv \int_{-1}^{\eta} \left(u^2 + p\right) dz, \tag{2.8}$$

$$\mathcal{F}(x,t) \equiv \int_{-1}^{\eta} u\left(\frac{1}{2}u^2 + \frac{1}{2}w^2 + p + z\right) dz, \tag{2.9}$$

$$\mathcal{E}(x,t) = \int_{-1}^{\eta} \left(\frac{1}{2}\left(u^2 + w^2\right) + p + z\right) dz. \tag{2.10}$$

Any set of exact solutions of the governing equations (2.1)-(2.6) satisfies the conservation laws for mass, momentum, and energy:

$$\partial_t \eta + \partial_x \mathcal{I} = 0, \tag{2.11}$$

$$\partial_t \mathcal{I} + \partial_x \mathcal{M} = 0, \tag{2.12}$$

$$\partial_t \mathcal{E} + \partial_x \mathcal{F} = 0. \tag{2.13}$$

Denote by $\langle\ \rangle$ the time-average over a period $T$: $\langle\varphi\rangle = \frac{1}{T}\int_0^T \varphi dz$. If the solutions are periodic, then time-averaging (2.11 )-(2.13) over the period leads to

$$\langle\mathcal{I}\rangle \equiv \text{constant}, \tag{2.14}$$

$$\langle\mathcal{M}\rangle \equiv \text{constant}, \tag{2.15}$$

$$\langle\mathcal{F}\rangle \equiv \text{constant}. \tag{2.16}$$

## 2.3 Linear monochromatic solutions of the homogeneous problem

The homogeneous problem is defined as the equilibrium state of wave-current interaction, at which the current profile and the wave properties do not change in space and time. In the following we will show that for any linear monochromatic wave, the homogeneous problem is characterized by a dispersion relation that relates the wave frequency, the wave length, and the parameters of the current profile.

### 2.3.1 General Solution

We define linear monochromatic solutions of the homogeneous problem as $\eta$, $u$, $w$, and $p$ given in the form of

$$\eta = a\cos\theta + \eta_0, \tag{2.17}$$

$$u = U(z) + \hat{u}(z)\cos\theta, \tag{2.18}$$

$$w = \hat{w}(z)\sin\theta, \tag{2.19}$$

$$p = -z + \eta_0 + \hat{p}(z)\cos\theta, \tag{2.20}$$

with $a$ the wave amplitude and $\eta_0$ the mean free surface elevation. Here $U(z)$ gives the current profile, which may be arbitrary. The wave phase is given by

$$\theta = kx - \omega t + \theta_0,$$

with $\omega$ the angular wave frequency, $k$ the wave number, and $\theta_0$ an initial wave phase. In the homogeneous problem $a$, $k$, $\eta_0$, and $\theta_0$ are constant. We assume that

$$a = \mathcal{O}(\epsilon), \epsilon \ll 1. \tag{2.21}$$

We also assume that $\hat{u}$, $\hat{w}$, and $\hat{p}$ are all $\mathcal{O}(\epsilon)$. In (2.19) the amplitude function $\hat{w}(z)$ must satisfy the Rayleigh equation,

$$\frac{d^2\hat{w}}{dz^2} - f(z)\hat{w} = 0, \quad -1 < z < \eta_0, \tag{2.22}$$

$$\hat{w} = 0 \text{ at } z = -1. \tag{2.23}$$

where

$$f(z) = k^2 + \frac{k\frac{d^2U}{dz^2}}{kU - \omega}, \tag{2.24}$$

The Rayleigh equation is also coupled to the wave and current properties by the requirement that

$$\left.\frac{\hat{w}'}{\hat{w}}\right|_{z=\eta_0} - \beta = 0, \tag{2.25}$$

where $\hat{w}' = d\hat{w}/dz$ and

$$\beta = \left( \frac{k^2}{(kU-\omega)^2} + \frac{k\frac{dU}{dz}}{kU-\omega} \right)_{z=\eta_0}. \tag{2.26}$$

We call (2.25) the exact dispersion relation. Since the solution $\hat{w}$ depends on the current profile $U(z)$ (see (2.22)), the quotient $\left.\frac{\hat{w}'}{\hat{w}}\right|_{z=\eta_0}$ in (2.25) depends functionally on $U(z)$, $k$, and $\omega$. Also, from (2.26) we see that $\beta$ depends on $U|_{z=\eta_0}$, $\left.\frac{dU}{dz}\right|_{z=\eta_0}$, $k$, and $\omega$. In other words, for any given current profile $U(z)$, (2.25) relates $k$ and $\omega$ nonlinearly.

For the solution $\hat{w}$ to be unique, we must prescribe together with (2.23) its value at the boundary; the kinematic boundary condition gives the relation with the wave amplitude:

$$\hat{w} = a(\omega - kU) \text{ at } z = \eta_0. \tag{2.27}$$

Finally, (2.18) and (2.20) are completed with the following expressions for $\hat{u}$ and $\hat{p}$:

$$\hat{u} = \frac{\hat{w}'}{k}, \tag{2.28}$$

$$\hat{p} = \frac{1}{k}\left( \hat{w}\frac{dU}{dz} + (\omega - kU)\frac{\hat{w}'}{k} \right). \tag{2.29}$$

If $\hat{w}$, $\hat{u}$, $\hat{p}$, and $k$ satisfy (2.22)-(2.29), then the residues of the governing equations (2.1)-(2.6) are all of higher order, $O\left(\epsilon^2\right)$. Then it is justified to call it a linear solution.

**Remark 2.3.1.1** *In the linear wave theory the dispersion relation does not depend on the wave amplitude. However, linear wave theory does not mean that a linear combination of two sets of linear solutions for $\eta(x,t)$, $u(x,z,t)$, $w(x,z,t)$, $p(x,z,t)$ is also a linear solution. This is because the nonlinearity of the dispersion relation in terms of $U$ implies that the current is nonlinearly related with the wave.*

Throughout this dissertation we only consider the case that $f(z)$ is continuous in the interval $[-1, \eta_0]$.

**Proposition 2.3.1.1** *When $f(z)$ is continuous in the interval $[-1, \eta_0]$ (i.e. $\omega - kU \neq 0$ for all $z \in [-1, \eta_0]$ or, in other words, there is no critical point inside the fluid layer (Drazin and Reid [18])), there exists a unique continuous solution $\hat{w}(z)$ valid in $[-1, \eta_0]$.*

To prove this, first of all the boundary-value problem is transformed into a second-order initial value problem as in Appendix B.1. The rest of the proof is straightforward, by following the theorem given in page 291 of Pearson [49], in which the proof is given in Brand [9]. Even though existence and uniqueness of solutions are guaranteed provided that $f(z)$ is continuous in $[-1, \eta_0]$, exact analytical solutions of (2.22)-(2.6) can only be found for a few types of current profiles.

Summarizing, we conclude that if (for a specific current profile) we know the solution of the Rayleigh equation (2.22), we have explicit expressions for the linear solutions (2.17)-(2.20) and exact analytical expression for the dispersion relation (2.25). A special case where an exact solution of the Rayleigh equation exists is presented in the following subsection. In the beginning of Chapter 4 we will discuss the case when an exact analytical solution is not known. We will show that there exist approximate solutions of the Rayleigh equation and approximate wave number $k$ such that all residues of the governing equations (2.1)-(2.6) are $\mathcal{O}\left(\epsilon^2\right)$, i.e. of the same order as the error from linearization.

### 2.3.2 Linear currents

If $U''(z) = 0$, i.e uniform or linear current, the exact solution of the Rayleigh equation is given by

$$\hat{w} = \frac{a\left(\omega - k\, U|_{z=\eta_0}\right)}{\sinh\left(k\left(1+\eta_0\right)\right)} \sinh k\left(z+1\right), \tag{2.30}$$

and with this the exact dispersion relation (2.25) is given by

$$\left(\omega - k\, U|_{z=\eta_0} + \frac{1}{2}\frac{dU}{dz}\bigg|_{z=\eta_0} \tanh k\left(1+\eta_0\right)\right)^2 = \left(\frac{1}{4}\left(\frac{dU}{dz}\right)^2\bigg|_{z=\eta_0} \tanh^2 k\left(1+\eta_0\right) + k\tanh k\left(1+\eta_0\right)\right). \tag{2.31}$$

The dispersion relation for linear current (2.31) is also given in Dingemans [17]. For the special case that $\frac{dU}{dz} = 0$, i.e. uniform current $U = U_0 \equiv$ constant, and $\eta_0 = 0$ (2.31) leads to

$$\omega = kU_0 + k\sqrt{\frac{\tanh k}{k}}. \tag{2.32}$$

We define *following current* as a current which velocity in $x-$direction is nonnegative for all $z \in [-1, \eta_0]$ and *adverse current* as a current which velocity is nonpositive for all $z \in [-1, \eta_0]$. Currents for which the velocity is partly positive and partly negative, are called *currents with backflow*. In Figure 2.1 we plot (2.31) and (2.32) for various following/adverse uniform and linear currents, taking $\eta_0 = 0$. Given a value $\omega$, observe that for cases with following currents the wave number $k$ is smaller

than the one of the current-free wave; while for cases with adverse currents the wave number $k$ is larger. Observe also that for each case with adverse current, there is a value $\omega$ at which the group velocity $\frac{d\omega}{dk}$ vanishes. At this point the wave action (energy) transport velocity vanishes (Suastika [63]). In Figure 2.2 we give another presentation of the dispersion relation (2.31), now for currents with backflow. We take $U(z) = U_0 + sz$. In Figure 2.2, we take $\omega = 1$ and plot $k$ as a function of $U_0$ or $s$. The corresponding wave number of the current-free wave is given by the solid straight line. We observe that the dispersion relations intersect this line. At the point of intersection, the wave number $k$ is the same. This means that the length of the wave is not affected by the presence of these linear currents. A similar analysis that determines the equivalent uniform current for a given depth-varying current is given by Hedges and Lee [27].

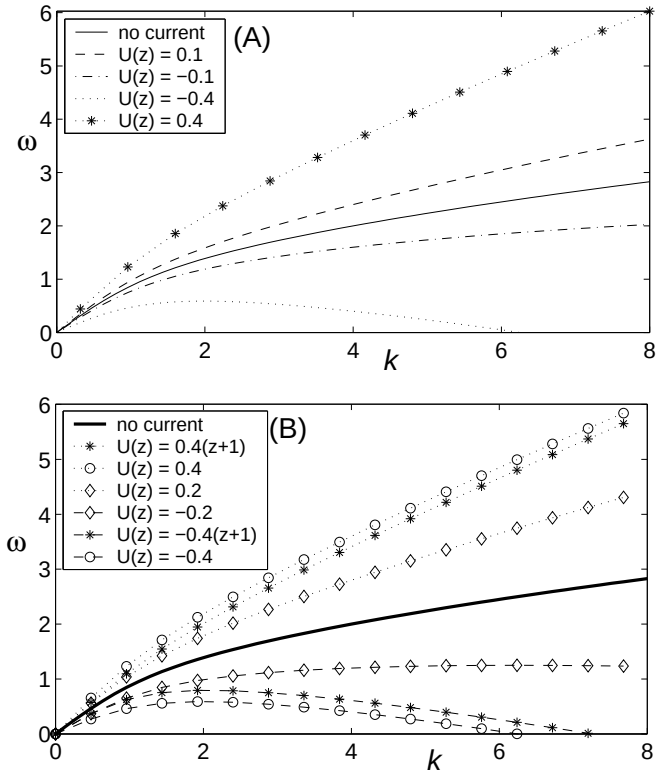


Figure 2.1: Figure (A): Plots of the dispersion relation 3.4, for various uniform currents. Figure (B): Plots of the dispersion relation 2.31, for various uniform and linear currents

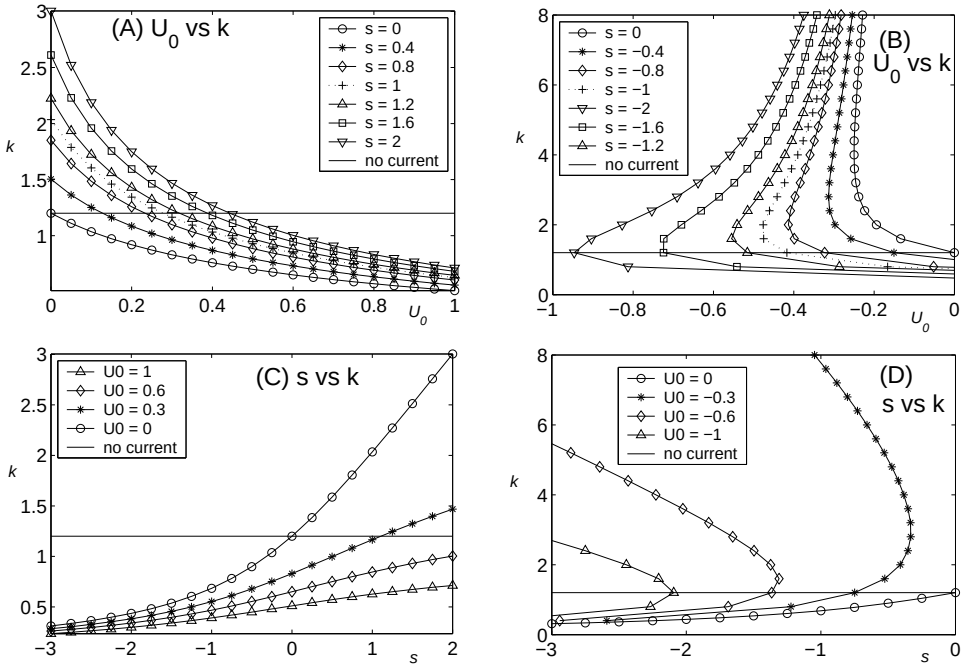


Figure 2.2: Plots of the dispersion relation 2.31, for $\omega = 1$. We take $U(z) = U_0 + sz$. Figure (A) and (B): $k$ vs $U_0$; Figure (C) and (D): $k$ vs $s$.

### 2.3.3 Nonlinear Currents

For water of finite depth, exact analytical solutions of (2.22)-(2.27) as well as the dispersion relation can only be found for a few types of current profiles (see [17]). If the current profile is not linear, $U''(z) \neq 0$, then in general we cannot find explicit solutions of the Rayleigh equation. In this case the dispersion relation has to be approximated. In Chapter 3 we present a method to approximate the dispersion relation. We will show that the proposed approximation works well for cases with nonlinear currents $U(z)$.

## 2.4 Overview of the model

We have shown that the set of solutions of the linearized homogeneous problem is characterized by the dispersion relation. Therefore before discussing the quasi-homogeneous approximation, a variational characterization of the dispersion relation will be presented in Chapter 3. This leads to an analytical expression that approximates the dispersion relation.

In Chapters 4 and 5 we propose and validate a low dimensional model that describes the adaptation process of a surface water wave that encounters a depth dependent current. Wave and current simultaneously adapt and reach an equilibrium condition determined by the Rayleigh equation (2.22) and characterized by the dispersion relation (2.25) (or its approximation).

In the mathematical model presented in Chapter 4, the problem is approached by seeing the interaction as an adaptation process of wave and current that takes place spatially. In practice, the current is defined as the mean (time-average) horizontal velocity. The process starts with a linear wave above a current free layer, that meets a current at a certain position in the free surface. At this position the adaptation starts. Before the start of the adaptation, the wavelength is determined from the wave-only dispersion relation; and the spatial adaptation results to a wavelength which agrees with the dispersion relation of steady wave-current interaction determined by the solution of the Rayleigh equation.

In the model that we propose, we allow the fluid properties (i.e. the free surface elevation, the velocities, and the pressure) to be parameterized by four parameters that may change quasi-homogeneously in one horizontal direction. The four parameters that describe the wave-current environment in the model are the wave amplitude $a$, the wave number $k$, the mean-free surface elevation $\eta_0$, and one parameter to describe the deformation of the current profile $U(z)$ denoted by $P_c$. The parameter $P_c$ gives, for example, uniform or quadratic change in the current profile.

Changes of the parameters are determined by requiring that the kinematic free surface boundary condition (2.1) and the continuity equation (2.5) are satisfied pointwise, and that conservations of the total mass, momentum, and energy density-fluxes (2.14)-(2.16) are satisfied. This can be stated differently: we derive the model by considering the full Euler equations (2.3)-(2.4), and instead of requiring them to hold pointwise, we project these equations in a number of specific directions. The directions are chosen such that changes in relevant physical quantities mentioned above are modeled in a valid way. A-priori estimates for the errors are derived which show that the errors introduced by the interaction are of higher order.

# Chapter 3

# Variational Characterization of the Dispersion Relation

An approximate dispersion relation for water waves propagating on a depth-dependent current is formulated without the necessity to solve the Rayleigh equation. Taking particular trial functions, the approximate dispersion relation is close to the exact one. The approximate dispersion relation is expressed analytically, from which approximations of certain quantities such as the phase velocity, the group velocity, or the wave blocking criteria can be derived.

## 3.1 Introduction

In Chapter 2 we show that for the homogeneous problem of linear waves propagating on a (steady) depth-varying current, the governing equations reduce to the Rayleigh equation (or the inviscid Orr-Sommerfeld equation) (2.22), which is an ordinary differential equation for the wave motion part of the vertical velocity. Kinematic boundary conditions are derived for the impermeable bottom and free surface. The dynamic boundary condition at the free surface contributes to an equation which can be interpreted as a representation of the exact dispersion relation. It should be observed that the dispersion relation is implicitly given by (2.25) once a nonzero solution $\hat{w}$ is found from (2.22)-(2.23). Although in the linear theory the dispersion relation is not affected by the wave amplitude, it relates nonlinearly the wave and the current.

A dispersion relation gives the essential character of the homogeneous problem, for each class of current profiles. The dispersion relation can be expressed analytically as long as analytical solutions of the Rayleigh equation are found. However, exact analytical solutions can only be found for a few classes of current profile or under the assumption that the wave is stationary ($c = \omega/k = 0$) or the water depth is infinite ($h \to \infty$). Reviews on this problem are given by Dingemans [17], Peregrine [50], Thomas and Klopman [70]. A separate collection of analytical solutions of the Rayleigh equation for some classes of mean flow (current) with shearing profiles is given by Russell [53], in which the solutions are given in terms of transcendental functions like the Gauss hypergeometric function.

Analytical expressions of the dispersion relation are useful for deriving and studying quantities such as the group velocity and the wave blocking criteria.

There are a number of analytical models which give approximations to the dispersion relation. Each model has advantages and disadvantages and a certain range of applicability. Skop [59] and Kirby and Chen [32] present models for arbitrary small current; a related expression for deep water has been found by Stewart [60]. In these models, the current is relatively small compared to the phase velocity. For deep water, Shrira [57] constructed the exact solution of the boundary-value problem in terms of an absolutely converging series in powers of a small parameter defined as the ratio of the averaged mean flow vorticity gradient $U^{'}(z)$ and the product of a characteristic wave number and wave frequency. A variational formulation for deep water is presented by Miles [47]. The formulation is applied to analyze the stability of exponential mean current profiles in deep water for two asymptotic cases, slow waves and short waves under the condition that $|c/U(0)| \ll 1$. In another paper by Miles [46], in which the water depth is finite, two variational integrals that provide an upper bound and a lower bound to the true value of the Froude number are formulated. Although these formulations are made for currents which have zero gradient at the surface ($U^{'}(0) = 0$), they also hold when $U'(0) \neq 0$. In [46], two cases were studied: the long wave approximation ($k \to 0$) and stationary waves ($c = 0$).

For some practical applications, getting the corresponding wavenumber $k$ from a given wave frequency $\omega$ is more demanding than getting the solution of the Rayleigh equation. Therefore, it is of practical interest to derive analytical or numerical models in which the task of finding $k$ is decoupled from that of finding the solution of the Rayleigh equation. We can do this by using the variational formulation for the boundary value problem as the ones given by Miles [46], [47]. We aim to find, for waves on water of finite depth, analytical approximations of the dispersion relation that are accurate for various current profiles and a large range of frequencies. The model is derived through variational formulations of the governing boundary value problem. In this way, the task of finding the dispersion relation becomes decoupled from that of finding the solution of the boundary value problem. We characterize the dispersion relation as the critical value of the functional. By using an action functional, we establish two functionals that give complementary approximations for the exact dispersion relation. We point out that both approximations in this dual approach are good if trial functions are carefully chosen. We collect several candidates for the trial functions, give the range of applicability of each trial function, and demonstrate the performance of the approximation. We show that for cases with nonlinear large currents, the WKB approximated solution of the Rayleigh equation results to a good approximation for the dispersion relation. We also derive a simple formula for the case that the current profile is given by a piecewise linear function. In that case exact analytical solutions exist, but they are lengthy and difficult to simplify (see Appendix A). The piecewise linear profile is of practical interest since in most measurements the current is measured point-wise. Provided that the vorticity jump at each kink

is small, we present approximations of the dispersion relation for general piecewise linear currents with $N-$ kinks that is much simpler than the exact dispersion relation. From the examples it appears that the approximations are good and get better and better as the wave number increases. As an additional result, in Appendix B.3 we show that an implementation of the finite-element method transforms the problem into a generalized (linear or quadratic) eigenvalue problem, from which $k$ or $\omega$ can be calculated without calculating the solution of the Rayleigh problem.

## 3.2 Variational Characterization

### 3.2.1 Direct variational formulation

Here we only consider cases that the Rayleigh equation is non singular,

$$kU(z) \neq \omega \text{ for all } z \in [-1, \eta_0].$$

With the following analysis, we formulate a method to approximate the dispersion relation for linear waves on finite depth without any restriction to the current profile or magnitude. With this method, the task of finding the dispersion relation is decoupled from that of finding the vertical fluid velocity. First we provide a variational way of representing the boundary value problem (2.22)-(2.27), and consequently the dispersion relation (2.25). Then we exploit this variational formulation to approximate the dispersion relation.

**Claim 3.2.1.1** *Critical points (i.e. maximum/minimum/saddle points) of the functional*

$$\mathcal{L}(\hat{w}) = \frac{1}{2}\int_{-1}^{\eta_0}\left[(\hat{w}')^2 + f(z)\,\hat{w}^2\right]dz - \frac{1}{2}\beta\hat{w}(\eta_0)^2, \tag{3.1}$$

*for functions $\hat{w}$ that satisfy $\hat{w}(-1) = 0$, satisfy the boundary value problem (2.22), (2.23), (2.25). Moreover, at a critical point $\hat{w}$ the functional $\mathcal{L}$ vanishes:*

$$\mathcal{L}(\hat{w}) = 0. \tag{3.2}$$

To show this, observe that the directional derivative of the functional $\mathcal{L}$ in the direction of a function $v$ that satisfies $v(-1) = 0$ is given by

$$\begin{aligned}
\delta_{\hat{w}}\mathcal{L}(\hat{w}; v) &= \left.\frac{d}{d\epsilon}\right|_{\epsilon=0}\mathcal{L}(\hat{w} + \epsilon v) \\
&= \int_{-1}^{\eta_0}\left[\hat{w}'v' + f(z)\,\hat{w}v\right]dz - \beta\hat{w}(\eta_0)\,v(\eta_0) \\
&= -\int_{-1}^{\eta_0}\left[\hat{w}'' - f(z)\,\hat{w}\right]vdz + \left[\hat{w}'(\eta_0) - \beta\hat{w}(\eta_0)\right]v(\eta_0),
\end{aligned}$$

from which we conclude that a critical point $\hat{w}$ satisfies the Euler-Lagrange equation of the functional $\mathcal{L}$, which is precisely the Rayleigh equation (2.22) and the boundary condition (2.25). Since for a critical point $\hat{w}$

$$\mathcal{L}(\hat{w}) = -\frac{1}{2}\int_{-1}^{\eta_0} \hat{w}\left[\hat{w}'' - f(z)\,\hat{w}\right] dz + \left[\frac{1}{2}\hat{w}'\hat{w}\right]_{z=\eta_0} - \frac{1}{2}\beta\hat{w}(\eta_0)^2,$$

the vanishing is an immediate consequence of (2.22) and (2.25).

Taken together, these results express that the vanishing of the functional $\mathcal{L}$ can be seen as the formulation for the dispersion relation. To illustrate this, we give the simplest example, the case of a uniform or linear current, $U''(z) = 0$. Then the exact solution to (2.22) and (2.23) is known to be

$$\hat{w}(z) = \Gamma \sinh k\,(z+1), \tag{3.3}$$

for arbitrary $\Gamma$. In case the current $U$ is uniform, substitution of this into (3.2) gives

$$\frac{1}{\tanh k} - \frac{k}{(kU-\omega)^2} = 0.$$

which, after simplification, leads to the exact dispersion relation for linear waves on a uniform current (Dingemans [17]; Peregrine [50]):

$$\omega = kU + \sqrt{k \tanh k}. \tag{3.4}$$

In case the current is linear, $U(z) = U_0 + sz$, substitution of (3.3) in (3.2) gives a relation which is equivalent to (2.31).

### 3.2.2 Dual variational formulation

Now we present another variational formulation that enables us to find the dual approximation for the dispersion relation. The method is essentially based on a Legendre transformation and is well known in Classical Mechanics to describe a transformation from a Lagrangian description to a Hamiltonian description.

One way to motivate this is to rewrite the second order boundary value problem (BVP) (2.22), (2.23), (2.25) in an equivalent way as a system of two first-order differential equations (the 'Hamilton' equations):

$$\hat{w}' - \psi = 0, \tag{3.5}$$

$$-\psi' + f\hat{w} = 0, \tag{3.6}$$

with the boundary conditions:

$$\hat{w}(-1) = 0 \text{ and } \psi(\eta_0) - \beta\hat{w}(\eta_0) = 0. \tag{3.7}$$

Then it can be observed that this system for $(\hat{w}, \psi)$ is the critical point of the functional (the *canonical action functional* $\mathcal{A}(\psi, \hat{w})$ in Classical Mechanics for the 'position' and 'momentum' variables $\hat{w}$ and $\psi$ respectively):

$$\mathcal{A}(\psi, \hat{w}) = \int_{-1}^{\eta_0} \left( \psi \hat{w}' - \frac{1}{2}\psi^2 + \frac{1}{2} f \hat{w}^2 \right) dz - \frac{1}{2}\beta \hat{w} (\eta_0)^2 .$$

The relation between the original *Lagrangian functional* $\mathcal{L}(\hat{w})$ and this action functional is actually given by

$$\mathcal{L}(\hat{w}) = \sup_{\psi} \mathcal{A}(\psi, \hat{w}) .$$

Now, because of the fact that the problem is quadratic, we can continue and eliminate the variable $\hat{w}$ in favor of the variable $\psi$. In fact, defining the *dual functional*

$$\mathcal{B}(\psi) = \operatorname*{crit}_{\hat{w}} \mathcal{A}(\psi, \hat{w}) ,$$

the elimination of $\hat{w}$ leads to the explicit expression

$$\mathcal{B}(\psi) = -\frac{1}{2} \int_{-1}^{\eta_0} \left( \frac{1}{f} \left( \psi' \right)^2 + \psi^2 \right) dz + \frac{1}{2\beta} \psi (\eta_0)^2 .$$

The critical point of this functional satisfies

$$-\frac{d}{dz}\left( \frac{\psi'}{f} \right) + \psi = 0, \ \psi'(-1) = 0, \ -\frac{\psi'(\eta_0)}{f(\eta_0)} + \frac{\psi(\eta_0)}{\beta} = 0$$

which is the same result as would have been found by eliminating $\hat{w}$ from the Hamilton equations (3.5)-(3.7) above.

The relation between the critical points of the functionals can be described as

$$\operatorname*{crit}_{\hat{w}} \mathcal{L}(\hat{w}) = \operatorname*{crit}_{\hat{w}} \operatorname*{crit}_{\psi} \mathcal{A}(\psi, \hat{w}) = \operatorname*{crit}_{\psi} \operatorname*{crit}_{\hat{w}} \mathcal{A}(\psi, \hat{w}) \equiv \operatorname*{crit}_{\psi} \mathcal{B}(\psi) .$$

In case the critical points are related by the Legendre transformation, the critical value of $\mathcal{B}$ of course also vanishes as is the case for $\mathcal{L}$. Also, when the function that is the conjugate of (3.3) given by

$$\psi = \Gamma k \cosh(k(z+1)) \tag{3.8}$$

is substituted into $\mathcal{B}(\psi) = 0$ we get indeed (3.4) for uniform current and (2.31) for linear current.

## 3.3 The approximate dispersion relation

For a current with a nonlinear profile it is in general not possible to find analytic solutions of the Rayleigh equation, and therefore of the exact dispersion relation. If an approximate solution of the Rayleigh equation is taken for the exact vertical

velocity amplitude, say a trial function $\hat{w}_{\text{trial}}(z)$, which satisfies $\hat{w}_{\text{trial}}(-1) = 0$, then an approximate dispersion relation is given by the relation

$$\mathcal{L}(\hat{w}_{\text{trial}}) = 0. \tag{3.9}$$

We can formulate this in a somewhat different way as follows. Define the functional $\mathcal{D}(\hat{w})$ that is homogeneous of degree zero:

$$\mathcal{D}(\hat{w}) = \frac{1}{\hat{w}(\eta_0)^2} \int_{-1}^{\eta_0} \left[ (\hat{w}')^2 + f(z)\,\hat{w}^2 \right] dz. \tag{3.10}$$

Then $\mathcal{L}(\hat{w}) = \frac{\hat{w}(\eta_0)^2}{2} [\mathcal{D}(\hat{w}) - \beta]$ so the exact dispersion relation is given by

$$\mathcal{D}(\hat{w}) = \beta.$$

Realising that both expressions are functions of $\omega$ and $k$, the equality can be viewed as the intersection of two surfaces, the 'Rayleigh-surface' $(\omega, k) \to \mathcal{D}(\hat{w})$, and the '$\beta$-surface' $(\omega, k) \to \beta$, with the dispersion relation as intersection curve.

Taking a trial function $\hat{w}_{\text{trial}}$, the approximate dispersion relation (3.9) can then be written as the intersection of the $\beta$-surface with the approximate Rayleigh surface $(\omega, k) \to \mathcal{D}(\hat{w}_{trial})$:

$$\mathcal{D}(\hat{w}_{\text{trial}}) = \beta; \tag{3.11}$$

this is illustrated in Figure (3.1).

**Remark 3.3.0.1** *It is important to realize that the 'quality' of the approximate dispersion relation is essentially better than the quality with which the Rayleigh equation is solved. Indeed, from the fact that for the exact dispersion relation the functional derivative vanishes, the error in the value of the functional is quadratic with respect to the error in the trial function from the exact solution.*

We use the functional $\mathcal{B}(\psi)$ to derive the second approximation for the dispersion relation,

$$\mathcal{B}(\psi_{\text{trial}}) = 0, \tag{3.12}$$

taking a suitable trial function $\psi_{\text{trial}}$.

Define $\mathcal{R}$ as

$$\mathcal{R}(\psi) = \psi(\eta_0)^2 \Big/ \int_{-1}^{\eta_0} \left( \frac{1}{f} \left( \psi' \right)^2 + \psi^2 \right) dz \tag{3.13}$$

then $\mathcal{B}(\psi) = \frac{\psi(\eta_0)^2}{2} \left[ \frac{1}{\beta} - \frac{1}{\mathcal{R}(\psi)} \right]$ and the approximate dispersion relation (3.12) can be written like:

$$\mathcal{R}(\psi_{\text{trial}}) - \beta(k, \omega) = 0, \tag{3.14}$$

which again can be interpreted as the intersection of the $\beta$-surface with the approximate 'dual Rayleigh-surface' $(\omega, k) \to \mathcal{R}(\psi_{\text{trial}})$ (see Figure 3.1).

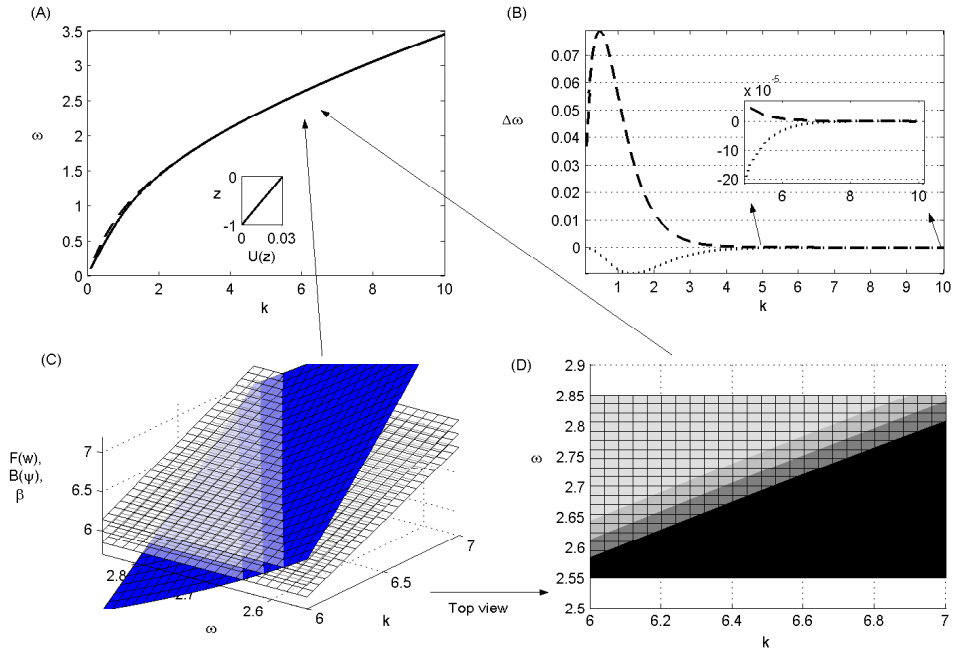


Figure 3.1: Fig.(A): The exact and approximate dispersion relations for linear current given by (3.15a) (shown in the inset). The solid line represents the exact dispersion relation, the dotted line is approximation (3.11) and the dashed line is approximation (3.14). Trial functions are given by (3.16a) and (3.16b).
Fig.(B): Differences from the exact solution, line styles are the same as for Fig.(A).
Fig.(C): The *β-surface* (the dark surface), the *approximate Rayleigh surface* $\mathcal{D}(\hat{w}_{trial})$ (the upper light surface), the *dual Rayleigh surface* $R(\psi_{trial})$ (the lower light surface), and the *exact Rayleigh surface* $\mathcal{D}(\hat{w}_{\text{exact}})$ (the surface in between $\mathcal{D}(\hat{w}_{trial})$ and $R(\psi_{trial})$).
Fig.(D): Figure (C) shown from the top. The dispersion relations in Figure (A) are shown as the three borders of areas with different grey color.

### 3.3.1 The trial functions

The quality of the approximate dispersion relation depends on the choice of the trial function. In table below we list several trial functions and the condition of applicability of each of them.

| Trial function | Application |
|---|---|
| $\hat{w}_{\text{trial}} = \sinh(k(z+1))$ | weakly nonlinear current $U''(z) \ll 1$ or short waves $k \to \infty$ (Miles [46]). |
| $\hat{w}_{\text{trial}} = \exp\left((z-\eta_0)\sqrt{k^2+1/d^2}\right)$ | (Miles [47]) deep water where $U(z) = U_0 \exp(z/d)$ under the assumption that $\lvert c/U_0 \rvert \ll 1$. |
| $\hat{w}_{\text{trial}} = U(z)\left[1 - k^2 \int_z^{\eta_0} \frac{P}{U^2} dz\right]$ | (Miles [46]) stationary long-wave ($c = 0$ and $k \to 0$). |
| $\hat{w}_{\text{trial}} = U(z)\frac{R(z)}{R(1)}$, where $R(z) = \int_{-1}^{z} \frac{dz}{(U-c)^2}$ | ([46]) long wave approximation for running waves ($c \neq 0,\ k \to 0$) |
| $\hat{w}_{\text{trial}}(z) = \frac{\sinh \int_{-1}^{z} \sqrt{f(\zeta)} d\zeta}{f(z)^{1/4}}$ (WKB approximation) | nonlinear current $U''(z) \gg 0$, provided that $f(z) \neq 0$ at any $z \in [-1, \eta_0]$. |

### 3.3.2 Bounds for the exact dispersion relation

Given $\hat{w}_{\text{trial}}$ and $\psi_{\text{trial}}$, by investigating the monotonicity of the functionals with respect to $\omega$ we can analyze whether each approximation provides an upper or a lower bound to the exact dispersion relation (in the $k - \omega$ plane). Note that the word 'bound' here has a different meaning than the one used by Miles [46] in which the word 'bound' refers to the correct value of the functionals (which is the Froude number $F = U(\eta_0)/\sqrt{gh}$). In the present discussion it refers to the correct value of the wave frequency, $\omega = \Omega(k)$.

Under the condition that $\hat{w}_{\text{trial}}$ does not depend on $\omega$ and $\omega < k \cdot \min_{-1 \le z \le \eta_0} U(z)$ or $\omega > k \cdot \max_{-1 \le z \le \eta_0} U(z)$, it follows that when $U''(z)$ is sign-definite over the whole depth, $\mathcal{D}(\hat{w}_{\text{trial}})$ depends monotonically on $\omega$ :

$$\text{if } U'' > 0 \text{ for all } z \text{ then } \mathcal{D}(\hat{w}) \text{ monotonically increases in } \omega,$$
$$\text{if } U'' < 0 \text{ for all } z \text{ then } \mathcal{D}(\hat{w}) \text{ monotonically decreases in } \omega,$$

From the expression (2.26) for $\beta$ we calculate $\frac{d\beta}{d\omega}$ and observe that when $\omega > k \cdot \max_{-1 \le z \le \eta_0} U(z)$,

$$\frac{\partial \beta}{\partial \omega} > 0 \text{ if } (2 + U(\eta_0) U'(\eta_0)) k < U'(\eta_0)\omega,$$
$$\frac{\partial \beta}{\partial \omega} < 0 \text{ if } (2 + U(\eta_0) U'(\eta_0)) k > U'(\eta_0)\omega,$$

and reversed inequalities when $\omega < k \min_{-1\leq z\leq \eta_0} (U(z))$.

From this, when $\hat{w}_{\text{trial}}$ does not depend on $\omega$ and $\omega = \Omega(k)$ is the exact dispersion relation and $\mathcal{L}(\hat{w}_{\text{trial}})$ increases with $\omega$, the approximation $\mathcal{L}(\hat{w}_{\text{trial}}) = 0$ leads to a lower bound for $\Omega(k)$ if $\mathcal{L}(\hat{w}_{\text{trial}})|_{\Omega(k),k} > 0$ and to an upper bound for $\Omega(k)$ if $\mathcal{L}(\hat{w}_{\text{trial}})|_{\Omega(k),k} < 0$; the same holds true for $\mathcal{B}$.

To illustrate this, take $\eta_0 = 0$ and consider as an example four different current profiles:

$$U(z) = 0.03(z+1) \tag{3.15a}$$

$$U(z) = 0.03\exp(z) \tag{3.15b}$$

$$U(z) = \begin{cases} 0.05z + 0.065 & , \ -1 \leq z < -0.3 \\ 0.5z + 0.2 & -0.3 \leq z \leq 0 \end{cases}, \tag{3.15c}$$

$$U(z) = \begin{cases} -0.05z - 0.065 & , \ -1 \leq z < -0.3 \\ -0.5z - 0.2 & -0.3 \leq z \leq 0 \end{cases}. \tag{3.15d}$$

In Figure 3.2 we present monotonicity for $F(\hat{w}_{\text{trial}})$ and $B(\psi_{\text{trial}})$, for the current profiles (3.15a)-(3.15d) given above. In Figure 3.2(a) we take as trial functions

$$\hat{w}_{\text{trial}} = \exp(k(z+1)) - 1, \tag{3.16a}$$

$$\psi_{\text{trial}} = \exp(k(z+1)), \tag{3.16b}$$

while for Figure 3.2(b, c, d), we take (3.3) and (3.8). Functions (3.3) and (3.8) are the asymptotic solutions of the Rayleigh equation for large $k$ and are exact solutions if the current is linear. In Figure 3.2(a, d), $\mathcal{L}(\hat{w}_{\text{trial}})|_{\Omega(k),k} > 0$, $\mathcal{B}(\hat{w}_{\text{trial}})|_{\Omega(k),k} < 0$, and inside the shaded area both $\mathcal{L}(\hat{w}_{\text{trial}})|_{\omega,k}$ and $\mathcal{B}(\hat{w}_{\text{trial}})|_{\omega,k}$ increase with $\omega$. This explains why the approximation (3.9) gives a lower bound and (3.12) gives an upper bound to the exact dispersion relation. With a similar reasoning, the result given in Figure 3.2(c), where both approximations give lower bounds to the exact dispersion relation, is explained.

From the results presented in Figure 3.2(c) and Figure 3.3, we observe that the exact dispersion relation $\omega_{\text{exact}}(k)$ is not always flanked by the two approximations. We can take as the final approximation the average value of the two approximations, $\omega_{\text{mid}}(k)$. In any case, when not knowing the exact value and its distance to approximations (3.9) and (3.12), it is safer to use the average value $\omega_{\text{mid}}$ than either (3.9) or (3.12) separately.

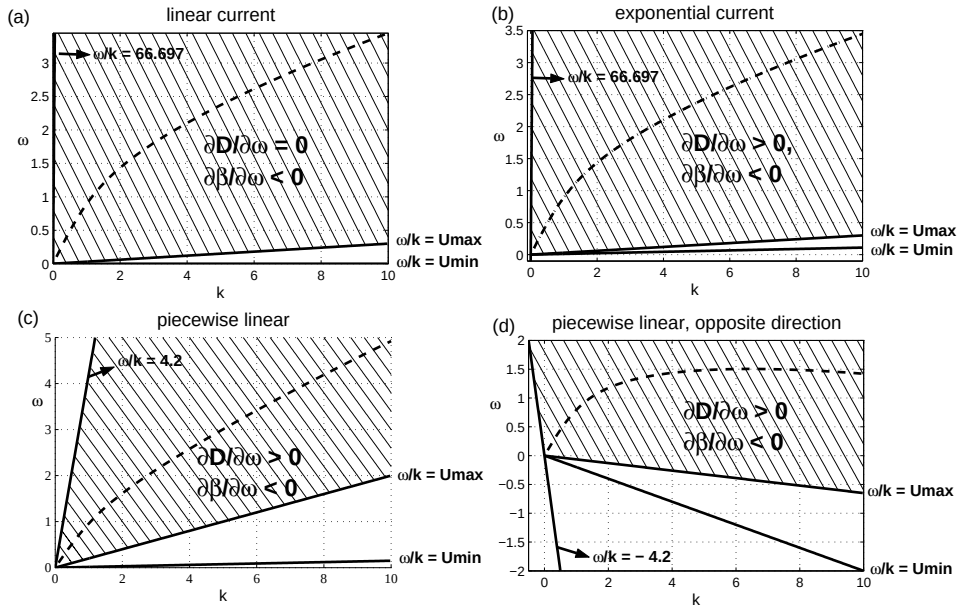


Figure 3.2: The four approximations for current profiles given by (3.15a )-(3.15d). The exact dispersion relation is given by the dashed line. Inside the shaded areas, $\mathcal{L}\left(\hat{w}_{\text{trial}}\right)$ and $\mathcal{B}\left(\hat{w}_{\text{trial}}\right)$ increase monotonically. In figures (a, d), $\mathcal{L}\left(\hat{w}_{\text{trial}}\right)|_{\Omega(k),k} > 0$ and $\mathcal{B}\left(\hat{w}_{\text{trial}}\right)|_{\Omega(k),k} < 0$; and in figure (c) $\mathcal{L}\left(\hat{w}_{\text{trial}}\right)|_{\Omega(k),k} > 0$ and $\mathcal{B}\left(\hat{w}_{\text{trial}}\right)|_{\Omega(k),k} > 0$.

## 3.4 Some examples

### 3.4.1 General formula for piecewise linear currents

When a current profile is approximated by a piecewise linear function

$$U(z) = \begin{cases} s_0 (z - \eta_0) + U_0 & z_1 < z \leq \eta_0, \\ s_1 (z - z_1) + U_1 & z_2 < z \leq z_1, \\ s_2 (z - z_2) + U_2 & z_3 < z \leq z_2, \\ \vdots & \vdots \\ s_N (z - z_N) + U_N & -1 \leq z \leq z_N, \end{cases} , \tag{3.17}$$

where $U(z)$ is continuous at each kink, it is known that exact analytical solutions can be derived by satisfying $2N$ matching conditions (see Appendix A). However, the resulting dispersion relations are lengthy and difficult to simplify.

If the 'vorticity jump' at each kink is small, simple expressions which approximate the dispersion relations are derived by using (2.20) and (3.12), taking as trial functions $\hat{w}_{\text{trial}} = \sinh\left(k\left(z+1\right)\right)$ and $\psi_{\text{trial}} = \cosh\left(k\left(z+1\right)\right)$. The approximate dispersion

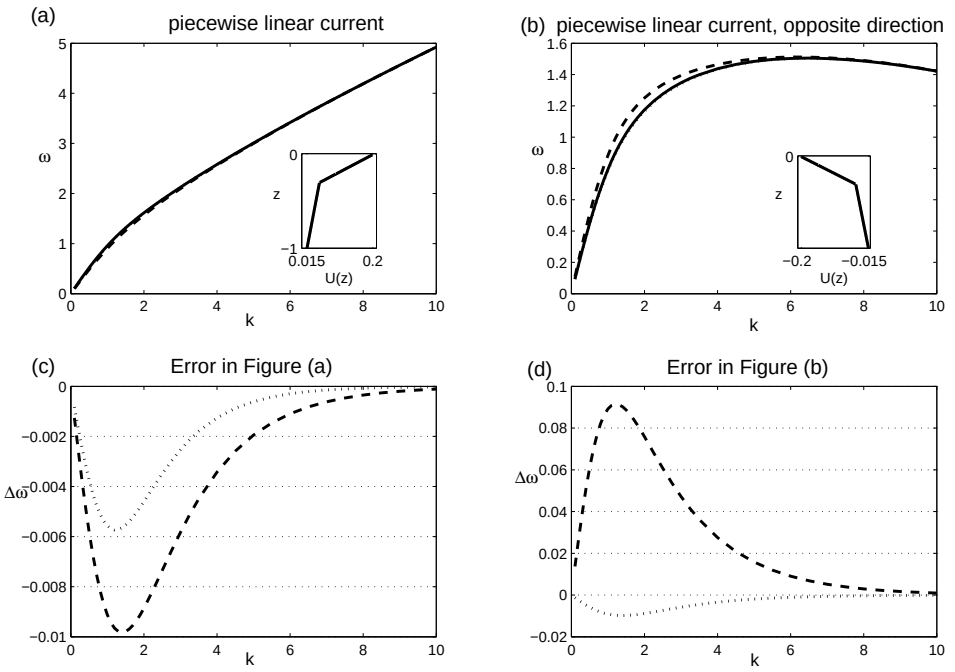


Figure 3.3: Approximations (3.9) and (3.12) when the current profile is given by piecewise linear functions as shown in the insets. The trial functions are given by (3.3) and (3.8). Approximation (3.9) is presented by the dotted line, and approximation (3.12) is presented by the dashed line. The exact dispersion relation is given by the solid line

relations are given by

$$\cosh(k\,(1+\eta_0))\sinh(k\,(1+\eta_0)) + \left(\sum_{i=1}^{N}\frac{s_i - s_{i-1}}{kU_i-\omega}\sinh^2\left(k\,(z_i+1)\right)\right) - \left(\frac{k^2}{(kU_0-\omega)^2}+\frac{ks_0}{kU_0-\omega}\right)\sinh^2\left(k\,(1+\eta_0)\right) = 0, \tag{3.18}$$

and

$$\cosh(k\,(1+\eta_0))\sinh(k\,(1+\eta_0)) - \frac{(kU_0-\omega)^2\cosh^2\left(k\,(1+\eta_0)\right)}{k+s_0\,(kU_0-\omega)} = 0. \tag{3.19}$$

An example for a single kink, where $N = 1$ is given in Figure 3.3, which shows the approximations (3.9) and (3.12) for currents given by piecewise-linear functions (3.15c) and (3.15d), taking as trial functions (3.3) and (3.8) and $\eta_0 = 0$. The approximate dispersion relations (3.18) and (3.19) are compared with the exact dispersion

relation, which is given by (A.4) in Appendix A. Although the vorticity jump at the kink is as large as 0.45, we observe that (3.18) and (3.19) give good approximations for the dispersion relation. For multiple kinks ($N > 1$) expressions (3.18) and (3.19) are easier to analyze than the exact, but intricate, dispersion relation. Because of their simplicity approximations (3.18) and (3.19) can be used (for example) to derive approximate analytical expressions for the group velocities.

### 3.4.2 Approximation using the irrotational-wave solution

In Figure 3.4, for $\eta_0 = 0$ we present the error from the approximate dispersion relation (3.9) when the current profile is given by $U(z) = -\exp(\alpha z)$ (adverse exponential current). As a trial function we take (3.3). As the current profile is nonlinear, the exact solution and the exact dispersion relation plotted in this Chapter are calculated numerically by the method given in (Fenton [19]) and (Thomas [69]).

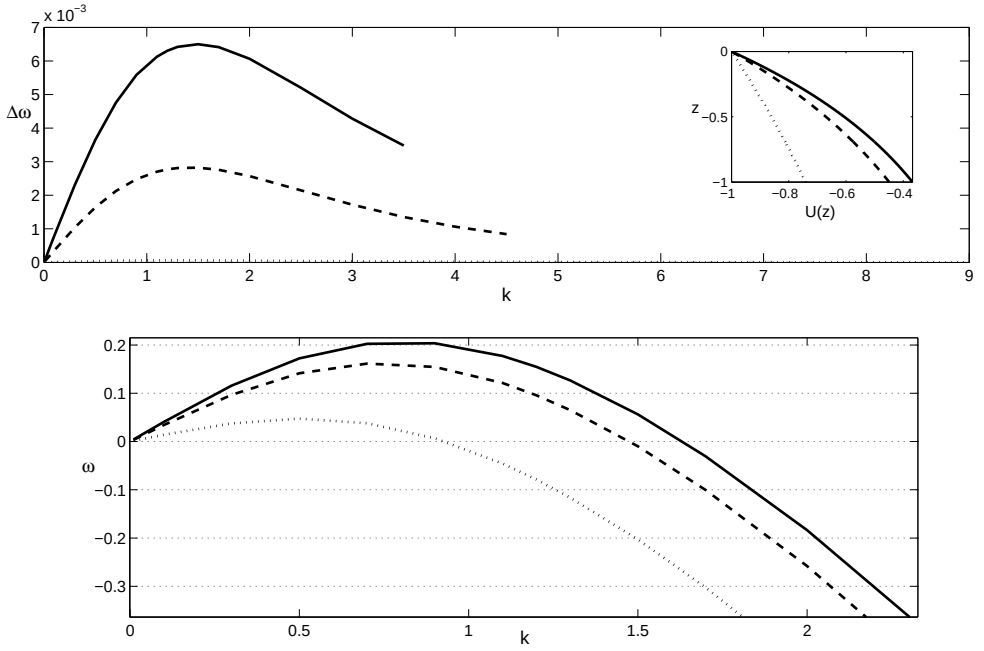


Figure 3.4: The error of the approximate dispersion relation with the choice (3.3) as the trial function when the current profile is given by $U(z) = -\exp(\alpha z)$ for various value of $\alpha$. In all pictures the solid line, the dashed line, and the dotted line are related to $\alpha = 1$, $\alpha = 0.8$, and $\alpha = 0.3$, respectively. In the lower picture, with the same line coding, the exact dispersion relations are plotted.

In Figure 3.5 we present the error in $\hat{w}$ for $k = 1.5$. As expected, we observe that

when using $\hat{w}_{\text{trial}} = \sinh(k(z+1))$ the less curved the current profile the better the approximation. From Figure 3.4 and Figure 3.5 we observe that the error to the dispersion relation is quadratic with respect to error in $\hat{w}$, in agreement with Remark 3.3.0.1.

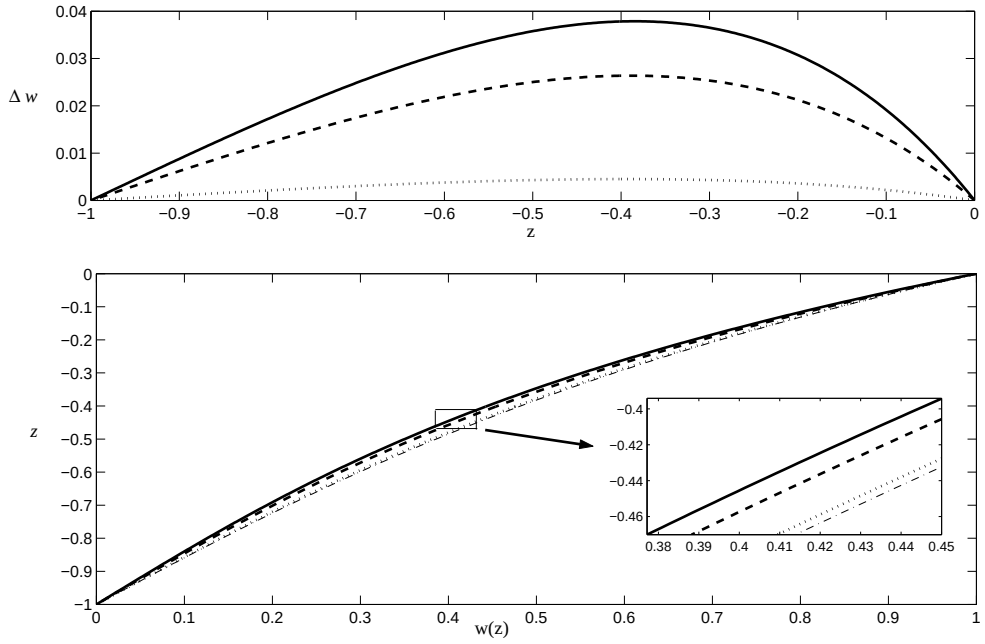


Figure 3.5: Related to the results presented in the previous figure: The error in $\hat{w}$ if $\hat{w}$ is given by (3.3) and the exact (numerical) solution for $\hat{w}$ for $k = 1.5$. The current profile is given by $U(z) = -\exp(\alpha z)$ for various value of $\alpha$. The solid line: $\alpha = 1$, the dashed line: $\alpha = 0.8$, the dotted line: $\alpha = 0.3$, and the (thin) dashed-dotted line is $\hat{w}_{\text{trial}}$. In the lower picture, the exact vertical velocities are plotted.

### 3.4.3 Approximation using the WKB approximate solution

To improve the approximation in such a way that the trial function depends on the curvature of the current, we choose the following trial function which is motivated by the WKB approximative solution of an equation of the form $u_{zz} + n(\sigma z)^2 u = 0$, with a slowly varying inhomogeneous function $n(\sigma z)$ with $\sigma$ small (see the paper of van Groesen [25] and Vainberg [74]). When $n(\sigma z)^2 = -f(z) = -\left(k^2 + \frac{kU''(z)}{kU(z)-\omega}\right)$, in which $\sigma$ is the parameter related to the curvature of the current, this equation is

the Rayleigh equation. For $f(z) \geq 0$ we take

$$\hat{w}_{\text{trial}}(z) = A(z) \sinh \int_{-1}^{z} \sqrt{f(\zeta)} d\zeta, \tag{3.20}$$

and for $f(z) \leq 0$ we take

$$\hat{w}_{\text{trial}}(z) = A(z) \sin \int_{-1}^{z} \sqrt{-f(\zeta)} d\zeta,$$

where

$$A(z) = \frac{\Gamma}{|f(z)|^{1/4}}, \tag{3.21}$$

for an arbitrary $\Gamma$. When the current profile is given by $U(z) = -\exp(5z)$ error of the present model, taking (3.20), is given in Figure 3.6.

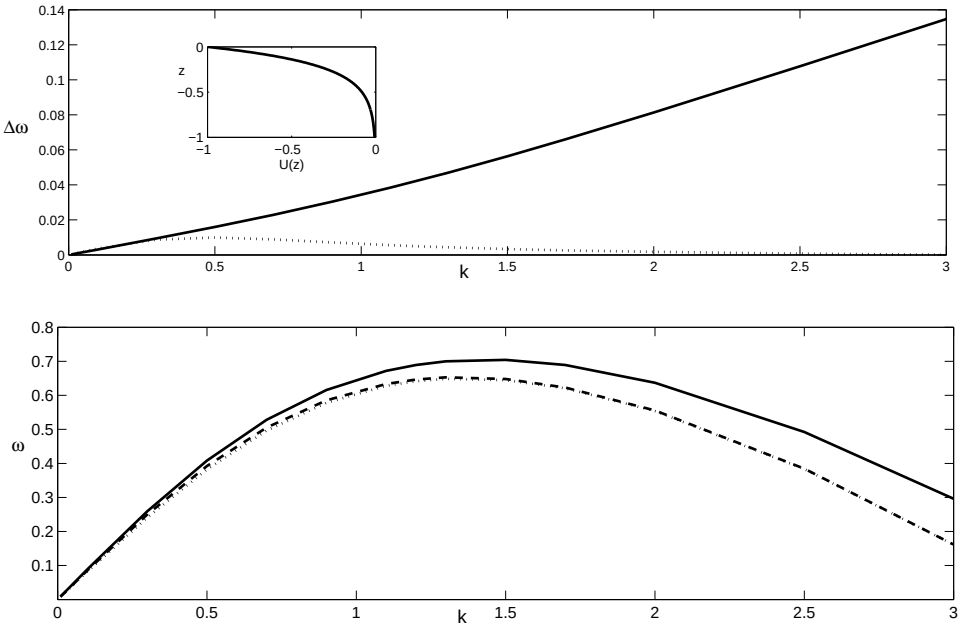


Figure 3.6: Error from approximation, when $U(z) = -\exp(5z)$, using (3.20) as the trial function. The dotted line is the error from the present model, and the solid line is the error from the Kirby and Chen model. The current profile is given in the inset and the resulting dispersion relation is given in the lower picture.

For a comparison, in Figure 3.6 we plot also the error from the Kirby and Chen's model. We observe that for very long waves ($k \to 0$) the present model is slightly worse than the Kirby and Chen's model but the approximation gets better and better

as the wave number increases (i.e. for $k > 0.5$). Also for a comparison, the exact velocity $\hat{w}(z)$ and the trial functions (3.3) and (3.20) are plotted in Figure 3.7, for $k = 1.3$.

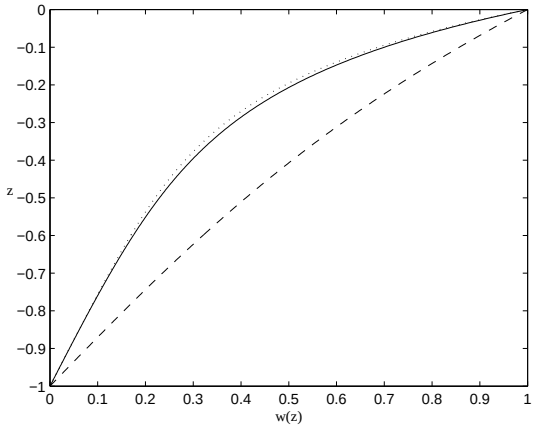


Figure 3.7: The exact solution for $\hat{w}$ (solid line) compared to the trial functions (3.3) (dashed line) and (3.20) (dotted line) for current given by $U(z) = -\exp(5z)$.

For cases when $\frac{kU''(z)}{kU(z)-\omega}$ is small compared to $k^2$ we can take a simpler trial function that is an approximation of (3.20) by taking the first order terms of the Taylor series expansions of $\frac{1}{f(z)^{1/4}}$ and $\sqrt{f(z)}$. This leads to:

$$\hat{w}_{\text{trial}} = A(z)\sinh\left(k(z+1) + \int_{-1}^{z} \frac{1}{2}\frac{kU''(\zeta)}{kU(\zeta)-\omega}d\zeta\right), \tag{3.22}$$

where

$$A(z) = \Gamma\left(\frac{1}{\sqrt{k}} - \frac{1}{4\sqrt{k}}\frac{kU''(z)}{kU(z)-\omega}\right).$$

In case of a current profile given by $U(z) = U_s\cos\left(\frac{\pi}{2}z\right)$, the error from the Kirby and Chen's model [32] is presented in Figure 5b of their paper. For a comparison, in Figure 3.8 we show the error in the phase velocity for $k = 3$, for the same cosine profile. In this figure we plot the error versus $U_s$. We observe that taking (3.22) the present model performs better.

From this observation, we see that a careful selection of the trial function gives a better approximation.

## 3.5 The group velocity

Analytical models are useful for deriving approximations for certain quantities such as the group velocity and the wave blocking criteria. These results can also be

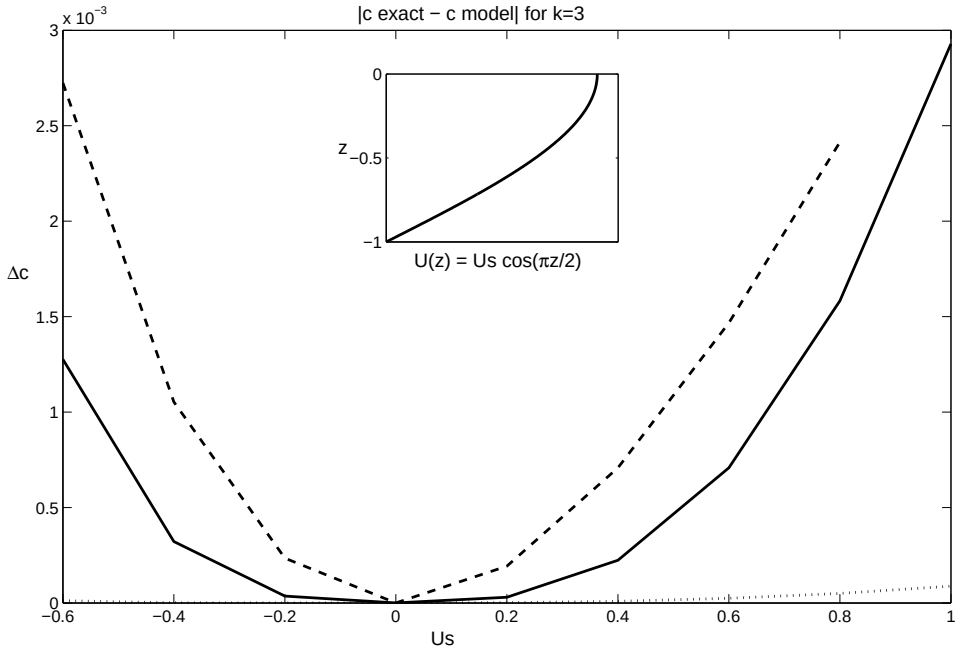


Figure 3.8: Error in the phase velocity $\frac{\omega}{k}$ vs $U_s$. Here $k = 3$ and $U(z) = U_s \cos\left(\frac{\pi}{2} z\right)$. The error resulting from taking (3.22) is presented by the dotted line (very close to the $U_s-$axis); the error resulting from taking (3.3) is given by the dashed line; and the error from the Kirby and Chen's model is given by the solid line.

applied in models for calculating reflected waves in the the presence of depth-varying currents (i.e., modifications of models given by Kyung et al. [34] and Suryanto [64]. Below we will present the approximate group velocity and wave blocking criteria derived from the analytical model presented in this chapter.

Some wave-current interaction models (for example the ones used for coastal waves models) require computation of the group velocity $c_g = \frac{d\omega}{dk}$ for many different current profiles and wave lengths. By using models which give analytical (implicit/explicit) expressions of $\omega(k)$, we can directly calculate the corresponding group velocity for a given $k = k_0$ (by firstly calculating $\omega(k_0)$). This is more efficient than calculating $\frac{d\omega}{dk}$ by using a numerical solver of the exact dispersion relation, by which we have to calculate also the values of $\omega$ at some neighboring points of $k = k_0$.

Observe that the dispersion relation $\omega(k)$ is given implicitly by the present model.

The expression for the group velocity $\frac{d\omega}{dk}$ can be derived as follow:

$$\begin{aligned} 0 &= \frac{d\mathcal{L}\left(k,\omega\left(k\right),\hat{w}_{\text{trial}}\left(\omega\left(k\right),k\right)\right)}{dk} \\ &= \left[\left\langle \delta_{\hat{w}}\mathcal{L},\frac{\partial\hat{w}}{\partial k}\right\rangle + \frac{\partial\mathcal{L}}{\partial k} + \frac{d\omega}{dk}\left\{\left\langle \delta_{\hat{w}}\mathcal{L},\frac{\partial\hat{w}}{\partial\omega}\right\rangle + \frac{\partial\mathcal{L}}{\partial\omega}\right\}\right]_{\hat{w}=\hat{w}_{\text{trial}}} \end{aligned}$$

which gives

$$\frac{d\omega}{dk} = \frac{-\left[\left\langle \delta_{\hat{w}}\mathcal{L},\frac{\partial\hat{w}}{\partial k}\right\rangle + \frac{\partial\mathcal{L}}{\partial k}\right]_{\hat{w}=\hat{w}_{\text{trial}}}}{\left[\left\langle \delta_{\hat{w}}\mathcal{L},\frac{\partial\hat{w}}{\partial\omega}\right\rangle + \frac{\partial\mathcal{L}}{\partial\omega}\right]_{\hat{w}=\hat{w}_{\text{trial}}}}, \tag{3.23}$$

where we define

$$\left\langle \delta_{\hat{w}}\mathcal{L},\varphi\right\rangle = -\frac{1}{2}\int_{-1}^{\eta_0}\left(\hat{w}'' - f\left(z\right)\hat{w}\right)\varphi dz + \frac{\varphi\left(\eta_0\right)}{2}\left[\hat{w}'\left(\eta_0\right) - \beta\hat{w}\left(\eta_0\right)\right],$$

which is equal to zero only if $\hat{w}$ is the exact solution of the boundary value problem. Relation (3.23) gives a direct approximation to the group velocity $c_g = \frac{d\omega}{dk}$. Havelock [26] and Lighthill [35] show that $c_g$ is also the velocity of the propagation of the energy. The condition in which $c_g = 0$ is a special condition that states that the wave energy cannot propagate further. This may happen when waves propagate against an adverse current. From (3.23), we can approximate the criteria for wave blocking, which is the relation between $\omega, k$, and $U\left(z\right)$ for which $\frac{d\omega}{dk} = 0$. In this approximation, the wave-blocking criteria is given by

$$\left\langle \delta_{\hat{w}}\mathcal{L},\frac{\partial\hat{w}}{\partial k}\right\rangle_{\hat{w}=\hat{w}_{\text{trial}}} = -\left.\frac{\partial\mathcal{L}}{\partial k}\right|_{\hat{w}=\hat{w}_{\text{trial}}}. \tag{3.24}$$

The integration in (3.24) can be carried out numerically. From (3.24) we can approximate the pair $(\omega, k)$ that results to the stopping of the propagation of the energy, when the current $U\left(z\right)$ is given.

## 3.6 Concluding remarks

We have developed a method to derive an analytical expression that approximates the dispersion relation, without the need to solve the Rayleigh equation. Two models are derived through complementary variational formulations of the governing boundary value problem. These approximate analytical expressions are given in integral form. When the primitives of the integrands cannot be found analytically, the approximate dispersion relations are obtained by calculating the integrals numerically.

Approximate dispersion relations for waves propagating on arbitrary current have been formulated. The performance of both approximations depend on the trial functions that are chosen. For short waves or for weakly nonlinear current, taking the asymptotic solution for large $k$ (3.3) and the corresponding conjugate solution (3.8) as trial functions, gives good approximations. As the final approximation we can take the average value of the two approximations.

The WKB solution of the Rayleigh equation gives a good approximate dispersion relation for waves on nonlinear large currents.

A preliminary investigation on the properties of $f(z)$ for the chosen class of current profile is necessary before deciding which trial function to take. From numerical experiment using different current profiles (avoiding cases that critical points, $z^*$ at which $kU(z^*)-\omega=0$, exist) we observe that when the current profile is almost linear,

$$\max_{z\in[-1,\eta_0]} U^{''}(z) < 1, \tag{3.25}$$

taking (3.3) gives good a approximation. But when the current profile is not linear

$$\max_{z\in[-1,\eta_0]} U^{''}(z) \gg 0, \tag{3.26}$$

we have to improve the trial function. The improvement depends on whether we consider long waves or short waves ($k \ll 1$ or $k \gg 0$); the sign of $U(z)$; and the sign of $U^{''}(z)$. In general when $f(z)$ is sign-definite and when critical points do not exist, trial functions (3.20) or (3.22) give good approximations for short waves ($k \gg 0$).

The observation that the approximation is good throughout the wave-number space, and is better for high wave-numbers, is important for estimation of the current profile from measurements by remote-sensing, where the dispersion relationship can be estimated from radar measurements in time and space. High wave-numbers can be used to estimate the near surface velocity and low wave-numbers to estimate the current profile at greater depth.

The approximate dispersion relation presented here will be used to characterize the equilibrium of the parameter dynamics in the model to follow.

# Chapter 4

# A Low-Dimensional Model for the Spatial Adaptation of Waves Encountering a Current

We propose and validate a low dimensional model that describes the adaptation process when a surface water wave meets a current. Changes in wave length, wave amplitude, mean surface elevation, and change in a parametric representation of the current profile are described in a quasi-homogeneous way. This quasi-homogeneous approximation is based on satisfying the basic conservation laws and the kinematic free-surface boundary condition. Wave and current simultaneously adapt in order to reach an equilibrium condition characterized by the wave-current dispersion relation derived from the solution of the Rayleigh equation. We describe the model and give theoretical error estimates.

## 4.1 Introduction

This work deals with wave-current interaction with particular emphasis on situations as they appear in hydrodynamic laboratories. There waves are generated by wave flaps, and currents are injected from one side of the basin. The water is re-circulated with a given constant discharge that maintains a specific horizontal mass-transport in the basin. The injected currents meet the waves at the free surface at a certain position where the adaptation of the interacting waves and current sets in. The model presented here is practical for the laboratory purpose, i.e. to generate wave and current environments requested for testing models of ships or other structures. The difficulty of getting a requested wave and current environment is due to the interaction between wave and current. In the presence of a current, the wave maker motion will produce waves that are different from the waves produced (by the same wavemaker motion) in the absence of currents. Kemp and Simons [29] [30], Klopman [33], and Swan et al. [67] conducted experiments that show that the interaction also changes the current profile, especially in the region near the free surface.

A number of models for fully-established wave-current interaction (i.e. when wave and current properties do not change in space and time) have been given in a number of review articles, e.g. Jonsson [28], Peregrine [50], Thomas and Klopman [70]. For uniform current, Baddour and Song [3] and Longuet-Higgins and Stewart [36] present models that predict the steady-state of the interaction, using given initial situations describing pure waves and pure current. In these models, the spatial/temporal dynamics describing the adaptation of wave and current is not described.

For uniform currents, a number of models assuming slowly-varying wave parameters are found in the literature, such as the models given by Boussinesq-type equations, e.g., Chen et al. [11]. Other models in this class are given by Longuet-Higgins and Stewart [37] and Peregrine [50], which describe the slow deformation of waves when propagating on given, slowly-varying uniform currents. Models assuming slowly-varying wave parameters are relevant for describing phenomena in the ocean/sea, where wave and current interaction takes place in an long open domain. This is not the case for a laboratory basin, which has limited length. In a laboratory basin as in MARIN (the Maritime Research Institute Netherlands) wave-current environment is made by entering waves into a current region, and it is observed that the most visible deformation of the surface waves takes place in a short interaction region.

Swan et al. [67] present a model to calculate the deformation of a regular wave propagating on a depth-dependent current. In that model, the change of the current profile must be known a-priory. Using results from laboratory experiments, Swan et al. demonstrate the validity of the prediction of the model, i.e. the wave amplitude and the wave length. However, as remarked in that paper, in practice the change of the current profile is not known a priori. Therefore, for practical application Swan et al. suggest to couple their model with, for example, the model presented by Groeneweg and Klopman [23].

For depth-dependent current, good models for predicting and explaining deformation of the current profile for the equilibrium condition (i.e., the homogeneous problem) have been given by Groeneweg and Klopman [23] for 1D flow and by Groeneweg and Battjes [24] for 2D flow. However, these models do not deal with the inverse problem that we investigate because the related current-free wave is not accommodated in these models. The reason why we are interested to know the related current-free wave is because when current is absent, reliable wavemaker theories are available, e.g. in Dean and Dalrymple [14], Schäffer [54], Schäffer and Klopman [55], Schäffer and Steenberg [56]. Thus, in the absence of currents it is relatively easy to get a desired wave in the basin. By generating a specific current-free wave, interaction with the current changes both the wave and the current into the desired wave-current combination.

For the problem addressed in this dissertation we need a model that can predict both changes in the waves and current. We approach the problem by seeing the interaction as a spatial adaptation process of wave and current. It starts with a linear wave above a current free layer, that meets at a certain position a current

underneath. Before and after entering the current zone, the wavelength is determined by two different dispersion relations, thus the wavelength can change significantly. A set of measurements at MARIN indicates that before and after the adaptation region, the wave length is significantly different; a quantitative analysis of these measurements is reported by Margaretha [39] and Voluer [75] and is summarized in Chapter 6 of the dissertation. Before the adaptation region, the measured wave length is close to the one calculated from the wave-only dispersion relation, and after that region it agrees with the theoretical wave-current dispersion relation. The change in the wave length clearly corresponds to observed spatial variations in wave amplitude.

These observations motivate us to make a model which allows a continuous change in the wave and current properties. In this chapter we propose a low dimensional model that describes the adaptation process of a surface water wave abruptly meeting a (depth dependent) current. Wave and current simultaneously adapt and reach an equilibrium condition characterized by the dispersion relation of the homogeneous problem. We use the linear theory to describe the waves, so that the equilibrium condition is determined by the Rayleigh equation. In the model to follow, we allow the fluid properties parameterized by four parameters to change quasi-homogeneously in the $x-$ direction. The actual change is determined by requiring that the continuity equation and the kinematic free-surface boundary condition are satisfied pointwise; furthermore it is required that the mass, momentum, and energy density fluxes are conserved. This can be stated differently: we derive the model by considering the full Euler equations, and instead of requiring them to hold pointwise we project these equations in a number of specific directions. The directions are chosen such that changes in relevant physical quantities mentioned above, are modeled in a valid way.

Somewhat related to the problem that we address, is the method of Green and Naghdi [22], [21]. In Section 4.4.3 of this chapter we briefly describe the GN method and also compare the characteristics of the present model and the GN method. We show the characteristics of the GN method and the problem that is encountered when the wavenumber varies. Briefly speaking, if the range of the wavenumber is not small, the GN method will result in a large set of nonlinear equations that has to be solved.

In this chapter, we describe details of the model and give an analysis of its accuracy. In the next chapter, we study special cases of current profiles and compare the results with laboratory experiments found in the literature. These comparisons show that the model predicts both qualitatively and quantitatively the result of the interaction process.

To simplify the notation when dealing with approximate solutions, and to keep track of the order of errors, we introduce the notation of the residues as follows:

$$\mathcal{R}^{\mathrm{kbc}} \equiv (\partial_t \eta + u\eta_x - w)|_{z=\eta}\,, \tag{4.1}$$

$$\mathcal{R}^{\mathrm{dbc}} \equiv p|_{z=\eta}\,, \tag{4.2}$$

$$\mathcal{R}^{\mathrm{E}_1} \equiv (\partial_t u + u\partial_x u + w\partial_z u + \partial_x p)\,, \qquad -1 \le z \le \eta \tag{4.3}$$

$$\mathcal{R}^{\mathrm{E}_2} \equiv (\partial_t w + u\partial_x w + w\partial_z w + \partial_z p + 1)\,, \qquad -1 \le z \le \eta \tag{4.4}$$

$$\mathcal{R}^{\mathrm{CE}} \equiv (\partial_x u + \partial_z w)\,, \qquad -1 \le z \le \eta \tag{4.5}$$

$$\mathcal{R}^{\mathrm{bottom}} \equiv w|_{z=-1}\,. \tag{4.6}$$

When the residues are zero, the right-hand sides of (4.1)-(4.6) are the governing equations (2.1)-(2.6).

## 4.2 Linear solutions of the homogeneous problem for weakly nonlinear currents

In Chapter 2, the general solution is defined, and we show the exact solution for the case when the current profile is linear. It is known that for water of finite depth, exact analytical solutions of the Rayleigh equation can be found for only a few types of current, including linear and piecewise linear currents (see [17]). If the current profile is not linear, $U''(z) \neq 0$, then in general analytical exact solutions of the Rayleigh equation cannot be found. Any approximate solution will introduce errors in the Rayleigh equation and the dispersion relation. Now the question is, how big are the residues (4.1)-(4.6) if the Rayleigh equation is not satisfied exactly?

Denote the approximate solution by $\hat{w}_{\mathrm{a}}$, and introduce the residue of the Rayleigh equation (2.22) and the residue of the dispersion relation (2.25):

$$\mathcal{R}^{\mathrm{Rayleigh}} = \frac{d^2\hat{w}}{dz^2} - f(z)\,\hat{w}, \tag{4.7}$$

$$\mathcal{R}^{\mathrm{DR}} = \left.\frac{\hat{w}'}{\hat{w}}\right|_{z=\eta_0} - \beta. \tag{4.8}$$

We require that the values of $\hat{w}_{\mathrm{a}}$ at the free surface and the bottom satisfy (2.23) and (2.27). Take $\hat{u}$ and $\hat{p}$ related to $\hat{w} = \hat{w}_{\mathrm{a}}$ by (2.28) and (2.29). After substituting (2.17)-(2.20) into (4.1 )-(4.6 ), we find for the residues:

$$\mathcal{R}^{\mathrm{E}_2} \overset{(2.28),(2.29)}{=} \frac{(\omega - kU)}{k^2}\mathcal{R}^{\mathrm{Rayleigh}}\cos(\theta) + \mathcal{O}\left(\epsilon^2\right) \tag{4.9}$$

$$\mathcal{R}^{\mathrm{dbc}} \overset{(2.29),(2.27)}{=} \hat{w}k^2(\omega - kU)\,\mathcal{R}^{\mathrm{DR}}\cos\theta + \mathcal{O}\left(\epsilon^2\right), \tag{4.10}$$

while $\mathcal{R}^{\mathrm{kbc}}$ and $\mathcal{R}^{\mathrm{E}_1}$ are $\mathcal{O}\left(\epsilon^2\right)$; $\mathcal{R}^{\mathrm{CE}}$ and $\mathcal{R}^{\mathrm{bottom}}$ are zero.

From these we see that the full equations (2.1)-(2.6) are still satisfied to $\mathcal{O}\left(\epsilon^2\right)$ if

$$\mathcal{R}^{\mathrm{Rayleigh}} = \mathcal{O}\left(\epsilon^2\right) \tag{4.11}$$

and

$$\mathcal{R}^{\mathrm{DR}} = \mathcal{O}(\epsilon)\,. \tag{4.12}$$

First we show how (4.12) can be satisfied if we have an approximate solution that satisfies (4.11). To that end, let $\omega$, $U(z)$, and $\eta_0$ be given. Notice that if the Rayleigh equation is approximated, then relation (2.25) does not give the correct wavenumber $k$ anymore. Therefore we need a good approximation for the wavenumber $k$. In the literature there are several models to approximate the wavenumber $k$ (or, equivalently, the wave velocity $\frac{\omega}{k}$). In the next chapter we will use the approximate dispersion relation given in Chapter 3. Below we will show that if the dispersion relation is approximated in this way, then (4.12) is a direct implication of (4.11).

The relation that approximates the dispersion relation given in Chapter 3 is rewritten like:

$$\frac{1}{2}\int_{-1}^{\eta_0}\left[\left(\hat{w}_{\mathrm{a}}'\right)^2 + f(z)\,\hat{w}_{\mathrm{a}}{}^2\right]dz - \frac{1}{2}\beta\hat{w}_{\mathrm{a}}(\eta_0)^2 = 0. \tag{4.13}$$

Here $\hat{w}_{\mathrm{a}}$ is the approximate solution of the Rayleigh equation that satisfies the boundary conditions (2.27) and (2.23), $\beta$ is given by (2.26), and $f(z)$ is given by (2.24).

**Remark 4.2.0.1** *If $\hat{w}_a$ in (4.13) is the exact solution of the boundary value problem (so $\mathcal{R}^{Rayleigh} = 0$), then (4.13) leads to a relation that is equivalent to the exact dispersion relation.*

Notice that we may write (4.13) like

$$\frac{-\int_{-1}^{\eta_0}\hat{w}_{\mathrm{a}}\left[\hat{w}_{\mathrm{a}}'' - f(z)\,\hat{w}_{\mathrm{a}}\right]dz}{\hat{w}_{\mathrm{a}}(\eta_0)^2} + \left(\frac{\hat{w}_{\mathrm{a}}'(\eta_0)}{\hat{w}_{\mathrm{a}}(\eta_0)} - \beta\right) = 0,$$

which gives

$$\mathcal{R}^{\mathrm{DR}} = \frac{\int_{-1}^{\eta_0}\hat{w}_{\mathrm{a}}\mathcal{R}^{\mathrm{Rayleigh}}dz}{\hat{w}_{\mathrm{a}}(\eta_0)^2}. \tag{4.14}$$

The approximation $\hat{w}_{\mathrm{a}}$ satisfies the boundary conditions (2.27) and (2.23), and since $a = \mathcal{O}(\epsilon)$ it follows that $\hat{w}_{\mathrm{a}} = \mathcal{O}(\epsilon)$. Consequently, it follows from (4.14) that $\mathcal{R}^{\mathrm{DR}} = \mathcal{O}(\epsilon)$ if $\mathcal{R}^{\mathrm{Rayleigh}} = \mathcal{O}\left(\epsilon^2\right)$.

Now consider the case where $U''(z) \neq 0$ and $\hat{w}_{\mathrm{a}}$ is given by the solution (2.30) for linear current. Substituting this to the Rayleigh equation gives

$$\mathcal{R}^{\mathrm{Rayleigh}} = aU''\frac{k(\omega - kU(\eta_0))}{\sinh(k(1+\eta_0))}\frac{\sinh(k(z+1))}{(\omega - kU(z))}.$$

Therefore if $(\omega - kU(z))$ is never zero and $U''(z) = \mathcal{O}(\epsilon)$ then it immediately follows that

$$\mathcal{R}^{\mathrm{Rayleigh}} = \mathcal{O}\left(\epsilon^2\right),$$

and hence that for $U''(z) = \mathcal{O}(\epsilon)$ the approximation (2.17)-(2.20) with the solution for the linear current (2.30) satisfies the full equations (2.1 )-(2.6) up to $\mathcal{O}\left(\epsilon^2\right)$.

Now we show that for currents having larger curvature,

$$U''(z) = \mathcal{O}\left(\epsilon^{\frac{1}{2}}\right), \tag{4.15}$$

we still satisfy (4.11) if we use a WKB approximate solution (see [25], [74]). For (2.22) and (2.23), this approximation is given by (3.20) where the amplitude $\Gamma$ is taken to satisfy the boundary condition (2.27):

$$\Gamma = Ia\left(k\,U|_{z=\eta_0} - \omega\right)\frac{f\left(\eta_0\right)^{1/4}}{\sinh\int_{-1}^{\eta_0}\sqrt{f\left(\zeta\right)}d\zeta}.$$

Subtituting $\hat{w} = \hat{w}_{\mathrm{WKB}}$ into the Rayleigh equation (2.22) gives

$$\mathcal{R}^{\mathrm{Rayleigh}} = \frac{\hat{w}_{\mathrm{WKB}}}{16f\left(z\right)^2}\left(5\left(\frac{df}{dz}\right)^2 - 4f\left(z\right)\frac{d^2f}{dz^2}\right). \tag{4.16}$$

With $f\left(z\right)$ given by (2.24), $(\omega - kU\left(z\right))$ nonvanishing, and $U$ that is slowly varying in the sense that

$$U = U\left(\sqrt{\sigma}z\right), \tag{4.17}$$

for some small parameter $\sigma$, it follows that $\mathcal{R}^{\mathrm{Rayleigh}} = \mathcal{O}\left(\epsilon\sigma^2\right)$. Hence for $\sigma = \epsilon^{\frac{1}{2}}$ it follows that $\mathcal{R}^{\mathrm{Rayleigh}} = \mathcal{O}\left(\epsilon^2\right)$. So, also in this case all residues of the governing equations (4.1)-(4.6) are $\mathcal{O}\left(\epsilon^2\right)$ and therefore are not larger than the error from linearization.

## 4.3 The quasi-homogeneous approximation

### 4.3.1 Description of the model

In this Section we introduce the low dimensional model that describes the adaptation process when a surface water wave meets a current. The model predicts changes of both wave and current and gives the dynamics of those changes. Wave and current simultaneously adapt in order to reach an equilibrium condition giving a linear solution of the homogeneous problem.

We use four parameters to describe the spatial variation of the wave-current environment: the wave amplitude $a$, the wave number $k$, the mean-free surface elevation $\eta_0$, and one parameter $P_c$. to describe the deformation of the current profile. Write

$$\begin{aligned}\eta &= \eta\left(\mathbf{P};x,t\right), \quad u = u\left(\mathbf{P};x,z,t\right),\\ w &= w\left(\mathbf{P};x,z,t\right), \quad p = p\left(\mathbf{P};x,z,t\right),\end{aligned}$$

where $\mathbf{P} = (a,k,\eta_0,P_c)$. In the quasi-homogeneous approximation (QHA), $\mathbf{P}$ varies in the $x-$direction.

In this QHA we generalize (2.17)-(2.20) and add a term $\bar{p}_2$ given in the form of the second-order mean pressure of the homogeneous problem (4.24). In detail, we take $\eta$,

$u$, $w$, and $p$ given by

$$\eta = \eta_0(x) + a(x)\cos\theta(x,t), \tag{4.18}$$

$$u = U(\mathbf{P}(x);z) + \hat{u}(\mathbf{P}(x);z)\cos\theta(x,t), \tag{4.19}$$

$$w = \hat{w}(\mathbf{P}(x);z)\sin\theta(x,t) - \frac{d\mathbf{P}}{dx}\cdot\left(\int_{-1}^{z}\left(\frac{\partial\hat{u}}{\partial\mathbf{P}}\cos\theta(x,t) + \frac{\partial U}{\partial\mathbf{P}}\right)dz\right), \tag{4.20}$$

$$p = -z + \eta_0(x) + \hat{p}(\mathbf{P}(x);z)\cos\theta(x,t) + \bar{p}_2(\mathbf{P}(x);z). \tag{4.21}$$

Here the wave phase $\theta$ is related to the wave number $k$ and the wave frequency $\omega$ by:

$$\partial_x\theta = k,\ \partial_t\theta = -\omega. \tag{4.22}$$

In the approximation (4.19)-(4.21) $\hat{w}$ is the solution (or approximate solution) of (2.22), (2.23), (2.27). It determines $\hat{u}$ and $\hat{p}$ by (2.28) and (2.29).

**Remark 4.3.1.1** *In the next chapter, we use the solution for a linear current (2.30) to construct the Ansatz for the quasi-homogeneous approximation if the current is uniform or if the curvature of the initial (wave-free) current is small or zero. In case the curvature of the initial current is moderate, we improve the model by using the WKB approximated solution (3.20).*

**Remark 4.3.1.2** *The second-order mean pressure $\bar{p}_2$ contributes to the second-order term of the momentum density flux $\langle\mathcal{M}\rangle$ and the energy density flux $\langle\mathcal{F}\rangle$ . For the homogeneous problem, after substituting (2.18)-(2.19) and (2.28) into (2.4) and time-averaging the result we get the total mean pressure:*

$$\langle p\rangle = -\frac{1}{2}\hat{w}^2 - z + \eta_0 + h.o.t. \tag{4.23}$$

*Here the term $-z+\eta_0$ gives the zeroth-order mean pressure, and the second-order mean pressure of the homogeneous problem is given by*

$$\overline{p}_2 = -\frac{1}{2}\hat{w}^2. \tag{4.24}$$

*For uniform current, $U \equiv$constant, (4.24) is equivalent with the second-order mean pressure derived by Whitham [78].*

For the current profile during interaction we take

$$U(\mathbf{P}(x);z) = U_c(z) + U_{\text{change}}(\mathbf{P}(x);z), \tag{4.25}$$

where $U_c(z)$ is the profile of the initial current (when waves are absent) and $U_{\text{change}}$ gives the deformation due to the presence of waves. Besides depending on $P_c$, $U_{\text{change}}$ may also depend on the wave parameters $a$, $k$, and $\eta_0$ like

$$U_{\text{change}}(\mathbf{P};z) = U_1(P_c;z) + U_2(a,k,\eta_0;z).$$

Here $U_2(a, k, \eta_0; z)$ is the part of $U_{\text{change}}$ that depends on the wave parameters. In this model, $U_2(a, k, \eta_0; z)$ is restricted to $\mathcal{O}(\epsilon^2)$.

The vertical velocity (4.20) has been taken to guarantee that the continuity equation and the bottom boundary condition are satisfied exactly, $\mathcal{R}^{\text{CE}} = 0$ and $\mathcal{R}^{\text{bottom}} = 0$. In order to consistently work with perturbations of $\mathcal{O}(\epsilon)$, the vertical velocity $w$ may not be larger than $\mathcal{O}(\epsilon)$. Therefore we have the following requirement for $a'(x)$:

$$\text{at each } x \geq 0,\ a'(x) \text{ must not be larger than } \mathcal{O}(\epsilon). \tag{4.26}$$

The model for the adaptation process of wave and current is now defined by the equations for the parameter dynamics. We will show that the following requirements lead to a model that is physically motivated and furthermore sufficiently accurate:

$$\mathcal{R}^{\text{kbc}} = \mathcal{O}(\epsilon^2), \tag{4.27}$$
$$\langle \mathcal{I} \rangle = \mathcal{I}_0, \tag{4.28}$$
$$\langle \mathcal{M} \rangle = \mathcal{M}_0, \tag{4.29}$$
$$\langle \mathcal{F} \rangle = \mathcal{F}^{\infty}, \tag{4.30}$$

Here, the angle brackets denote time-averaging over a wave period,

$$\langle \varphi \rangle = \frac{1}{T} \int_0^T \varphi \, dt$$

with $T = 2\pi/\omega$.

Conditions (4.28)-(4.30) mean that these three fluxes are conserved during the evolution in the adaptation interval. The constants $\mathcal{I}_0$, $\mathcal{M}_0$, and $\mathcal{F}^{\infty}$ will be chosen appropriately in the following discussion (see (4.49), (4.50) and (4.52)). The dynamics require that wave and current simultaneously adapt and reach an equilibrium condition characterized by the dispersion relation of the homogeneous problem. Therefore the parameters converge to constant values (which are not a priori given) as the distance $x$ increases, i.e.

$$\lim_{x \to \infty} \mathbf{P}(x) = \mathbf{P}^{\infty} = (a^{\infty}, k^{\infty}, \eta_0^{\infty}, P_c^{\infty}) \equiv \text{ constant}. \tag{4.31}$$

In the model, the equilibrium values $k^{\infty}$, $\eta_0^{\infty}$, $P_c^{\infty}$ and $\omega$ are related by the (approximate) dispersion relation of the homogeneous problem (3.9).

### 4.3.2 The parameter dynamics

We will now investigate how the requirements (4.27)-(4.30) for the model lead to specific conditions for the parameters collected in $\mathbf{P}$, namely three algebraic relations (of which two are nonlinear) and one ODE.

#### 4.3.2.1 Conservation of mass and momentum-density fluxes

After substituting (4.18) and (4.19) into (4.28), we get

$$\int_{-1}^{\eta_0} U dz + \frac{1}{2}\left(\frac{a^2}{2}\left(\partial_z U\right)_{z=\eta_0} + a\ \hat{u}|_{z=\eta_0}\right) + \text{h.o.t} = \mathcal{I}_0. \tag{4.32}$$

And after substituting (4.25) for $U$ and a solution for $\hat{u}$ into (4.32), we get the first relation for the parameters $a$, $k$, $\eta_0$, $P_c$. Since no differentiation with respect to $x$ is included, the resulting relation is algebraic.

In the same way, after substituting (4.18), (4.19), and (4.21) into (4.29) we get

$$\int_{-1}^{\eta_0}\left(U^2 + \frac{1}{2}\hat{u}^2 - z + \eta_0 + \bar{p}_2\right) dz + \\ \frac{1}{2}a\left(2U\hat{u} + \hat{p}\right)_{z=\eta_0} + \frac{a^2}{2}\left(U\partial_z U\right)_{z=\eta} - \frac{a^2}{4} + \text{h.o.t} = \mathcal{M}_0. \tag{4.33}$$

For the quasi-homogeneous evolution, this leads to the second relation for the parameters, again a nonlinear algebraic relation.

**Remark 4.3.2.1** *Notice that the $x-$derivatives of the left hand sides of (4.32) and (4.33) must be identical to zero. From this, it can be shown that*

$$\frac{dP_c}{dx} = \frac{da}{dx}\cdot\mathcal{O}\left(\epsilon\right), \qquad \frac{d\eta_0}{dx} = \frac{da}{dx}\cdot\mathcal{O}\left(\epsilon\right). \tag{4.34}$$

*This means that $P_c'\left(x\right)$ and $\eta_0'\left(x\right)$ are of the same order, and each is of one order of magnitude larger than $a'\left(x\right)$.*

#### 4.3.2.2 The kinematic boundary condition: conservation of 'wave volume'

First, we write $\hat{w}$ as

$$\hat{w} = a\left(\omega - k\ U|_{z=\eta_0}\right)\hat{w}_{\text{norm}}, \tag{4.35}$$

where $\hat{w}_{\text{norm}}$ is a normalized solution of the Rayleigh equation (2.22), that does not depend on $a$ and $\eta_0$:

$$\hat{w}_{\text{norm}} = 1 \quad \text{at} \quad z = \eta_0, \qquad \hat{w}_{\text{norm}} = 0 \quad \text{at} \quad z = -1. \tag{4.36}$$

After substituting (4.18)-(4.20), (4.34) into (4.1), assuming (4.26), we get

$$\mathcal{R}^{\text{kbc}} = \left\{a\left(\omega - k\ U|_{z=\eta_0}\right) - \hat{w}|_{z=\eta_0}\right\}\sin\theta + \\ \left\{a'\ U|_{z=\eta_0} + a'\int_{-1}^{\eta_0}\frac{\partial\hat{u}}{\partial a}dz + k'\int_{-1}^{\eta_0}\frac{\partial\hat{u}}{\partial k}dz\right\}\cos\theta + \mathcal{O}\left(\epsilon^2\right). \tag{4.37}$$

The coefficient of $\sin\theta$ in the formula above vanishes as a consequence of (2.27). Condition (4.27) leads to the condition

$$a'\,U|_{z=\eta_0} + a'\int_{-1}^{\eta_0}\frac{\partial\hat{u}}{\partial a}dz + k'\int_{-1}^{\eta_0}\frac{\partial\hat{u}}{\partial k}dz = 0. \tag{4.38}$$

An expression for $\int_{-1}^{\eta_0}\frac{\partial\hat{u}}{\partial a}dz$ can be derived from (2.28) and (4.35)-(4.36):

$$\begin{aligned}\int_{-1}^{\eta_0}\frac{\partial\hat{u}}{\partial a}dz &= \frac{I}{k}\int_{-1}^{\eta_0}\frac{\partial}{\partial a}\frac{d\hat{w}}{dz}dz \\ &= \left(\omega - k\,U|_{z=\eta_0}\right)\frac{1}{k}\left[\hat{w}_{\text{norm}}|_{z=\eta_0} - \hat{w}_{\text{norm}}|_{z=-1}\right] \\ &= \frac{\omega}{k} - U|_{z=\eta_0}\,. \end{aligned}\tag{4.39}$$

So (4.38) can be simplified as follows

$$a'\frac{\omega}{k} + k'\int_{-1}^{\eta_0}\frac{\partial\hat{u}}{\partial k}dz = 0 \overset{(2.28),(4.35)}{\Leftrightarrow}$$

$$a'\frac{\omega}{k} + k'\frac{\partial}{\partial k}\frac{a\left(\omega - kU\left(\eta_0\right)\right)}{k}\left\{\hat{w}_{\text{norm}}|_{z=\eta_0} - \hat{w}_{\text{norm}}|_{z=-1}\right\} = 0 \overset{(4.36)}{\Leftrightarrow}$$

$$a'k - k'a = 0 \Leftrightarrow \tag{4.40}$$

$$\frac{a}{k} = \alpha \equiv \text{constant}. \tag{4.41}$$

The third algebraic relation for the QHA model is given by (4.41). This relation can also be written like $a\lambda \equiv$constant, with $\lambda$ the wave length. Since $a\lambda$ has an interpretation as 'wave volume', this result means that the wave volume is conserved in the $x-$direction.

**Remark 4.3.2.2** *Relation (4.40) implies that*

$$\frac{da}{dx} = \frac{dk}{dx}\cdot\mathcal{O}\left(\epsilon\right). \tag{4.42}$$

*This means that $\frac{dk}{dx}$ is one order of magnitude smaller than $\frac{da}{dx}$. This already shows that the change of the wave number (wave length) will be relatively large compare to the change of the wave amplitude, in agreement with experimental observations (see the next chapter).*

#### 4.3.2.3 Conservation of energy-density flux

The fourth equation for the parameter dynamics results into an ODE for $k\left(x\right)$ and is obtained by substituting (4.18)-(4.21) into (4.30). Derivatives of the parameters $\frac{d\mathbf{P}}{dx}$ appears only in the approximation for $w$. In the expression for the energy flux (2.9) $w$ appears quadratically; and after time-averaging, only terms containing multiplication of a pair of parameter derivatives and terms without any derivative remain. The

order of each term can be analyzed using (4.34) and (4.42). After replacing $\frac{da}{dx}$ with $\frac{dk}{dx}$ using (4.40), and neglecting higher order terms, the resulting ODE can be written like

$$\mathcal{F}_0\left(a,k,\eta_0,P_c\right)+\mathcal{F}_2\left(a,k,\eta_0,P_c\right)\left(\frac{dk}{dx}\right)^2+\text{h.o.t}=\mathcal{F}^{\infty}\equiv\text{constant}. \tag{4.43}$$

where

$$\mathcal{F}_0=\int_{-1}^{\eta_0}\left(\frac{U^3}{2}+U\left(\overline{p}_2+\eta_0\right)+\frac{U}{4}\left(3\hat{u}^2+\hat{w}^2\right)+\frac{\hat{u}\hat{p}}{2}\right)dz+$$
$$\frac{3}{4}U^2\left(a\;\hat{u}|_{z=\eta_0}+\frac{a^2}{2}\left.\frac{\partial U}{\partial z}\right|_{z=\eta_0}\right)+\frac{a}{2}\left(U\hat{p}\right)_{z=\eta_0}, \tag{4.44}$$

$$\mathcal{F}_2=\int_{-1}^{\eta_0}\frac{U}{4}\left(\frac{a}{k}\int_{-1}^{z}\frac{\partial\hat{u}}{\partial a}dz+\int_{-1}^{z}\frac{\partial\hat{u}}{\partial k}dz\right)^2dz. \tag{4.45}$$

From (4.43), $\frac{dk}{dx}$ can be calculated directly:

$$\frac{dk}{dx}=\pm\sqrt{\frac{\mathcal{F}^{\infty}-\mathcal{F}_0\left(a,k,P_c,\eta_0\right)}{\mathcal{F}_2\left(a,k,P_c,\eta_0\right)}}. \tag{4.46}$$

When the wave propagates in the same direction as the current, the wave length increases (i.e. $\frac{dk}{dx}>0$): for this case we choose the negative sign for (4.46). On the other hand, when the wave opposes the current, the wavelength decreases(i.e. $\frac{dk}{dx}<0$), and the positive sign is chosen.

If from the three algebraic relation above we assume that the parameters $a$, $\eta_0$, and $P_c$ are all expressed in terms of $k$, the relation (4.46) can be integrated to give

$$x=\pm\int_{k_0}^{k(x)}\sqrt{\frac{\mathcal{F}_2\left(a\left(k\right),k,P_c\left(k\right),\eta_0\left(k\right)\right)}{\mathcal{F}^{\infty}-\mathcal{F}_0\left(a\left(k\right),k,P_c\left(k\right),\eta_0\left(k\right)\right)}}dk, \tag{4.47}$$

with sign as stated above. This will produce the adaptation length $L$ by choosing a certain value that is sufficiently close to the asymptotic value $k^{\infty}$ as the end of the integration interval.

### 4.3.3 The initial condition and the steady state of the parameters

The spatial dynamics of the parameters is determined by (4.43), and the three algebraic equations (4.32), (4.33) and (4.41).

To describe the evolution we first have to specify the initial situation: the wave and current properties at the start of the interaction. In this model we take the amplitude and wave number of the current-free wave, $a_0$ and $k_0$, as conditions for $a$ and $k$ at $x=0$. The wave number $k_0$ is related to the wave frequency $\omega$ by the 'current-free' dispersion relation:

$$\omega^2=k_0\tanh k_0. \tag{4.48}$$

The value of the mean free surface elevation at $x = 0$ is taken to be zero, $\eta_0(0) = 0$. Taking $\mathcal{I}_0$ given by

$$\mathcal{I}_0 = \int_{-1}^{0} U_c(z)\, dz, \tag{4.49}$$

the remaining condition for $P_c$ at $x = 0$ is calculated from the conservation of mass (4.32).

The constants $\mathcal{M}_0$ in (4.33) and $\alpha$ in (4.41) are calculated from the conditions for the parameters at $x = 0$:

$$\mathcal{M}_0 = \overline{\mathcal{M}}(a_0, k_0, 0, P_c(0)), \tag{4.50}$$

$$\alpha = \frac{a_0}{k_0}. \tag{4.51}$$

Having specified these values at the start of the interaction, let

$$\mathbf{P}^\infty = (a^\infty, k^\infty, \eta_0^\infty, P_c^\infty)$$

denote the equilibrium values of the parameters at the end of the interaction, (see (4.31)), satisfying the (approximate) dispersion relation of the homogeneous problem (3.9). In other words, the equilibrium values give a solution of the linear homogeneous problem. The values of $\mathbf{P}^\infty = (a^\infty, k^\infty, \eta_0^\infty, P_c^\infty)$ are calculated by solving four algebraic equations (of which three are nonlinear): (4.32), (4.33), (4.41), and (3.9), for $a = a^\infty$, $k = k^\infty$, $\eta_0 = \eta_0^\infty$ and $P_c = P_c^\infty$. Note that the limiting values can be found without using the specific evolution of the parameters. To find the dynamics, first the value of the total energy-density flux $\mathcal{F}^\infty$ has to be specified. It is calculated from the equilibrium values of the parameters:

$$\mathcal{F}^\infty = \mathcal{F}_0(a^\infty, k^\infty, \eta_0^\infty, P_c^\infty). \tag{4.52}$$

After determining $\mathcal{F}^\infty$, the dynamics can be calculated from (4.46).

### 4.3.4 A geometrical view of the parameter dynamics

The dynamics of the four parameters $a$, $k$, $\eta_0$, and $P_c$ are determined by two nonlinear algebraic relations (4.32), (4.33), one linear algebraic relation (4.41), and the ODE (4.43). Each algebraic relation can be seen as a 3D subspace in the four-dimensional parameter space. An illustration is given in Figure 4.1. The intersection of the three subspaces (4.32), (4.33), (4.41) defines a curve in the four-dimensional space. The adaptation of $a(x)$, $k(x)$, $\eta_0(x)$, and $P_c(x)$ is represented by this curve. This curve depends on four constants: $\omega$, $\mathcal{I}_0$, $\mathcal{M}_0$, and $\alpha$. Here $\omega$ is given while $\mathcal{I}_0$, $\mathcal{M}_0$, and $\alpha$ is calculated from (4.49), (2.7) and (4.51). In this four dimensional space, there is a manifold given by (3.9), which is the (exact/approximate) dispersion relation of the homogeneous problem. Each point $(a, k, \eta_0, P_c)$ in this manifold represents a linear solution of the homogeneous problem. This manifold is called the dispersion manifold.

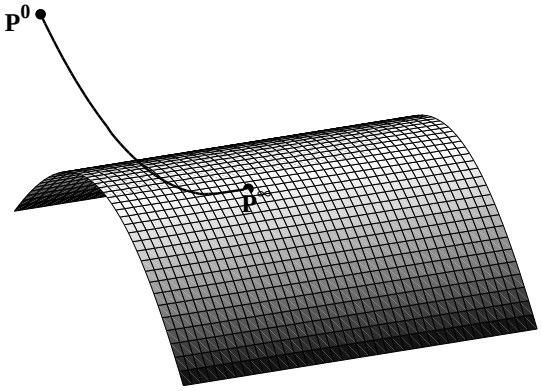


Figure 4.1: A geometrical view of the parameter dynamics

Since $\mathbf{P}^\infty = (a^\infty, k^\infty, \eta_0^\infty, P_c^\infty)$ denotes the intersection point of the evolution curve and the dispersion manifold, the model represents the case where the parameters evolve from a starting point $\mathbf{P}^0$ (where we have the current-free dispersion relation) into a steady state $\mathbf{P}^\infty$ where the parameters are related by the wave-current dispersion relation of the homogeneous problem.

## 4.4 Accuracy of the model

### 4.4.1 Accuracy in the governing equations

The description of the adaptation of the wave-current by the four parameter model is necessarily approximative. In this Subsection we will show that after the start of the interaction the errors in the governing equations are of higher order than linear. We discuss in particular the residues of the Euler equations and the dynamic boundary condition. The residues of the other equations, i.e. the kinematic boundary condition, continuity equation, and bottom boundary condition, will already be small $\left(\mathcal{O}\left(\epsilon^2\right)\right)$ or zero by the requirements of the model.

After substituting (4.18)-(4.21), (2.28), (2.29) and (4.41), into (4.2)-(4.4), assuming (4.11), these residues are given by:

$$\mathcal{R}^{\mathrm{E}_1} \overset{(4.34),(4.42)}{=} \frac{dk}{dx} \cdot \mathcal{O}\left(\epsilon\right) + \mathcal{O}\left(\epsilon^2\right), \tag{4.53}$$

$$\mathcal{R}^{\mathrm{E}_2} \overset{(4.34),(4.42),(4.11)}{=} \frac{dk}{dx} \cdot \mathcal{O}\left(\epsilon\right) + \mathcal{O}\left(\epsilon^2\right), \tag{4.54}$$

$$\mathcal{R}^{\mathrm{dbc}} = \mathcal{O}\left(\epsilon\right) \cdot \mathcal{R}^{\mathrm{DR}} \cdot \cos\theta + \mathcal{O}\left(\epsilon^2\right). \tag{4.55}$$

In the residues above, $\frac{dk}{dx}$ is a direct consequence from quasi-homogenization, and the term $\mathcal{R}^{\mathrm{DR}}$ in (4.55) is given by (4.8). In the discussion below, we will analyze the size

of $\frac{dk}{dx}$ and $\mathcal{R}^{\mathrm{DR}}$ both at $x=0$ and as the distance $x$ increases.

First of all, notice that the value of $\frac{dk}{dx}$ at each $x$ can be approximated by expanding the numerator in (4.46) with $\Delta k = k(x) - k^{\infty}$ as variable:

$$\frac{dk}{dx} = \pm\sqrt{\frac{\mathcal{F}^{\infty} - \mathcal{F}_0\left(a(k), k, \eta_0(k), P_c(k)\right)|_{k=k^{\infty}+\Delta k}}{\mathcal{F}_2(k)}}$$
$$\overset{(4.52)}{=} \pm\sqrt{\frac{\Delta k\left[\left(\frac{\partial}{\partial k} + \frac{da}{dk}\frac{\partial}{\partial a} + \frac{dP_c}{dk}\frac{\partial}{\partial P_c} + \frac{d\eta_0}{dk}\frac{\partial}{\partial \eta_0}\right)\mathcal{F}_0\right]_{k=k^{\infty}}}{\mathcal{F}_2(k)}} + h.o.t. \tag{4.56}$$

From (4.45) and (4.44) it can be shown that $\mathcal{F}_2 = \mathcal{O}\left(\epsilon^2\right)$, $\frac{\partial \mathcal{F}_0}{\partial k}\big|_{k=k^{\infty}} = \mathcal{O}\left(\epsilon^2\right)$, $\frac{\partial \mathcal{F}_0}{\partial a}\big|_{k=k^{\infty}} = \mathcal{O}(\epsilon)$, $\frac{\partial \mathcal{F}_0}{\partial P_c}\Big|_{k=k^{\infty}} = \mathcal{O}(1)$, $\frac{\partial \mathcal{F}_0}{\partial \eta_0}\Big|_{k=k^{\infty}} = \mathcal{O}(1)$. Also, from (4.42) and (4.34) we have $\frac{da}{dk} = \mathcal{O}(\epsilon)$, $\frac{dP_c}{dk} = \mathcal{O}\left(\epsilon^2\right)$, $\frac{d\eta_0}{dk} = \mathcal{O}\left(\epsilon^2\right)$. These imply that (4.56) will be of the same order as $\sqrt{\Delta k}$.

In the same way, with $k$ as parameter we write

$$\mathcal{R}^{\mathrm{DR}} = \mathcal{R}^{\mathrm{DR}}\big|_{\mathbf{P}=\mathbf{P}^{\infty}} + \Delta k\left[\left(\frac{\partial}{\partial k} + \frac{da}{dk}\frac{\partial}{\partial a} + \right.\right.$$
$$\left.\left.\frac{d\eta_0}{dk}\frac{\partial}{\partial \eta_0} + \frac{dP_c}{dk}\frac{\partial}{\partial P_c}\right)\mathcal{R}^{\mathrm{DR}}\right]_{\mathbf{P}=\mathbf{P}^{\infty}} + h.o.t. \tag{4.57}$$

In the model we require that $\mathbf{P}^{\infty}$ satisfies the (approximate) dispersion relation (3.9). Then $\mathcal{R}^{\mathrm{DR}}\big|_{\mathbf{P}=\mathbf{P}^{\infty}}$ (but not its derivatives) must be either zero or $\mathcal{O}(\epsilon)$. This implies that the right-hand side of (4.57) must be either $\mathcal{O}(\epsilon)$ or of the same order as $\Delta k$.

At $x=0$, the value of $k$ is determined by the wave-only dispersion relation (4.48), and at $x \to \infty$ the limiting value $k^{\infty}$ is determined by the (approximate) dispersion relation of the homogeneous problem (3.9). In general, because $k(0)$ and $k^{\infty}$ are determined from two different dispersion relations, then $\Delta k|_{x=0} = \mathcal{O}(1)$. In other words both $\frac{dk}{dx}$ and $\mathcal{R}^{\mathrm{DR}}$ are $\mathcal{O}(1)$ at $x=0$; and this implies that $\mathcal{R}^{\mathrm{E}_1}$, $\mathcal{R}^{\mathrm{E}_2}$, and $\mathcal{R}^{\mathrm{dbc}}$ are $\mathcal{O}(\epsilon)$ at $x=0$.

As the distance $x$ increases, $\Delta k$ goes to zero, so both $\frac{dk}{dx}$ and the terms of (4.57) containing $\Delta k$ decrease to zero. In other words after the start of the interaction, $\mathcal{R}^{\mathrm{E}_1}$, $\mathcal{R}^{\mathrm{E}_2}$, $\mathcal{R}^{\mathrm{dbc}}$ decrease smoothly from $\mathcal{O}(\epsilon)$ to $\mathcal{O}\left(\epsilon^2\right)$. So for $x > 0$ these residues are of higher order. Furthermore, from the relations for the residues (4.53)-(4.55), we notice that there must be a position $x = L$ such that for $x \geq L$ error from quasi-homogenization are smaller than $\mathcal{O}\left(\epsilon^2\right)$ error from homogenization. The distance $L$ is called 'the distance of adaptation'.

### 4.4.2 Consequences of the flux conservations

Having investigated the residue of the equations, we now investigate in a different way consequences of the flux conservations. To investigate this, first observe that for an approximate solution of the full equation, the conservation laws will also

only be satisfied approximately and the right-hand sides of (2.11)-(2.13) are not zero anymore. For the case that the velocity field satisfies the bottom boundary condition and the continuity equation exactly, relations between the conservation laws for mass, momentum, and energy and the residues are given by

$$\partial_t \eta + \partial_x \mathcal{I} = \mathcal{R}^{\mathrm{kbc}}, \tag{4.58}$$

$$\partial_t \mathcal{I} + \partial_x \mathcal{M} = \int_{-1}^{\eta} \mathcal{R}^{\mathrm{E}_1} dz + u|_{z=\eta} \mathcal{R}^{\mathrm{kbc}} + \eta_x \mathcal{R}^{\mathrm{dbc}}, \tag{4.59}$$

$$\begin{aligned} \partial_t \mathcal{E} + \partial_x \mathcal{F} = & \int_{-1}^{\eta} \left( u\mathcal{R}^{\mathrm{E}_1} + w\mathcal{R}^{\mathrm{E}_2} \right) dz + \\ & \mathcal{R}^{\mathrm{kbc}} \left( \frac{1}{2}u^2 + \frac{1}{2}w^2 + \eta \right)_{z=\eta} + (u\eta_x - w)_{z=\eta} \mathcal{R}^{\mathrm{dbc}}, \end{aligned} \tag{4.60}$$

where expressions for $\mathcal{I}$, $\mathcal{M}$, $\mathcal{F}$, $\mathcal{E}$ are given by (2.7)-(2.10).

If all quantities $\eta$, $u$, $w$, and $p$, are periodic in time, then after time-averaging (4.58)-(4.60) we will get the following relations between the residues of the governing equations and the mass, momentum, and energy density fluxes:

$$\partial_x \langle \mathcal{I} \rangle = \left\langle \mathcal{R}^{\mathrm{kbc}} \right\rangle, \tag{4.61}$$

$$\partial_x \langle \mathcal{M} \rangle = \left\langle \int_{-1}^{\eta} \mathcal{R}^{\mathrm{E}_1} dz \right\rangle + \left\langle u|_{z=\eta} \mathcal{R}^{\mathrm{kbc}} \right\rangle + \left\langle \eta_x \mathcal{R}^{\mathrm{dbc}} \right\rangle, \tag{4.62}$$

$$\begin{aligned} \partial_x \langle \mathcal{F} \rangle = & \left\langle \int_{-1}^{\eta} \left( u\mathcal{R}^{\mathrm{E}_1} + w\mathcal{R}^{\mathrm{E}_2} \right) dz \right\rangle + \left\langle (u\eta_x - w)_{z=\eta} \mathcal{R}^{\mathrm{dbc}} \right\rangle + \\ & \left\langle \mathcal{R}^{\mathrm{kbc}} \left( \frac{1}{2}u^2 + \frac{1}{2}w^2 + \eta \right)_{z=\eta} \right\rangle. \end{aligned} \tag{4.63}$$

In the linear approximation, conserving $\langle \mathcal{I} \rangle$, $\langle \mathcal{M} \rangle$, and $\langle \mathcal{F} \rangle$ as is required by the model means that $\partial_x \langle \mathcal{I} \rangle$, $\partial_x \langle \mathcal{M} \rangle$, and $\partial_x \langle \mathcal{F} \rangle$ vanish in the order of approximation (i.e. they are smaller than $\mathcal{O}\left(\epsilon^2\right)$).

The first relation (4.61) means that conserving $\langle \mathcal{I} \rangle$ implies the vanishing of all $\mathcal{O}\left(\epsilon^2\right)$ terms of the time-average of $\mathcal{R}^{\mathrm{kbc}}$. From this, and from the second and third relations (4.62)-(4.63), the vanishing of $\partial_x \langle \mathcal{M} \rangle$ and $\partial_x \langle \mathcal{F} \rangle$ implies that

$$\left\langle \int_{-1}^{\eta} \mathcal{R}^{\mathrm{E}_1} dz \right\rangle = \left\langle \frac{da}{dx} \cos\theta \mathcal{R}^{\mathrm{dbc}} \right\rangle + h.o.t, \tag{4.64}$$

$$\left\langle \int_{-1}^{\eta} \left( u\mathcal{R}^{\mathrm{E}_1} + w\mathcal{R}^{\mathrm{E}_2} \right) dz \right\rangle = \left\langle U|_{z=\eta} \frac{da}{dx} \cos\theta \mathcal{R}^{\mathrm{dbc}} \right\rangle + h.o.t. \tag{4.65}$$

As discussed previously, $\frac{dk}{dx}$ is $\mathcal{O}(1)$ at $x = 0$ and decreases to zero as the distance $x$ increases. Then we may say that $\frac{dk}{dx}$ is smaller than $\mathcal{O}(1)$ for $x > 0$. From (4.42), this means that $\frac{da}{dx}$ is smaller than $\mathcal{O}(\epsilon)$ for $x > 0$. We have shown also that $\mathcal{R}^{\mathrm{dbc}}$ is $\mathcal{O}(\epsilon)$ at $x = 0$ and after a finite distance it becomes $\mathcal{O}\left(\epsilon^2\right)$. Then we may say that $\mathcal{R}^{\mathrm{dbc}}$

is smaller than $\mathcal{O}(\epsilon)$ for $x > 0$. Then (4.64)-(4.65) imply that the right-hand side of (4.64) and (4.65) are of higher order (i.e., they are smaller than $\mathcal{O}(\epsilon^2)$):

$$\left\langle \int_{-1}^{\eta} \mathcal{R}^{\mathrm{E}_1} dz \right\rangle \approx 0 \text{ for } x > 0 \tag{4.66}$$

and

$$\left\langle \int_{-1}^{\eta} \left( u\mathcal{R}^{\mathrm{E}_1} + w\mathcal{R}^{\mathrm{E}_2} \right) dz \right\rangle \approx 0 \text{ for } x > 0. \tag{4.67}$$

This means that in the interaction the Euler equations are projected in two specific directions: $(1,0)^{\mathrm{T}}$ and $(u,w)^{\mathrm{T}}$. These are the implications of flux conservation. Conditions (4.66)-(4.67) are weak formulations for periodic waves of the condition implied by the GN method, which will be discussed in the following.

### 4.4.3 Comparison with the Green-Naghdi theory for fluid sheets

For water waves, the Green-Naghdi (GN) method is often used to derive model equations for water-structure interaction or to derive nonlinear wave solutions. Although the general theory does not assume that the flow is irrotational, in the literature we find that existing applications of the GN method for water waves are so far only for irrotational waves.

The GN method is based on a separation of variables, in which the velocities are described by using $N$ given interpolation functions $q_i(z)$. The fluid velocities are expressed in such a way that the continuity equation (2.5) holds automatically,

$$u = \sum_{i=1}^{N} q_i'(z)\, \xi_i(x,t), \tag{4.68}$$

$$w = -\sum_{i=1}^{N} q_i(z)\, \partial_x \xi_i(x,t), \tag{4.69}$$

in which $\xi_i(x,t)$ and the free surface elevation $\eta(x,t)$ are the unknown functions to be solved (Green and Naghdi [22], Green [21], and Kim et al. [31]). There are $2N+2$ unknowns: $\xi_i$, $p_i$, $\eta$, and $p_{bottom}$, where the $p_i$'s are weight-integrated pressures,

$$p_i = \int_{-h}^{\eta} p q_i dz,$$

and $p_{bottom}$ is the pressure at the bottom. The theory assumes that the free surface dynamic boundary condition holds. The $2N+2$ equations for the unknowns come from the free surface kinematic boundary condition and the bottom boundary condition, plus $2N$ weak formulations of the Euler equation,

$$\int_{-1}^{\eta} \mathcal{R}^{\mathrm{E}_1} q_i'(z)\, dz = 0, \tag{4.70}$$

$$\int_{-1}^{\eta} \mathcal{R}^{\mathrm{E}_2} q_i(z)\, dz = 0. \tag{4.71}$$

The mass is conserved since the continuity equation and the kinematic boundary condition are taken to hold. It is also clear that (4.70) and (4.71) imply

$$\int_{-1}^{\eta} \left( u\mathcal{R}^{\mathrm{E}_1} + w\mathcal{R}^{\mathrm{E}_2} \right) dz = 0.$$

This means that the right-hand side of (4.60) vanishes, thus the energy is conserved. Moreover, if one of the shape functions, for example $q_1$, is given by $q_1 = z$ then (4.70) implies $\int_{-1}^{\eta} \mathcal{R}^{\mathrm{E}_1} dz = 0$. This means that the right hand side of (4.59) vanishes, thus horizontal momentum is also conserved.

With the GN method, the conservation of mass, momentum, and energy are pointwise in time. These conservations are stronger than the conservations we require. However, although the GN method gives a good theoretical tool for formulating solutions of various fluid-dynamics problems, in practice it is not always easy to solve the set of $2N + 2$ nonlinear equations resulting from GN method. An example related to the problem considered in this dissertation is given below.

For the simplest example, i.e. an irrotational wave, the shape functions $q_i(z)$ are taken from the Stokes wave solution (or its approximations for water of infinite depth or shallow water): $q_0 = 1$, $q_1 = z$, $q_{n+1} = \sinh(nk(z+h))$, $n = 1 \ldots N-1$. For the case that the wavenumber $k$ varies in $x$, the shape functions above can be adapted by expressing them in terms of Taylor series expansions around a fixed number $k_0$. For our nondimensionalized linear wave problem, we will get the following set of shape functions:

$$\begin{aligned} q_0 = 1, \quad q_1 = z, \\ q_{2_j} = \frac{(z+1)^{j-1}}{(j-1)!\,(k_0)^{j-1}} \frac{d^{j-1}}{dz^{j-1}} \sinh(k_0(z+1)), \\ j = 1, 2, \ldots \frac{N-1}{2}. \end{aligned}$$

When we want to cover a large range of $k(x)$ (i.e. from $k_0$ that satisfies the wave-only dispersion relation until $k^{\infty}$ that satisfies the wave-current dispersion relation) it is necessary to take $N$ large. This means that we will end up with a large set of nonlinear equations that has to be solved.

## 4.5 Conclusions and Remarks

In this chapter, a model for wave-current interaction with particular emphasis on situations as they appear in laboratory basins is presented. The main aim of this research is to give a practical method for hydrodynamic laboratories like MARIN, so that they can easily make a prediction of the changes that will happen on the generated waves and current. By having a prediction of these changes, they can adapt their wave and current in such a way that the interaction will give the requested wave-current environment.

We approach the problem by seeing the interaction as a smooth adaptation process that takes place spatially. During this adaptation, we require the mass, the momentum, and the energy density fluxes to be conserved, and require the continuity equation and the kinematic boundary condition to be satisfied. In the model, wave and current simultaneously adapt and reach an equilibrium condition characterized by the dispersion relation of the homogeneous problem. We allow the free-surface elevation, the velocities, and the pressure to change quasi-homogeneously in one horizontal direction.

In this chapter we give an analysis of the model and its validity. We show that directly after the start of the interaction, the residues of the governing equations are of higher order, and these residues decrease. Furthermore, there will be a position $x = L$ such that for $x \geq L$ the error from the quasi-homogenization are smaller than the $\mathcal{O}\left(\epsilon^2\right)$ error from homogenization. The distance $L$, which precise definition will be given in the next chapter, is called 'the distance of adaptation'. We have shown also that the requirement that the mass, momentum, and energy-density fluxes must be conserved implies that residues of the full Euler equations are projected in two specific directions. These projections are weak formulations of the condition implied by the Green-Naghdi (GN) method.

A discussion on the Green-Naghdi method is given. It is shown there the characteristics of the GN method and the problem encountered if the range of the wavenumber $k\left(x\right)$ is large. With the GN method, the mass, momentum, and energy are automatically conserved. These conservations are pointwise in time, so they are stronger than the conservations we require. However, if the range of the wavenumber $k\left(x\right)$ is large, it is not so easy to solve the large set of nonlinear equations resulting from the GN method.

In the next chapter, we present case studies and a comparison with results from laboratory experiments found in the literature. Good agreements are found from these comparisons.

# Chapter 5

# Case Studies and Comparison with Experiments

For the problem that a surface water wave suddenly meets a current we investigate the changes in wave and current characteristics. The model described in Chapter 4 is used to study changes in waves and current for cases with uniform, linear, and nonlinear currents. The predicted increase/decrease of the wave length, the wave amplitude, the mean free-surface elevation, and the magnitude/curvature of the current profile are studied both for adverse and favourable currents. The distance of adaptation is calculated, and the results show that this distance is smaller than the wave length but it is large compared to the wave amplitude. Comparisons with laboratory experiments reported in the literature show that the model correctly predicts the qualitative results of the interaction process. Quantitatively, the predictions are good for experiments with following and adverse uniform currents reported by Thomas [69], Margaretha [39] and Voluer [75], for favourable uniform current reported by Swan et al. [67], for nonlinear current reported by Klopman [33], and for small amplitude waves on nonlinear strong current reported by Kemp and Simons [29].

## 5.1 Introduction

This chapter serves as the second part of an investigation on the spatial adaptation when a wave and a current start to interact. The model has been presented and explained in Chapter 4; in this chapter we present case studies and comparison with laboratory experiments reported in the literature.

The model deals with wave-current interaction with particular emphasis on situations as they appear in hydrodynamic laboratories. For accurately testing various designs for offshore structures and ships, a hydrodynamic laboratory must be able to provide precise scaled-versions of various conditions of the real sea. The objective of this research is to find a model for the accurate generation of wave and current conditions in a hydrodynamic laboratory. Interest is specifically also in the dependence on the water depth. The difficulty of getting a requested wave and current environment

is due to the interaction between wave and current. In the presence of a current, the wavemaker motion will produce waves that are different from the waves produced (by the same wavemaker motion) in the absence of currents. For the purpose of laboratory testing we need a model that can predict the changes of both waves and current.

The model discussed here describes the adaptation process that starts when a surface wave abruptly meets a depth dependent current. Before the start of the interaction, the wavelength is determined from the wave-only dispersion relation; and the spatial adaptation will afterwards result in a wavelength which agrees with the dispersion relation of steady wave-current interaction determined by the solution of the Rayleigh equation.

We apply the model to predict the increase/decrease of the wave length, the wave amplitude, the mean free surface elevation, and the magnitude/the curvature of the current profile for cases with uniform, linear, and weakly to moderately nonlinear currents. First of all, we will define 'the distance of adaptation', which is the distance that needed by the wave and current to come sufficiently close to a new equilibrium because of the interaction. This distance will be calculated for case studies with adverse and following uniform and linear currents. The results show that the distance of adaptation is smaller than the wave length, but it is large compared to the wave amplitude. Furthermore, results from the model show that within this distance the change of the wave length will be relatively large compared to the change of the wave amplitude, and the change of the current will be relatively small compared to the change of the wave amplitude.

For adverse currents, the model predicts interesting results if the wave frequency is close to the wave-blocking frequency. In the presence of a current, these waves are amplified much more than waves with smaller frequencies. The predicted distance of adaptation is also longer for this case.

Predicted results of the adaptation process are compared with laboratory experiments reported by Kemp and Simons [29], Klopman [33], Thomas [69], and Swan et al [67]. For the case with uniform current, we also present a comparison with a set of measurements from the Maritime Research Institute Netherlands (MARIN) (test no. 17710-1-OB (2002)). Data analysis of this experiment are reported Margaretha [39] and Voluer [75]. For most experiments the model predicts qualitatively and quantitatively results of the adaptation process; while for some experiments the model only correctly predicts the qualitative behaviour of the interaction process.

## 5.2 The distance of adaptation

In the model, the wave frequency $\omega$ is constant, while the wave number evolves in one-horizontal direction, starting from an initial value $k = k_0$ that satisfies the wave-only dispersion relation 4.48 and asymptotically goes to $k = k^\infty$ as the distance increases. The value $k^\infty$ is related to asymptotic values of the other parameters by the (approximate) wave-current dispersion relation of the homogeneous problem

(3.9). The evolution is described by the ODE (4.46) where the constant $\mathcal{F}^{\infty}$ is given by (4.52).

We define 'the distance of adaptation' $L$ as the distance for which the wavenumber goes from the initial value $k_0$ to the following value that is sufficiently close to $k^{\infty}$ :

$$k = k_1 = k^{\infty} \pm \left(a^{\infty}\right)^2. \tag{5.1}$$

Here the sign is positive if wave and current propagates in the same direction, and negative otherwise. The distance $L$ is calculated from (4.47), taking $k = k_1$ as the end of the integration boundary:

$$L = \pm \int_{k_0}^{k_1} \sqrt{\frac{\mathcal{F}_2\left(a\left(k\right), k, P_c\left(k\right), \eta_0\left(k\right)\right)}{\mathcal{F}^{\infty} - \mathcal{F}_0\left(a\left(k\right), k, P_c\left(k\right), \eta_0\left(k\right)\right)}} dk, \tag{5.2}$$

with negative sign if a wave propagates in the same direction as the current, and positive sign otherwise.

In the following we will show that at and after $x = L$, all residues of the governing equations (4.1)-(4.6) are either $O\left(\epsilon^2\right)$ or zero. In the model, the residues of the kinematic boundary condition, continuity equation, and bottom boundary condition, are already $O\left(\epsilon^2\right)$ or zero, while the residues of the dynamic boundary condition and the Euler equations are related to $\Delta k = k\left(x\right) - k^{\infty}$ by (4.53)-(4.57). Since $k\left(x\right)$ monotonically increases/decreases towards the asymptotic value $k^{\infty}$, then for $x \geq L$ we have

$$\left|\Delta k\right| = \left|k\left(x\right) - k^{\infty}\right| \leq \left(a^{\infty}\right)^2 = O\left(\epsilon^2\right) \tag{5.3}$$

Then, from (4.53)-(4.57) it follows that $\mathcal{R}^{\mathrm{dbc}}$, $\mathcal{R}^{\mathrm{E}_1}$, and $\mathcal{R}^{\mathrm{E}_2}$ are $O\left(\epsilon^2\right)$ for $x \geq L$.

## 5.3 Uniform current

In this section, predicted increase/decrease of the wave length, the wave amplitude, the mean free surface elevation, and the magnitude/curvature of the current profile are studied both for adverse and following uniform currents.

Equations for the parameter dynamics will be given first. Then for various combinations of wave and current, predicted changes are calculated numerically and the results are presented and analyzed. Afterwards comparison with laboratory experiments found in the literature will be given.

### 5.3.1 Equations for the parameter dynamics for uniform current

As a model for the current during the adaptation, we will take

$$U = U_c + P_c,$$

where $U_c$ gives the initial uniform current that exists in the absence of waves. The unknown parameter $P_c$ describes a (depth-independent) change of the uniform current that is necessary for accommodating the presence of waves in the basin.

Taking the wave amplitude $a$, the wave number $k$, the mean free surface elevation $\eta_0$, and the change of the current $P_c$ as the varying parameters, the model describing the free surface elevation $\eta$, the velocities $(u, w)$, and the pressure $p$ are given by (4.18)-(4.21), where $\hat{w}$, $\hat{u}$, $\hat{p}$, $\bar{p}_2$ are given by (2.30), (2.28), (2.29), and (4.24):

$$\eta = a\cos\left(\theta\left(x,t\right)\right) + \eta_0, \tag{5.4}$$

$$u = \left(U_c + P_c\right) + a\frac{\left(\omega - k\left(U_c + P_c\right)\right)}{\sinh\left(k\left(1+\eta_0\right)\right)}\cosh\left(k\left(z+1\right)\right)\cos\theta\left(x,t\right) \tag{5.5}$$

$$\begin{aligned} w = &-\frac{dP_c}{dx}\left(z+1\right) + \frac{a\left(\omega - k\left(U_c + P_c\right)\right)}{\sinh\left(k\left(1+\eta_0\right)\right)}\sinh\left(k\left(z+1\right)\right)\sin\theta\left(x,t\right) - \\ &\frac{d}{dx}\left(\frac{a\left(\omega - k\left(U_c + P_c\right)\right)}{k\sinh\left(k\left(1+\eta_0\right)\right)}\right)\sinh\left(k\left(z+1\right)\right)\cos\theta\left(x,t\right) - \\ &\left(\frac{ak'\left(\omega - k\left(U_c + P_c\right)\right)}{k\sinh\left(k\left(1+\eta_0\right)\right)}\right)\left(z+1\right)\cosh\left(k\left(z+1\right)\right)\cos\theta\left(x,t\right), \end{aligned} \tag{5.6}$$

$$\begin{aligned} p = &-z + \eta_0 + a\frac{\left(\omega - k\left(U_c + P_c\right)\right)^2}{k\left(x\right)\sinh\left(k\left(1+\eta_0\right)\right)}\cosh\left(k\left(z+1\right)\right)\cos\theta\left(x,t\right) - \\ &\frac{a^2}{2}\frac{\left(\omega - k\left(U_c + P_c\right)\right)^2}{\sinh^2\left(k\left(1+\eta_0\right)\right)}\sinh^2\left(k\left(z+1\right)\right), \end{aligned} \tag{5.7}$$

where the phase $\theta\left(x,t\right)$ is related to the wave number and wave frequency by

$$\partial_x\theta = k\left(x\right),\ \partial_t\theta = -\omega.$$

Here $\omega$ is prescribed and is independent of time and space.

The four parameters are related by four equations (4.32), (4.33), (4.41) and (4.43). For this case of uniform current these equations are summarized here:

$$\left(U_c + P_c\right)\left(1+\eta_0\right) + \frac{a^2}{2}\frac{\left(\omega - k\left(U_c + P_c\right)\right)}{\tanh\left(k\left(1+\eta_0\right)\right)} = \mathcal{I}_0, \tag{5.8}$$

$$\begin{aligned} &\left(\frac{1}{2} + \left(U_c + P_c\right)^2 + \frac{\eta_0}{2}\right)\left(1+\eta_0\right) + \\ &a^2\left(\frac{\frac{\left(\omega - k\left(U_c + P_c\right)\right)^2}{2k} + U\left(\omega - k\left(U_c + P_c\right)\right)}{\tanh\left(k\left(1+\eta_0\right)\right)} - \frac{1}{4}\right) + \\ &\frac{a^2}{4}\left(1+\eta_0\right)\frac{k\tanh\left(k\left(1+\eta_0\right)\right) - 3\left(\omega - k\left(U_c + P_c\right)\right)^2}{\sinh^2\left(k\left(1+\eta_0\right)\right)} = \mathcal{M}_0, \end{aligned} \tag{5.9}$$

$$\frac{a}{k} = \alpha, \tag{5.10}$$

and

$$\mathcal{F}_0\left(a,k,P_c,\eta_0\right)+\mathcal{F}_2\left(a,k,P_c,\eta_0\right)\left(\frac{dk}{dx}\right)^2=\mathcal{F}^{\infty}, \tag{5.11}$$

where

$$\begin{aligned}
\mathcal{F}_0 = &\left(\frac{\left(U_c+P_c\right)^3}{2}+\left(U_c+P_c\right)\eta_0\right)\left(1+\eta_0\right)+\\
&\frac{a^2}{4}\left(\frac{2\left(U_c+P_c\right)^3k^3+\omega^2-3\omega k^2\left(U_c+P_c\right)^2}{k\sinh^2\left(k\left(1+\eta_0\right)\right)}\right)\left(1+\eta_0\right)+\\
&\frac{a^2}{4}\left(\frac{\omega^3-k^3\left(U_c+P_c\right)^3}{k^2\tanh\left(k\left(1+\eta_0\right)\right)}+\frac{2\left(\omega-k\left(U_c+P_c\right)\right)\eta_0}{\tanh\left(k\left(1+\eta_0\right)\right)}-\right)+\\
&\frac{a^2}{4}\left(-\frac{2k\left(U_c+P_c\right)}{\sinh\left(2k\left(1+\eta_0\right)\right)}-\frac{k\left(U_c+P_c\right)\eta_0}{\tanh\left(k\left(1+\eta_0\right)\right)}\right),
\end{aligned} \tag{5.12}$$

$$\begin{aligned}
\mathcal{F}_2 = &\frac{a^2}{4}\frac{\omega^3+2k^3\left(U_c+P_c\right)^3-3\omega k^2\left(U_c+P_c\right)^2}{k\sinh^2\left(k\left(1+\eta_0\right)\right)}-\\
&\frac{a^2\eta_0}{2}\frac{\left(\omega-k\left(U_c+P_c\right)\right)}{\tanh\left(k\left(1+\eta_0\right)\right)}+\\
&\frac{a^2}{4}\left(\frac{2k\left(U_c+P_c\right)}{\sinh\left(2k\left(1+\eta_0\right)\right)}+\frac{\omega^3-k^3\left(U_c+P_c\right)^3}{k^2\tanh\left(k\left(1+\eta_0\right)\right)}\right).
\end{aligned} \tag{5.13}$$

The interaction will approach equilibrium values of the parameters

$$\mathbf{P}^{\infty}=\left(a^{\infty},k^{\infty},{\eta_0}^{\infty},{P_c}^{\infty}\right),$$

which are the values of $a$, $k$, $P_c$, and $\eta_0$ resulting from the adaptation process. This equilibrium gives a solution of the homogeneous problem. For uniform current, this solution is identified by the dispersion relation which relates (nonlinearly) $k^{\infty}$, $P_c^{\infty}$, and $\eta_0^{\infty}$ :

$$\left(\omega-k^{\infty}\left(U_c+P_c^{\infty}\right)\right)^2-k^{\infty}\tanh\left(k^{\infty}\left(1+\eta_0^{\infty}\right)\right)=0. \tag{5.14}$$

Summarizing, the equilibrium values of the parameters $a^{\infty}$, $k^{\infty}$, $P_c^{\infty}$, $\eta_0^{\infty}$ are calculated from four algebraic equations (of which three are nonlinear): (5.8), (5.9), (5.10), and (5.14) above. The constants $\mathcal{I}_0$, $\mathcal{M}_0$, $\alpha$ and $\mathcal{F}^{\infty}$ are calculated using the values of the parameters at $x=0$ or at $x\to\infty$ :

$$\begin{aligned}
\mathcal{I}_0 &= \int_{-1}^{0}U_c\left(z\right)dz,\\
\mathcal{M}_0 &= \overline{\mathcal{M}}\left(a_0,k_0,0,P_c\left(0\right)\right),\\
\alpha &= \frac{a\left(0\right)}{k\left(0\right)},\\
\mathcal{F}^{\infty} &= \mathcal{F}_0\left(a^{\infty},k^{\infty},\eta_0^{\infty},P_c^{\infty}\right).
\end{aligned}$$

Notice that (5.8), (5.9), and (5.14) are nonlinear algebraic relations for the parameters. This means that although the wave is linear, the adaptation process and the interaction are nonlinear.

### 5.3.2 Changes of the parameters and the distance of adaptation - Case studies

For this case of uniform current, we present some numerical results with wave and current conditions that are realistic for hydrodynamic laboratories. Characteristics of the initial wave and current are given in Table 5.1, for wave and current propagating in the same and opposite direction. Results of the adaptation process are presented in Table 5.2 and Table 5.3.

| Case | $a_0$ | $\omega$ | $k_0$ | $U_c$ | Case | $a_0$ | $\omega$ | $k_0$ | $U_c$ |
|---|---|---|---|---|---|---|---|---|---|
| 1a | 0.01 | 2.2 | 4.841 | 0.06 | 3a | 0.01 | 0.6 | 0.639 | -0.3 |
| 1b | 0.02 | 2.2 | 4.841 | 0.06 | 3b | 0.02 | 0.6 | 0.639 | -0.3 |
| 1c | 0.04 | 2.2 | 4.841 | 0.06 | 3c | 0.04 | 0.6 | 0.639 | -0.3 |
| 2a | 0.01 | 2.2 | 4.841 | 0.12 | 4a | 0.01 | 0.8 | 0.896 | -0.3 |
| 2b | 0.02 | 2.2 | 4.841 | 0.12 | 4b | 0.02 | 0.8 | 0.896 | -0.3 |
| 2c | 0.04 | 2.2 | 4.841 | 0.12 | | | | | |

Table 5.1: Properties of initial wave and current, for case studies with uniform current. Results are reported in Table 5.2 and Table 5.3

| Case | $P_c(0)$ | $a^\infty$ | $k^\infty$ | $P_c^\infty$ | $\eta_0^\infty$ $\times 10^3$ | $L$ | $\frac{\Delta a}{L}$ | $\frac{da}{dx}$ | |
|---|---|---|---|---|---|---|---|---|---|
| | | | | | | | | $x=0$ | $x=L$ |
| 1a | $-0.00010$ | 0.0080 | 3.875 | $-0.00006$ | $-0.0008$ | 0.113 | -0.018 | -0.036 | -0.00028 |
| 1b | $-0.00038$ | 0.0160 | 3.878 | $-0.00025$ | $-0.0030$ | 0.111 | -0.036 | -0.072 | -0.00114 |
| 1c | $-0.00153$ | 0.0321 | 3.887 | $-0.00101$ | $-0.0101$ | 0.107 | -0.074 | -0.145 | -0.00459 |
| 2a | $-0.00008$ | 0.0068 | 3.275 | $-0.00004$ | $-0.0080$ | 0.199 | -0.016 | -0.027 | -0.00018 |
| 2b | $-0.00032$ | 0.0135 | 3.276 | $-0.00016$ | $-0.0317$ | 0.195 | -0.033 | -0.054 | -0.00074 |
| 2c | $-0.00130$ | 0.0271 | 3.280 | $-0.00065$ | $-0.1248$ | 0.191 | -0.068 | -0.110 | -0.00297 |

Table 5.2: Predicted results of the adaptation process for cases with following uniform currents (Cases 1a - 2c) in Table 5.1.

It is explained in Chapter 4 that the adaptation of $a(x)$, $k(x)$, $\eta_0(x)$, and $P_c(x)$ can be represented by a curve in a four dimensional space. In Figure 5.1 and 5.2 we give two examples of this adaptation curve when projected to the planes $k$ vs $a$, $k$ vs $P_c$, $\eta_0$ vs $k$, and $\eta_0$ vs $P_c$. Figure 5.1 corresponds to case 2c in Table 5.1 and 5.2 while Figure 5.2 corresponds to case 4a in Table 5.1 and 5.3.

| Case | $P_c\,(0)$ | $a^\infty$ | $k^\infty$ | $P_c^\infty$ | $\eta_0^\infty$ $\times 10^3$ | $L$ | $\frac{\Delta a}{L}$ | $\frac{da}{dx}$ | |
|---|---|---|---|---|---|---|---|---|---|
| | | | | | | | | $x=0$ | $x=L$ |
| 3a | 0.00007 | 0.0169 | 1.076 | 0.00018 | −0.0480 | 0.097 | 0.071 | 0.111 | 0.00298 |
| 3b | 0.00028 | 0.0338 | 1.078 | 0.00072 | −0.1942 | 0.088 | 0.157 | 0.222 | 0.01187 |
| 3c | 0.00112 | 0.0680 | 1.085 | 0.00294 | −0.8122 | 0.077 | 0.364 | 0.442 | 0.04665 |
| 4a | 0.00007 | 0.0239 | 2.143 | 0.00047 | −0.1599 | 0.459* | 0.030* | 0.135 | 0.00091* |
| 4b | 0.00030 | 0.0489 | 2.189 | 0.00200 | −0.6852 | 0.308* | 0.094* | 0.269 | 0.00331* |

Table 5.3: Predicted results of the adaptation process for cases with adverse uniform currents (Cases 3a - 4b) in Table 5.1.

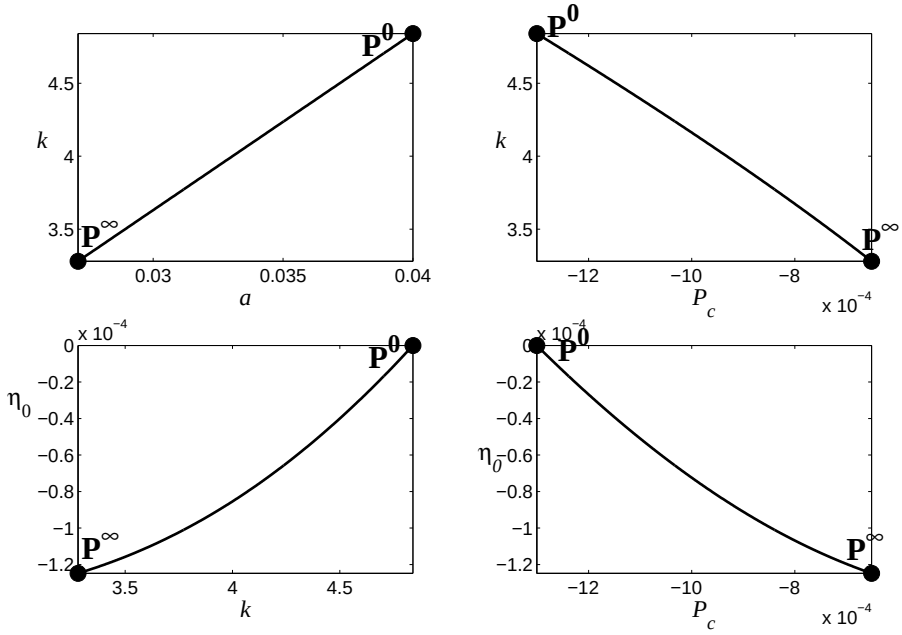


Figure 5.1: Wave on following uniform current. The evolution curve projected to the $a$ vs. $k$, $U$ vs. $k$, $\eta_0$ vs. $U$, and $\eta_0$ vs. $k$ planes.

#### 5.3.2.1 Following current

In Table 5.2 we present numerical results for three different initial wave amplitudes and two initial current values (cases 1-2 in Table 5.1). The results in Table 5.2 and Figure 5.1 show that when wave and current propagate in the same direction the wave amplitude decreases, the wave length increases, the mean free surface elevation decreases, and the current after the adaptation is smaller than the initial (wave-free)

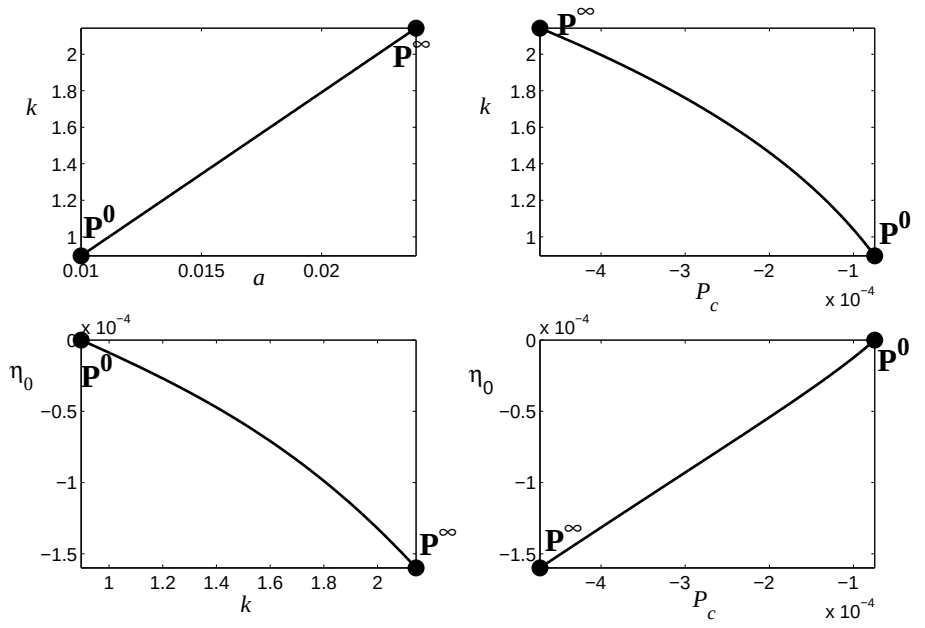


Figure 5.2: As Figure 5.1, but for wave on adverse uniform current.

current $U_c$.

We observe, as can be expected, that the higher the initial current $U_c$ is, the smaller $a^\infty$ and the longer $\lambda^\infty = \frac{2\pi}{k^\infty}$ are. It is also observed that the higher the initial current $U_c$, the longer the distance of adaptation $L$ and the larger the change in the mean free surface elevation $\eta_0{}^\infty$. In these calculations, the distance of adaptation varies between $10\% - 20\%$ of the water depth. Expressed differently, the ratio between $L$ and the initial wave length $\lambda_0 = \frac{2\pi}{k_0}$varies between $0.08 - 0.16$. This means that the largest deformation of wave and current will occur within the distance of one wavelength.

In the last two-columns of Table 5.2 we present the value of $\frac{da}{dx}$ both at the start of the interaction, $x = 0$, and at the end of the defined 'adaptation region', $x = L$. The value of $\frac{da}{dx}$ can be calculated exactly from the ODE (4.46) and relation (4.40). We observe that if $a_0$ increases two times then $\frac{da}{dx}\big|_{x=0}$ increases two times as well and $\frac{da}{dx}\big|_{x=L}$ increases four times. This shows that at $x = 0$ $\frac{da}{dx}$ is $O(\epsilon)$, and at $x = L$ it is $O\left(\epsilon^2\right)$. Since $\frac{da}{dx}$ is continously and monotonically decreasing in $x$, this means that between $x = 0$ and $x = L$ the size of $\frac{da}{dx}$ decreases from $O(\epsilon)$ to $O\left(\epsilon^2\right)$. This result is consistent with requirement (4.26), which is the condition in the model that has to be satisfied to consistently work with $O(\epsilon)$ perturbation (i.e. linear wave theory).

The value $\frac{\Delta a}{L}$ reported in Table 5.2 can be interpreted as an average $\frac{da}{dx}$ in the interval $x \in [0, L]$. Numerical results shows that this value is a bit smaller than $O(\epsilon)$.

#### 5.3.2.2 Adverse current

In Table 5.3 we present numerical results for three different initial wave amplitudes and two values of the wave frequency (cases 3-4 in Table 5.1).

As expected, the wave amplitude increases, the wave length decreases, the mean free surface elevation decreases, and the current $U$ resulting from the adaptation process is larger than the wave-free current $U_c$. The distance of adaptation $L$ varies between $7\% - 46\%$ of the water depth, and the ratio between $L$ and the initial wave length $\lambda_0 = \frac{2\pi}{k_0}$varies between $0.007 - 0.07$.

Wave blocking is a phenomena that is associated with adverse current, $U < 0$. Experiment on wave blocking was conducted by Suastika et al. [62]. The blocking frequency is defined as the value of $\omega$ for which $\frac{d\omega}{dk}$ is zero. From the dispersion relation (5.14) we see that if $\omega$ is smaller than the blocking frequency then one value of $\omega$ corresponds to two values of $k^\infty$: one related to the 'normal case' where $\frac{d\omega}{dk} \geq 0$ and $\frac{\omega}{k} > 0$ and the other one that describes a shorter wave is related to the case where $\frac{d\omega}{dk} \leq 0$ but $\frac{\omega}{k} > 0$. In Table 5.3 we only present the value of $k^\infty$ related to the 'normal case'.

We observe interesting behavior for waves with frequency close to the wave-blocking frequency (cases 4a-4b in Table 5.3). We observe that waves of case 4 are amplified much more than waves with a smaller frequency (case 3). We also observe that the distance of adaptation $L$ is much larger for waves with frequency close to the blocking frequency. This means that these waves need a longer distance to adapt to the presence of current. Maybe this is related to the speed of the wave energy, which is slower near the blocking frequency.

**Remark 5.3.2.1** *For cases 4a and 4b, we found that the square-root in formula (5.2) gives an imaginary value for $k > k_1^*$, with $k_1^* = 2.119$ for case 4a and $k_1^* = 2.049$ for case 4b. In Table 5.3, the value L for cases 4a-4b is calculated by taking $k_1^*$ as the upper boundary of the integral in (5.2). For these two cases $k_1^*$ is smaller than $k_1$ defined in (5.1). It was found that for $k > k_1^*$, the numerator of the term inside the square-root in (5.2) is smaller than $10^{-9}$. Thus higher-order terms (which are neglected in this approximation) and a break-down of the assumption on the Ansatz might change the character near the wave-blocking location.*

In Table 5.3 we also present the values of $\frac{da}{dx}$ at both $x = 0$ and $x = L$ and the value of $\frac{\Delta a}{L}$. We observe that if $a_0$ increases by a factor of two then $\frac{da}{dx}\big|_{x=0}$ increases around two times, $\frac{da}{dx}\big|_{x=L}$ increases around four times, and $\frac{\Delta a}{L}$ increases a bit more than two times. In other words, because $a_0$ is $O(\epsilon)$, we may say that $\frac{da}{dx}\big|_{x=0}$ is $O(\epsilon)$, $\frac{da}{dx}\big|_{x=L}$ is $O(\epsilon^2)$, and the 'average' $\frac{\Delta a}{L}$ less than $O(\epsilon)$. These results are consistent with requirement (4.26).

### 5.3.3 Comparison with experiments

An experiment using an adverse uniform current conditions conducted by Thomas [69] shows the effect of the interaction on the wave amplitude and the wave length (the change of the current was not reported). The experiment used one wave condition and with four different adverse current conditions. The wave has an amplitude $a_0 = 0.0918\,\mathrm{m}$ and length $\lambda_0 = 2.246\,\mathrm{m}$, which corresponds with a frequency $\omega = 5.027$ rad/ s . The water depth is $0.57\,\mathrm{m}$ . In Table 5.4 we present comparisons of the measured and the predicted steady-states of the interaction. When compared with the measured values from the experiment, the difference is small. The wave amplitude is slightly underpredicted by the present model while the wave length is well predicted.

| $\mathcal{I}_0$ | $a^\infty$ (cm) | | | $\lambda^\infty$ (m) | | | Me |
|---|---|---|---|---|---|---|---|
| (cm / s) | Me | Mo | D | Me | Mo | D | $a^\infty\lambda^\infty$ |
| 5.97 | 0.996 | 0.971 | 2.51% | 2.143 | 2.124 | -0.89% | 0.0213 |
| 11.62 | 1.061 | 1.029 | 3.02% | 2.007 | 2.004 | -0.15% | 0.0213 |
| 15.98 | 1.163 | 1.081 | 7.05% | 1.896 | 1.906 | 0.53% | 0.0221 |
| 20.30 | 1.202 | 1.1411 | 5.07% | 1.820 | 1.814 | -0.33% | 0.0219 |

Table 5.4: Comparison with the experiment by Thomas [69]. In this experiment, the wave volume of the initial wave is $a_0\lambda_0 = 0.0206\,\mathrm{m}^2$ .
Me = measured, Mo = Model, D = difference

In Chapter 4, the model predicts that the 'wave volume' $a\lambda$ is conserved. This means

$$a_0\lambda_0 = a^\infty\lambda^\infty. \tag{5.15}$$

In the experiment by Thomas, $a_0\lambda_0 = 0.0206\,\mathrm{m}^2$ . The value $a^\infty\lambda^\infty$ measured in the flume is given in the last column of Table 5.4. In this measurement, the difference between $a_0\lambda_0$ and $a^\infty\lambda^\infty$ is at most 7.3%.

An experiment on uniform current was conducted by Swan et al. [67]. In their experiment, the water depth is $0.7\,\mathrm{m}$ . Detailed information on changes of wave and current are reported in their paper. In Table 5.5 we summarize the experimental results for a uniform current and compare with the prediction from our model. In this experiment, Wave A interacted with a following uniform current $U_c = 0.171\,\mathrm{m}/\,\mathrm{s}$, and Wave B interacted with an adverse uniform current $U_c = -0.185\,\mathrm{m}/\,\mathrm{s}$ .

It is observed from Table 5.5 that the change of the current is predicted well, both for cases with following and adverse current, with a relative error of $1.8\% - 2\%$. The wave properties are also predicted well for the experiment with favorable current, but less good for the experiment with adverse current. We also calculate the 'wave volume' $a\lambda$ measured in the laboratory experiment. In this experiment the difference between $a^\infty\lambda^\infty$ and $a_0\lambda_0$ is 2.1% for the case with following current and it is 6.8% for the case with adverse current

| Wave | $\mathcal{I}_0$ | $2a^\infty$ (m) | | | $a^\infty k^\infty$ | | | $U^\infty$ | | | Measured | |
|---|---|---|---|---|---|---|---|---|---|---|---|---|
| | (m / s) | Me | Mo | D | Me | Mo | D | Me | Mo | D | $a_0\lambda_0$ | $a^\infty\lambda^\infty$ |
| A | 0.171 | 0.083 | 0.0793 | 4.5% | 0.22 | 0.2247 | 2.1% | 0.1598 | 0.1626 | 1.8% | 0.048 | 0.049 |
| B | -0.185 | 0.090 | 0.103 | 14.4% | 0.23 | 0.2880 | 25.2% | -0.1953 | -0.1992 | 2.0% | 0.059 | 0.055 |

Table 5.5: Comparison with an experiment by Swan et al. [67]. For Wave A, the initial height is $2a_0 = 0.1\,\mathrm{m}$, the initial steepness is $a_0k_0 = 0.33$, and the period is $0.75\,\mathrm{s}$. For wave B, the initial height is $2a_0 = 0.075\,\mathrm{m}$, the initial steepness is $a_0k_0 = 0.15$, and the period is $1\,\mathrm{s}$. Me = Measured, Mo = Model, D = Difference.

Another experiment on uniform current was conducted in the wave-current (offshore) basin of the Maritime Research Institute Netherlands (MARIN), test no. 17710-1-OB (2002). An analysis of this experiment is reported by Margaretha [39] and Voluer [75]. In that experiment waves are measured at several positions in the basin, with and without current. The water depth is $1.12\,\mathrm{m}$ and the wave period $0.965\,\mathrm{s}$ giving the initial wave length (without current) $1.454\,\mathrm{s}$. Two wave conditions are tested: Wave A has amplitude $0.02\,\mathrm{m}$ and Wave B $0.04\,\mathrm{m}$. A following uniform current having speed $0.3\,\mathrm{m/s}$(in the absence of waves) was generated. In Table 5.6 predictions from the present model are compared with the ensemble-average values of the measurements. In this experiment the difference between $a^\infty\lambda^\infty$ and $a_0\lambda_0$ is 2.2% for the case with smaller wave amplitude (Wave A) and it is 9.7% for the case with higher wave amplitude (Wave B). We observe that changes of the wave properties are predicted well by the model. Good agreement with MARIN's experiment indicates that the present model can be used for predicting wave and current that have to be generated in order to get a desired wave-current environment in the wave-current basin of MARIN.

| Wave | $a^\infty$ (m) | | | $\lambda^\infty$ (m) | | | Measured | |
|---|---|---|---|---|---|---|---|---|
| | Me | Mo | D | Me | Mo | D | $a_0\lambda_0$ | $a^\infty\lambda^\infty$ |
| A | 0.0148 | 0.0146 | -1% | 2.009 | 1.948 | -3% | 0.02908 | 0.02973 |
| B | 0.0308 | 0.0286 | -7% | 2.071 | 1.945 | -6% | 0.05816 | 0.06379 |

Table 5.6: Comparison with MARIN experiment no.17710-1-OB (2002). Me = Measured, Mo = Model, D = Difference.

## 5.4 Depth-dependent Current

We will now discuss cases for which the current profile is non-uniform, and we are also interested to investigate the change of the curvature of the current profile when interacting with a wave. Since in the model we can only assign one parameter to

describe the change in the current profile, we choose to model the deformation of the current profile with a quadratic function parameterized by one parameter. We take a quadratic shape function for which the largest change on the magnitude and the gradient (i.e., the vorticity) of the current happens at the free surface, while there is no change at the bottom, and the curvature of the current changes uniformly over the depth.

Details on the parametric representation for the deformation of the current profile will be given first for the specific case where the initial current profile is given by a linear function. For various combinations of wave and current, the formulas are treated numerically and the results are presented and analyzed.

Then we will present a comparison with laboratory experiments for currents with nonlinear profile. We will compare predictions from the model with results from two experiments reported by Kemp and Simons [29] and Klopman [33]. These experiments used a current profile known to be turbulent: A shear-current with profile that is almost linear near the free surface but is very curved near the bottom.

### 5.4.1 A parametric representation for the deformation of the current profile

In our model, the current profile during adaptation is given by (4.25), where $U_{\text{change}}$ still has to be chosen. Results of laboratory experiments by Kemp and Simons [29], Klopman [33], Swan [65], and Swan et al. [67], show that the deformation seems to be nonlinear in the sense that the curvature of the current profile changes. Therefore we took in the first instance

$$U^{(1)}_{\text{change}} = P_c\left(x\right)\left(z+1\right)^2, \tag{5.16}$$

where $P_c$ is a parameter that varies in the horizontal $x-$direction.

Later on, it turned out that an additional uniform shift of the current profile will improve results from the model. This shift is taken to be due to the changing wave:

$$U^{(2)}_{\text{change}} = P_c\left(x\right)\left(z+1\right)^2 \pm \left(U_w\left(0\right) - U_w\left(x\right)\right), \tag{5.17}$$

where $U_w$ is the wave mass-transport velocity,

$$U_w = \frac{1}{2}a^2\sqrt{\frac{k}{\tanh\left(k\left(1+\eta_0\right)\right)}}. \tag{5.18}$$

The plus sign in (5.17) is chosen if wave and current propagate in the same direction; otherwise the negative sign is chosen.

### 5.4.2 Case study: Linear currents

We will study the simplest case of shear-current, i.e. the case that the initial current profile varies linearly over the depth. The profile of the initial current is given by the following function

$$U_c\left(z\right) = U_1\left(z+1\right).$$

The change of the current profile is taken to be of the form as given in (5.16) or (5.17).

We want to study the change of a linear current when interacting with a monochromatic wave, as well as the changes of the wave characteristics. The results are presented in Table 5.7 -5.8 for cases with following currents and in Table 5.9 -5.10 for cases with adverse currents. An illustration is shown in Figure 5.3.

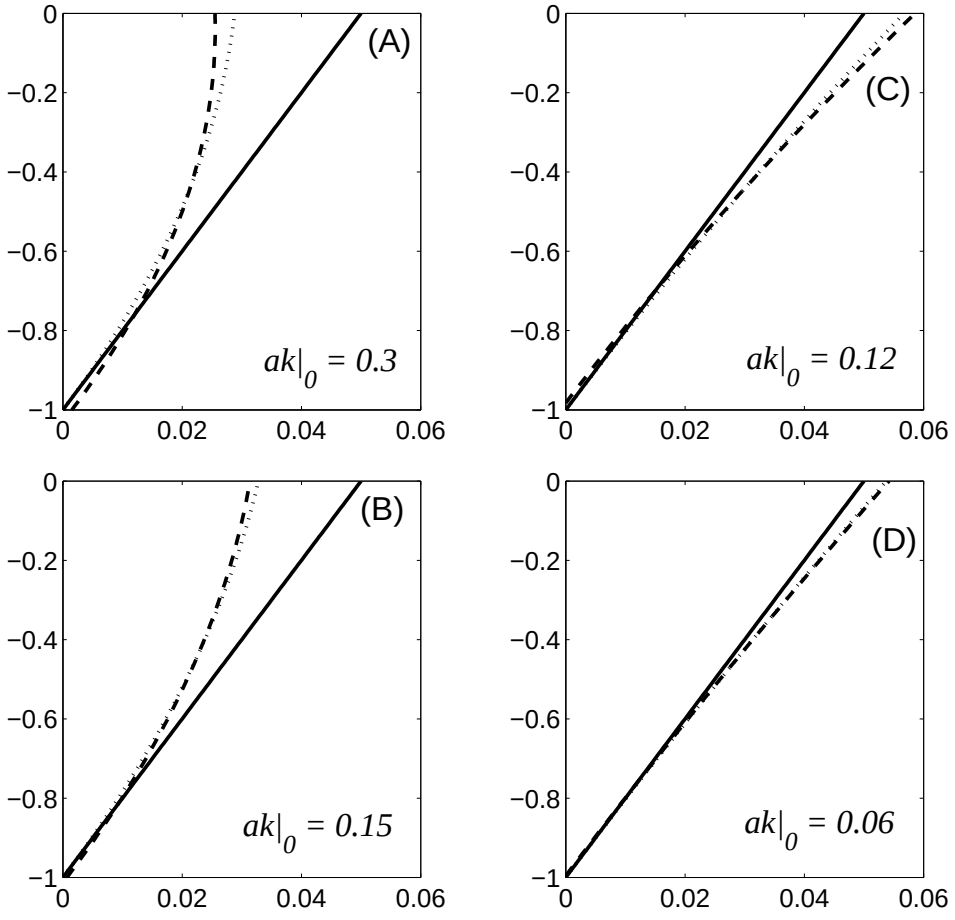


Figure 5.3: Change of current profile, the horizontal axis is the magnitude of the current, the vertical axis is the depth $z$. The initial current profile (linear current) is given by the solid line; while the dotted line and the dashed line give the prediction of the current profile in the presence of the wave using $U^{(1)}_{\text{change}}$ and $U^{(2)}_{\text{change}}$, respectively. Figures (A) and (B): following currents; Figure (C) and (D): adverse currents. The initial wave amplitude and wave number $(a_0, k_0)$ are given by $(0.1, 3)$ for Figure (A), $(0.1, 1.5)$ for Figure (B), $(0.04, 3)$ for Figure (C), $(0.04, 1.5)$ for Figure (D).

Model equations for the parameter dynamics are given by (4.32), (4.33), (4.41) and (4.43). Since the curvature of the initial current is zero and since for this case we do not expect a large change of the curvature of the current profile, we take the irrotational-wave solutions (2.30) to approximate $\hat{w}$. The expressions for $\hat{u}$, $\hat{p}$ and $\bar{p}_2$ are calculated from (2.28), (2.29), and (4.24). The dispersion relation of the homogeneous problem is approximated using formula (3.9).

In Table 5.7 and Table 5.9, $U_1$ gives the magnitude and the slope of the initial current, $a_0k_0$ gives the steepness of the initial wave. In Table 5.8 and Table 5.10 $P_c^\infty$ gives the change of the curvature of the current, ${\eta_0}^\infty$ gives the change of the mean free surface elevation, $\Delta a^{\mathrm{rel}}$ gives the relative change of the wave amplitude,

$$\Delta a^{\mathrm{rel}} = \frac{a^\infty - a_0}{a_0},$$

and $\Delta\left(ak\right)^{\mathrm{rel}}$ gives the relative change of the wave steepness

$$\Delta\left(ak\right)^{\mathrm{rel}} = \frac{a^\infty k^\infty - a_0k_0}{a_0k_0}.$$

#### 5.4.2.1 Following currents

Characteristics of the initial wave and the initial current are given in Table 5.7. Numerical results if the deformation of the current profile is modelled by $U^{(1)}_{\mathrm{change}}$ (5.16) and $U^{(2)}_{\mathrm{change}}$ (5.17) are given in Table 5.7 and 5.8 respectively.

| Case | Wave-only | | | Current | $U_{\mathrm{change}}$ given by (5.16 ) | | | | | |
|---|---|---|---|---|---|---|---|---|---|---|
| | $a_0$ | $k_0$ | $\omega$ | $U_1$ | $a^\infty$ | $\Delta a^{\mathrm{rel}}$ | $a^\infty k^\infty$ | $\Delta\left(ak\right)^{\mathrm{rel}}$ | $\eta_0^\infty \times 10^3$ | $P_c^\infty \times 10^3$ |
| 5a | 0.025 | 3 | 2.985 | 0.05 | 0.0221 | -11.5% | 0.0588 | -21.6% | -0.00155 | -1.203 |
| 5b | 0.025 | 3 | 2.985 | 0.1 | 0.0200 | -19.9% | 0.0481 | -35.9% | -0.01971 | -0.934 |
| 5c | 0.025 | 1.5 | 1.358 | 0.05 | 0.0235 | -6.1% | 0.0330 | -11.9% | -0.01412 | -1.038 |
| 5d | 0.025 | 1.5 | 1.358 | 0.1 | 0.0223 | -11.3% | 0.0295 | -21.4% | -0.03244 | -0.903 |
| 6a | 0.05 | 3 | 2.985 | 0.05 | 0.0446 | -10.8% | 0.1192 | -20.5% | -0.00251 | -4.897 |
| 6b | 0.05 | 3 | 2.985 | 0.1 | 0.0402 | -19.6% | 0.0971 | -35.3% | -0.07303 | -3.779 |
| 6c | 0.05 | 1.5 | 1.358 | 0.05 | 0.0471 | -5.9% | 0.0665 | -11.4% | -0.05301 | -4.181 |
| 6d | 0.05 | 1.5 | 1.358 | 0.1 | 0.0445 | -11.1% | 0.0593 | -21.0% | -0.12603 | -3.632 |
| 7a | 0.1 | 3 | 2.985 | 0.05 | 0.0921 | -7.9% | 0.2544 | -15.2% | 0.03570 | -21.187 |
| 7b | 0.1 | 3 | 2.985 | 0.1 | 0.0820 | -18.0% | 0.2017 | -32.8% | -0.19947 | -.15.857 |
| 7c | 0.1 | 1.5 | 1.358 | 0.05 | 0.0953 | -4.7% | 0.1363 | -9.1% | -0.15694 | -17.192 |
| 7d | 0.1 | 1.5 | 1.358 | 0.1 | 0.0898 | -10.3% | 0.1209 | -19.5% | -0.44399 | -14.854 |

Table 5.7: Characteristics of wave and current before interaction, for cases with following shear-currents. Also results from model for $U_{\mathrm{change}}$ given by (5.16). The initial current profile is given by $U_c = U_1\left(z+1\right)$.

| | $U_{\text{change}}$ given by (5.17) | | | | | | | | $\frac{da}{dx}$ | |
|---|---|---|---|---|---|---|---|---|---|---|
| Case | $a^\infty$ | $\Delta a^{\text{rel}}$ | $a^\infty k^\infty$ | $\Delta\,(ak)$ | $\eta_0^\infty \times 10^3$ | $P_c^\infty \times 10^3$ | $L$ | $\frac{\Delta a}{L}$ | $x=0$ | $x=L$ |
| 5a | 0.0221 | -11.4% | 0.0588 | -21.6% | 0.00187 | -1.628 | 0.12 | 0.0238 | -0.0495 | -0.00176 |
| 5b | 0.0200 | -19.9% | 0.0482 | -35.8% | -0.00833 | -1.626 | 0.33 | 0.0151 | -0.0310 | -0.00074 |
| 5c | 0.0235 | -6.1% | 0.0330 | -11.9% | -0.01276 | -1.120 | 0.05 | 0.0305 | -0.0569 | -0.00419 |
| 5d | 0.0222 | -11.3% | 0.0295 | -21.4% | -0.02755 | -1.199 | 0.14 | 0.0202 | -0.0394 | -0.00196 |
| 6a | 0.0447 | -10.7% | 0.1196 | -20.2% | 0.00906 | -6.509 | 0.06 | 0.0892 | -0.1684 | -0.01184 |
| 6b | 0.0403 | -19.4% | 0.0975 | -35.0% | -0.02998 | -6.501 | 0.17 | 0.0571 | -0.1216 | -0.00536 |
| 6c | 0.0472 | -5.8% | 0.0665 | -11.4% | -0.04810 | -4.817 | 0.03 | 0.0967 | -0.1580 | -0.02359 |
| 6d | 0.0445 | -11.1% | 0.0593 | -20.9% | -0.10730 | -4.796 | 0.08 | 0.0694 | -0.1257 | -0.01226 |
| 7a | 0.0926 | -7.4% | 0.2573 | -14.2% | 0.05059 | -25.991 | 0.02 | 0.370 | -0.5197 | -0.09603 |
| 7b | 0.0827 | -17.3% | 0.2052 | -31.6% | -0.06709 | -25.983 | 0.07 | 0.2471 | -0.4986 | -0.04207 |
| 7c | 0.0954 | -4.6% | 0.1366 | -9.0% | -0.14500 | -19.228 | 0.01 | 0.4600 | -0.4323 | -0.14666 |
| 7d | 0.0899 | -10.1% | 0.1212 | -19.2% | -0.38210 | -19.160 | 0.04 | 0.2525 | -0.3881 | -0.07646 |

Table 5.8: As Table 5.7, but for $U_{\text{change}}$ given by (5.17).

When using $U^{(2)}_{\text{change}}$ the model predicts a larger value of $P_c^\infty$ than when using $U^{(1)}_{\text{change}}$. We observe that the magnitude and the slope of the current at the free surface decrease in the presence of waves.

For both $U^{(1)}_{\text{change}}$ and $U^{(2)}_{\text{change}}$ the model gives the following predictions:

- For the same $U_1$ and $a_0k_0$: the larger $a_0$ is, the larger $|P_c^\infty|$ is but the smaller $\left|\Delta a^{\text{rel}}\right|$ and $\left|\Delta\,(ak)^{\text{rel}}\right|$ are.
- For the same $U_1$ and $a_0$: The larger $a_0k_0$ is, the larger $|P_c^\infty|$ is and also the larger $\left|\Delta a^{\text{rel}}\right|$ and $\left|\Delta\,(ak)^{\text{rel}}\right|$ are.
- For the same $a_0$ and $a_0k_0$: The larger $U_1$ is, the larger $|P_c^\infty|$, $\left|\Delta a^{\text{rel}}\right|$, and $\left|\Delta\,(ak)^{\text{rel}}\right|$ are.

In other words, the model predicts that the current profile bends more with the increase of the amplitude or the steepness of the current-free wave, as is to be expected. Also both wave amplitude/steepness and curvature of the current change more if the initial (wave-free) current has a larger slope or if the initial (current-free) wave has a larger steepness.

The distance of adaptation $L$ was also calculated. It turned out that by taking $U^{(1)}_{\text{change}}$ we get almost the same $L$ as by taking $U^{(2)}_{\text{change}}$. In Table 5.8 the resulting $L$ for model (5.17) is reported. For cases with favorable current, the ratio between $L$ and the length of the initial wave is around $0.002-0.16$. Observe also that an increase of $U_1$ or of the wave frequency (i.e. smaller wavelength $\lambda_0$) results in an increase of the distance $L$.

As in the case with a uniform current, in this case we also analyze the sizes of $\frac{\Delta a}{L}$ and $\frac{da}{dx}$ at both $x=0$ and $x=L$. From Table 5.8 we observe that if $a_0$ increases two

times then $\frac{da}{dx}\big|_{x=0}$ increases around three times, $\frac{da}{dx}\big|_{x=L}$ increases around six times, and $\frac{\Delta a}{L}$ increases around four times. In other words, because $a_0$ is $O(\epsilon)$, we may say that $\frac{da}{dx}\big|_{x=0}$ is $O\left(\epsilon^{1.5}\right)$, $\frac{da}{dx}\big|_{x=L}$ is $O\left(\epsilon^{2.5}\right)$, and the 'average' $\frac{\Delta a}{L}$ is $O\left(\epsilon^{2}\right)$. These results are consistent with requirement (4.26).

#### 5.4.2.2 Adverse currents

Characteristics of the initial wave and the initial current are given in Table 5.9. Numerical results are given in Table 5.9 and Table 5.10.

| Case | Wave-only | | | Current | $U_{\text{change}}$ given by (5.16 ) | | | | | |
|---|---|---|---|---|---|---|---|---|---|---|
| | $a_0$ | $k_0$ | $\omega$ | $U_1$ | $a^\infty$ | $\Delta a^{\text{rel}}$ | $a^\infty k^\infty$ | $\Delta(ak)^{\text{rel}}$ | $\eta_0^\infty \times 10^3$ | $P_c^\infty \times 10^3$ |
| 8a | 0.01 | 3 | 2.985 | -0.05 | 0.0118 | 18.1% | 0.0419 | 39.5% | -0.00627 | -0.395 |
| 8b | 0.01 | 3 | 2.985 | -0.1 | 0.0152 | 52.2% | 0.0695 | 131.6% | -0.03344 | -0.753 |
| 8c | 0.01 | 1.5 | 1.358 | -0.05 | 0.0108 | 7.9% | 0.0175 | 16.4% | 0.00122 | -0.231 |
| 8d | 0.01 | 1.5 | 1.358 | -0.1 | 0.0118 | 18.4% | 0.0210 | 40.2% | 0.00033 | -0.289 |
| 9a | 0.02 | 3 | 2.985 | -0.05 | 0.0237 | 18.6% | 0.0844 | 40.7% | -0.02614 | -1.598 |
| 9b | 0.02 | 3 | 2.985 | -0.1 | 0.0309 | 54.4% | 0.1430 | 138.5% | -0.14221 | -3.122 |
| 9c | 0.02 | 1.5 | 1.358 | -0.05 | 0.0216 | 8.0% | 0.0350 | 16.6% | 0.00488 | -0.925 |
| 9d | 0.02 | 1.5 | 1.358 | -0.1 | 0.0237 | 18.6% | 0.0422 | 40.7% | 0.00117 | -1.158 |

Table 5.9: As Table 5.7, but for cases with adverse shear-currents.

| | $U_{\text{change}}$ given by (5.17) | | | | | | | | $\frac{da}{dx}$ | |
|---|---|---|---|---|---|---|---|---|---|---|
| Case | $a^\infty$ | $\Delta a^{\text{rel}}$ | $a^\infty k^\infty$ | $\Delta(ak)^{\text{rel}}$ | $\eta_0^\infty \times 10^3$ | $P_c^\infty \times 10^3$ | $L$ | $\frac{\Delta a}{L}$ | $x=0$ | $x=L$ |
| 8a | 0.0118 | 18.2% | 0.0419 | 39.6% | -0.00742 | -0.530 | 0.30 | 0.006 | 0.01344 | 0.00018 |
| 8b | 0.0152 | 52.4% | 0.0697 | 132.4% | -0.04186 | -1.244 | 3.37 | 0.002 | 0.00437 | 0.00004 |
| 8c | 0.0108 | 7.9% | 0.0175 | 16.4% | 0.00090 | -0.269 | 0.02 | 0.032 | 0.06235 | 0.00192 |
| 8d | 0.0118 | 18.4% | 0.0210 | 40.2% | -0.00127 | -0.384 | 0.19 | 0.010 | 0.01802 | 0.00043 |
| 9a | 0.0238 | 18.7% | 0.0846 | 41.0% | -0.03119 | -2.159 | 0.10 | 0.037 | 0.05678 | 0.00120 |
| 9b | 0.0311 | 55.6% | 0.1454 | 142.3% | -0.18305 | -5.298 | 1.14 | 0.010 | 0.02391 | 0.00052 |
| 9c | 0.0216 | 8.0% | 0.0350 | 16.6% | 0.003572 | -1.079 | 0.01 | 0.160 | 0.24413 | 0.01628 |
| 9d | 0.0237 | 18.6% | 0.0422 | 40.7% | -0.00540 | -1.547 | 0.04 | 0.093 | 0.18240 | 0.00804 |

Table 5.10: As Table 5.9, but here $U_{\text{change}}$ is given by (5.17).

As expected, wave and current behave differently than in the cases with following currents: the magnitude and the slope of the current at the free surface increase in the presence of waves. The wave amplitude and wave steepness increase, while the wavelength decreases.

Similar behaviour as in the cases with following current are observed: first, when using $U_{\text{change}}^{(2)}$ the model results into a larger value for $P_c^\infty$ than when using $U_{\text{change}}^{(1)}$. Second, the model predicts that the current profile bends more with the increase

of the amplitude or the steepness of the current-free wave, and both wave amplitude/steepness and curvature of the current change more if the initial (wave-free) current has a larger slope or if the initial (current-free) wave has a larger steepness. Third, the higher $U_1$ or the higher the wave frequency is (i.e. the smaller the wavelength $\lambda_0$ is) the longer the distance $L$ is.

The ratio between $L$ and the length of the initial wave is around $0.002 - 1.6$. As in the cases with adverse uniform currents, with adverse linear currents we also observe that the predicted distance of adaptation $L$ is much longer, and both wave amplitude and wave steepness are amplified much more than if the wave frequency is close to the blocking frequency (cases 8b and 9b).

We observe that $\frac{\Delta a}{L}$, $\frac{da}{dx}\big|_{x=0}$, and $\frac{da}{dx}\big|_{x=L}$ increase more than four times if $a_0$ increases two times. This means that these three quantities are smaller than $O\left(\epsilon^2\right)$. These results are consistent with requirement (4.26)

### 5.4.3 Nonlinear currents: comparison with laboratory experiments

For a depth-dependent current, we validate the model using results from two laboratory experiments reported by Kemp and Simons [29] and Klopman [33]. Two different approximations for the solution of the Rayleigh equation $\hat{w}$ are used in the model equations (4.32), (4.33), (4.41) and (4.43): in the first approximation we apply the irrotational-wave solution (2.30), and in the second one we apply the WKB approximate solution (3.20). For both approximations, the dispersion relation is approximated by (3.9).

The results show that both when using the irrotational-wave solution (2.30) and with the WKB approximate solution approximations (3.20) we get almost the same results. This is because the irrotational wave solution is already close to the exact solution for $\hat{w}$, although the curvature of the current profiles themselves are large near the bottom. This is the reason why the WKB approximate solution does not give much improvement to the model.

In Figure 5.4 and 5.5 comparisons with experimental results reported by Kemp and Simons [29] and Klopman [33] are shown. We observe that the model gives a better prediction if the deformation of the current profile is modelled with $U^{(2)}_{\text{change}}$ (5.17). The predicted current profile agrees with the experiment by Klopman and the experiment by Kemp and Simons for smaller wave amplitude. However, when the model is compared with the experiment by Kemp and Simons for higher wave amplitude, the predicted current profile only qualitatively agrees with the measurement. This drawback could be caused by the fact that the current used in the experiment is very strong ($0.206\,\mathrm{m}\,/\,\mathrm{s}$ in water depth $0.2\,\mathrm{m}$).

In Table 5.11 the predicted wave amplitude and wave length are shown, and compared with the measured ones. It is shown there that except for Wave A, the wave length and the wave amplitude are quite well predicted by the model, even for waves with large amplitudes. We also calculated the value $a_0\lambda_0$ and $a^\infty\lambda^\infty$ from the mea-

| Wave | $H_0$ | $\lambda_0$ | $H^\infty$ (m) | | | $\lambda^\infty$ (m) | | | Measured | |
|---|---|---|---|---|---|---|---|---|---|---|
| | (m) | (m) | Me | Mo | Dm | Me | Mo | Dm | $a_0\lambda_0$ | $a^\infty\lambda^\infty$ |
| A | 0.0290 | 1.210 | 0.0207 | 0.0243 | 17.4% | 1.426 | 1.448 | 1.5% | 0.0175 | 0.0148 |
| B | 0.0378 | 1.212 | 0.0303 | 0.0317 | 4.6% | 1.425 | 1.444 | 1.3% | 0.0229 | 0.0216 |
| C | 0.0464 | 1.216 | 0.0394 | 0.0391 | -0.8% | 1.430 | 1.439 | 0.6% | 0.0282 | 0.0282 |
| D | 0.0544 | 1.222 | 0.0444 | 0.0460 | 3.6% | 1.433 | 1.434 | 0.07% | 0.0332 | 0.0318 |

Table 5.11: Comparison with an experiment by Kemp and Simons [29]. Here $H_0$ and $\lambda_0$ are the wave height and wave length when current is absent, $H^\infty$ and $\lambda^\infty$ are the ones when current is present. Me = Measured, Mo = Model, Dm = Difference. Predicted deformation on the current profile for Wave A and Wave D can be seen in Figure 5.4.

surement because we would like to see how well the conservation of wave volume (5.15) is verified by the experiment. The results show that except for Wave A, the experimental results satisfy (5.15) well with differences 5.7% for wave B, 0% for wave C, and 4.2% for Wave D. For Wave A, wave volume conservation is violated for almost 30%.

These comparison show good agreement between the model and laboratory experiments for the type of current profile used in the two experiments (i.e. turbulent current), in which most turbulence mixing happens near the bottom.

**Remark 5.4.3.1** *There is another type of current which is commonly asked to be generated in a laboratory but is not yet compared with the proposed QHA model. We call this type of current 'hurricane current', i.e. current which is strongly sheared near the free-surface with non-uniform vorticity distribution and is almost uniform near the bottom. An experimental study on hurricane currents is reported by Swan et al. [67], which provides good insights in the effect of wave-current interaction. As hinted in their paper, a significant effect from the wave-induced mixing might be that the wave motion encourages a transfer of energy into the turbulent components of the flow field. Another experiment using hurricane current was done at MARIN by van Dijk et al. [15]. It is indicated that a very sheared current does generates a lot of vortices. Since for hurricane currents, it is expected that most mixing will occur near the free surface and since at the present stage the QHA we propose does not incorporate turbulent components, we did not compare the present model with the experiment for hurricane currents by Swan et al. [67].*

## 5.5 Conclusions

We apply the model explained in Chapter 4 to predict the increase or decrease of the wave length, the wave amplitude, the mean free-surface elevation, and the

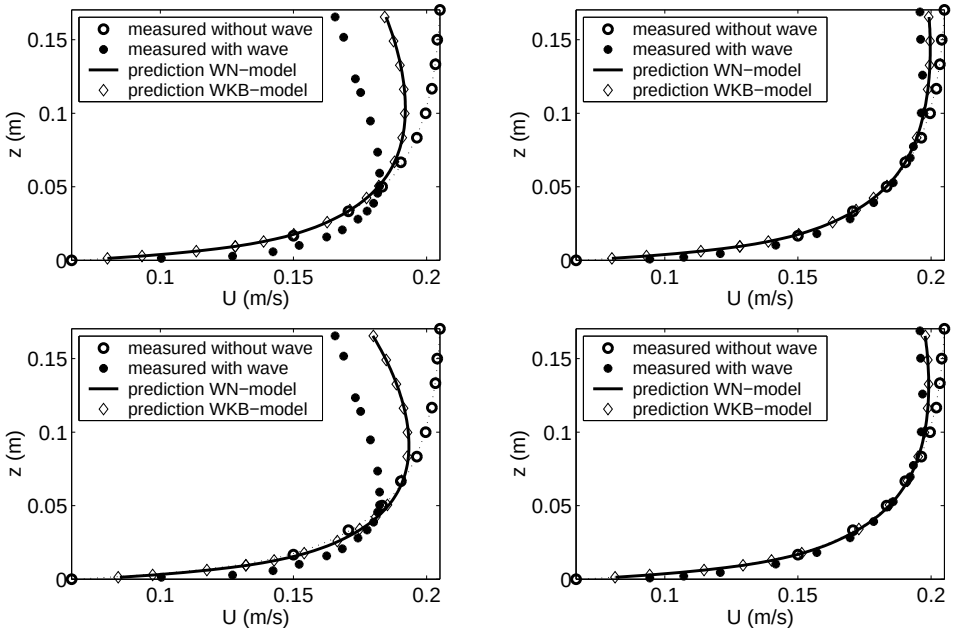


Figure 5.4: Current profile, comparison with experiments reported by Kemp and Simons [29]. In this experiment the water depth is 0.2 m and the wave period is 1 second. Left figures: $a_0 = 0.0272\,\mathrm{m}$. Right figures: $a_0 = 0.0145\,\mathrm{m}$. Upper figures: using $U^{(1)}_{\mathrm{change}}$. Lower figures: using $U^{(2)}_{\mathrm{change}}$. Results from experiment are compared with the QHA model for weakly nonlinear currents (denoted by solid lines) and with the QHA model improved by WKB approximation (denoted by diamonds).
Model for the wave-free (initial) current:
$U_c(z) = -0.75 + 0.9\,\mathrm{sech}\,(0.21z + 0.02) - 0.1\,\mathrm{sech}\,(8z + 9.36) - 0.14\,\mathrm{sech}\,(8z + 8.72)^6$.

magnitude or the curvature of the current profile for cases with uniform, linear, and nonlinear currents.

The aim of this research is to give a practical method for hydrodynamic laboratories like MARIN, to predicts the adaptation process and the changes in the generated wave and current. By having an idea on changes that will happen on the generated wave and current, the wave and current can be chosen in such a way that the interaction will give the desired wave-current environment that are requested for testing model structures.

Two case studies are presented here: uniform current and linear current. For adverse currents, we observe that the wave amplitude will be strongly amplified if the wave frequency is close to the wave-blocking frequency (case 4 in Table 5.3 and cases 8b and 9b in Table 5.9-5.10). In the presence of current, these waves are amplified much more (in agreement with the observation reported by Suastika et al. [62] [63]),

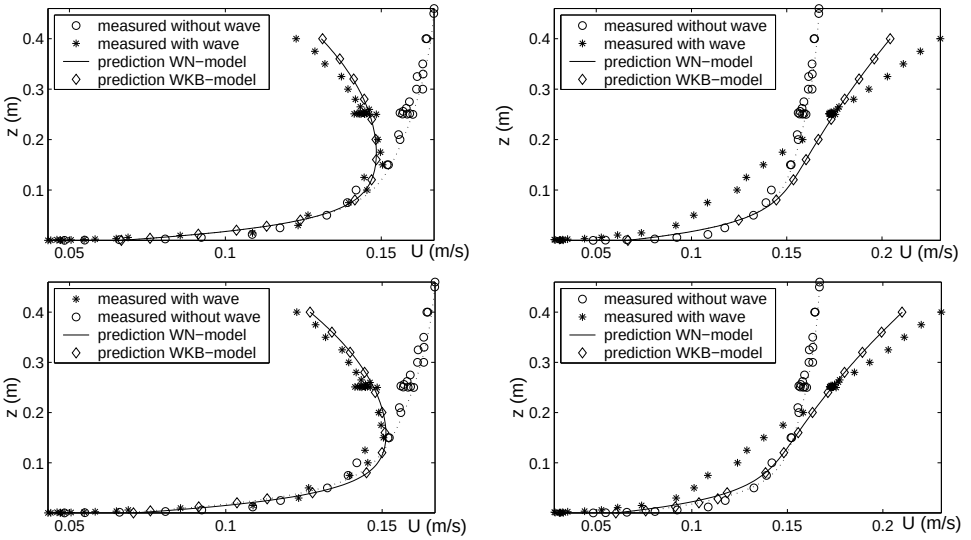


Figure 5.5: Current profile, comparison with experiments reported by Klopman [33]. In this experiment the water depth is 0.5 m, the wave amplitude established when current is present is 0.06 m and the wave period is 1.44 second. Left figures: favourable current. Right figures: adverse current. Upper figures: using $U^{(1)}_{\text{change}}$. Lower figures: using $U^{(2)}_{\text{change}}$. Results from experiment are compared with the QHA model for weakly nonlinear currents (denoted by solid lines) and with the QHA model improved by WKB approximation (denoted by diamonds).
Model for the wave-free (initial) current:
$U_c = 0.07546 + 0.00029z - 0.03322z^{16} - 0.01229z^2$

and these waves need a longer distance to adapt to the presence of currents.

For cases with linear currents (both following and adverse) the model predicts that a linear current will bend more with the increase of the amplitude or the steepness of the current-free wave. Also results from calculation show that both wave amplitude/steepness and curvature of the current change more if the initial (wave-free) current has a larger slope or if the initial (current-free) wave has a larger steepness.

For nonlinear current, the model is compared with results from experiments on turbulent currents conducted by Kemp and Simons [29] and Klopman [33]. The model gives a better prediction if the deformation of the current profile is modelled by (5.17) instead of (5.16).

When tested with experiments, the model gives good predictions to the changes on both wave and current, for experiments with uniform currents reported by Thomas [69], Swan et al. [67], Margaretha and Voluer [39] [75], and for experiments with turbulent currents reported by Kemp and Simons [29] and Klopman [33].

# Chapter 6

# An Experimental Study of Wave-Current Interaction in the Offshore Basin of MARIN

A series of tests with waves encountering a uniform current was conducted in the Offshore Basin of MARIN on 6 and 9 December 2002. The aim of the experiment is two-fold. First, we want to study the behaviour of interacting current and waves in the Offshore Basin of MARIN. Secondly, we want to verify the applicability of the QHA model for pre-adjusting wave and current in that basin.

## 6.1 Capturing the variation of wave and current

The QHA model is built on the assumption that in a laboratory basin wave and current vary spatially, and the largest variation happens in a region where the wave encounters the current.

There are two ways to capture the horizontal variation of the wave amplitude, wavelength, mean free surface elevation, and current profile: using a series of wave probes and current meters fixed at many different positions, or using a series of (a few) wave probes and one current meter attached to a carriage, that will move in the wave-opposing direction.

The first method implies that sufficient numbers of wave probes and current meters are needed. For the experiment at MARIN, the model predicts that the adaptation takes place in a length interval (much) smaller than the wavelength. Consequently, if we use the first method, the distance between the probes must be small (e.g. 8 cm or smaller). Then there is a risk that the recorded data will contain significant effects from probe interference. In addition to this, since the exact location in the basin where the wave and current meet is not known beforehand, we need to place many probes in order to cover a part in the basin that certainly contains the 'adaptation region'.

If we use the second method, the number of probes is reduced significantly and the measurement easily covers any length in the basin, even the whole length of the basin.

Provided that the velocity of the carriage is recorded, from the recorded data we can extract information on the wave amplitude, wave length, and the speed of the current as functions of the horizontal direction. This method requires that the carriage is able to move smoothly without generating extra vibrations or noise that will effect the measurement data. The speed of the carriage depends on the number of wave oscillations we want to capture in a certain length $L$ (e.g. six wave oscillations per 16 cm length). For quasi-harmonic waves, we can show that the speed of the carriage (denoted by $\gamma$) follows from:

$$\gamma = \frac{L\omega}{2\pi N - Lk_{\text{rel}}}, \tag{6.1}$$

where $\omega$ is the constant wave frequency, $L$ is the length of interest, $N$ is the number of wave oscillation per length $L$ that will be captured when the probes 'sweep' the basin, and $k_{\text{rel}}$ is a wavenumber significant to the problem of interest. In the experiment, we take

$$k_{\text{rel}} = k^{\infty},$$

where $k^{\infty}$ is the wave number of the steady interaction predicted by the model.

The implications of (6.1) are illustrated in Figure (6.1). The figure at the top is a plot of the free surface elevation $\eta(x,t)$ given by

$$\eta(x,t) = a(x)\cos(K(x) - \omega t),$$

where $a(x)$ and $K(x)$ are calculated using the QHA model, for one of the proposed tests. The wave is plotted from $x = 0$ to $x = L = 0.1713\,\text{m}$, and from $t = 0$ to $t = 6\,\text{s}$. Here $L$ is the distance of adaptation predicted for the test case. The dark plane intersecting the plot of $\eta(x,t)$ illustrates the case that the probe moves from $x = L$ to $x = 0$ with a constant speed $\gamma = 0.1713\,\text{m/s}$; while the gray plane corresponds to the case that $\gamma = 0.0286\,\text{m/s}$. The figures at the bottom are the recorded $\eta(x,t(x))$ for these two cases; the one at the right is for $\gamma = 0.1713\,\text{m/s}$ while the one at the left is for $\gamma = 0.0286\,\text{m/s}$. The variable $x$ in the lower figures is related to the time $t$ by

$$t = \frac{1}{\gamma}(L - x).$$

From this illustration, it is clear that the slower the speed of the probe, the larger the number of wave oscillations recorded in a given length $L$. However, in practice a carriage is not able to move smoothly if the speed is too slow. If this happens, the recorded data will be corrupted by noise due to the carriage vibrations.

The amplitude $a(x)$ and phase $K(x)$ can be extracted from the record of $\eta(x,t(x))$ by using, for example, the Hilbert transform:

$$a(x_i) = \sqrt{\eta(x_i,t(x_i))^2 + \hat{\eta}_H(x_i,t(x_i))^2},$$
$$K(x_i) = \tan^{-1}\left(\frac{\hat{\eta}_H(x_i,t(x_i))}{\eta(x_i,t(x_i))}\right),$$

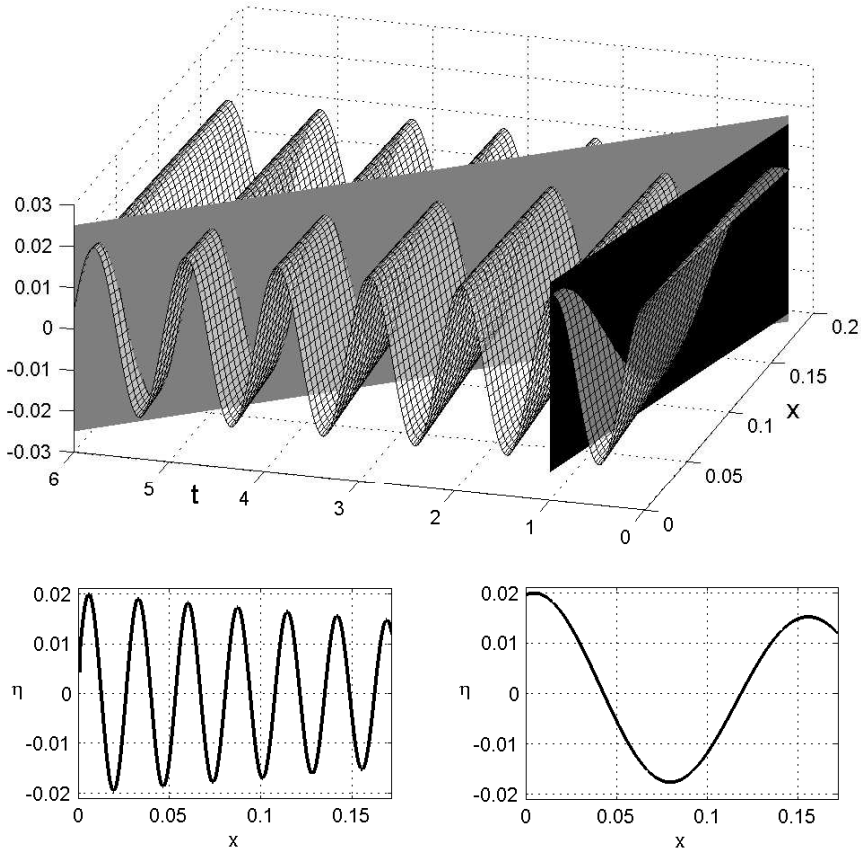


Figure 6.1: An illustration of the wave elevation recorded by a probe moving from $x = L$ to $x = 0$ with speed $\gamma = 0.1713\,\mathrm{m/s}$ (the dark plane at the right, leading to the signal at the bottom right) and $\gamma = 0.0286\,\mathrm{m/s}$ (the gray plane at the left, leading to the signal at the bottom left).

where $\hat{\eta}_H$ is the Hilbert transform of $\eta$. The Hilbert transform is related to the actual data by a 90° phase shift at each frequency contained in the signal $\eta\left(x_i, t\left(x_i\right)\right)$.

## 6.2 Set up of the experiment

### 6.2.1 Basin set up

The basin set-up is illustrated in Figure 6.2. Only the wavemakers at the west side were used. Wavemakers at the South side were not operated, but their angles were adjusted such that they formed a fixed vertical wall. The water depth was

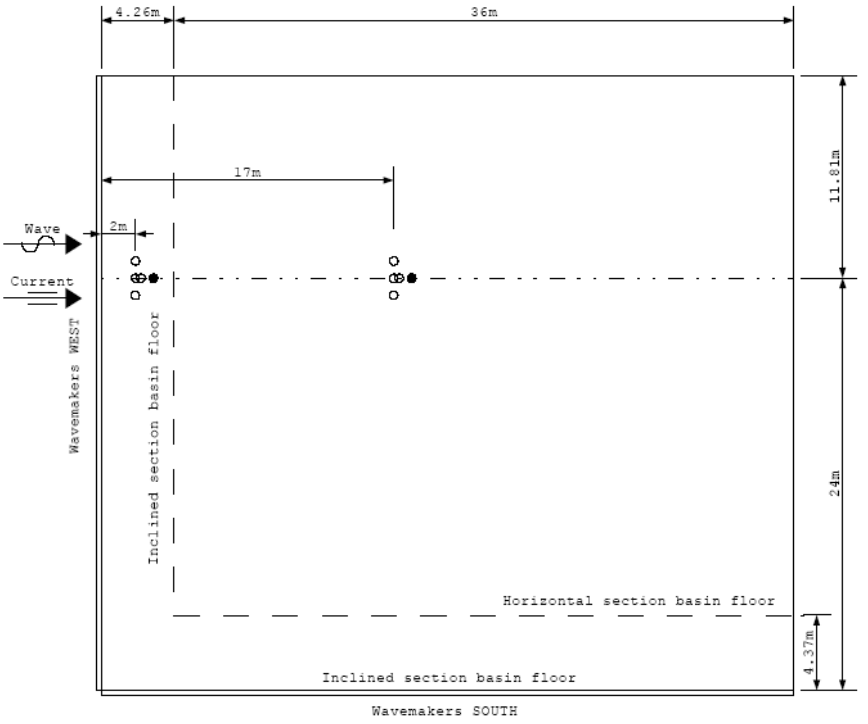


Figure 6.2: Layout of the basin: top view

1.12 m, which means that only the first layer of the current inlet system was used. A cross-section of the basin for this experiment is illustrated in Figure 6.3. See Chapter 1 for general information on the current circulation system.

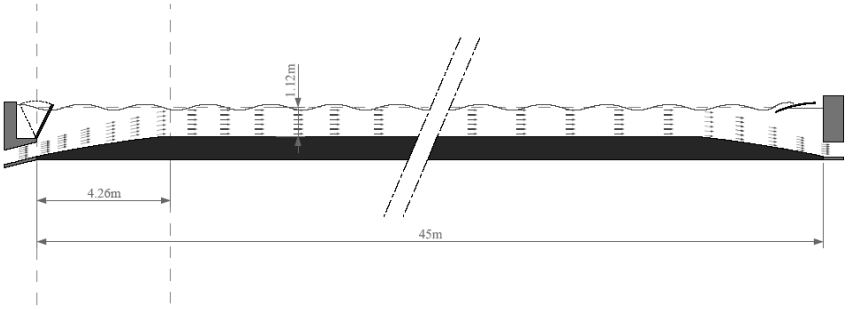


Figure 6.3: Layout of the basin: side view

Figure 6.4 illustrates the arrangement of the wave probes (the gray dots denoted

by CL, CLA, N, S) and the current meter (the black dot) attached to the carriage. A photograph of this arrangement is given in Figure 6.5.

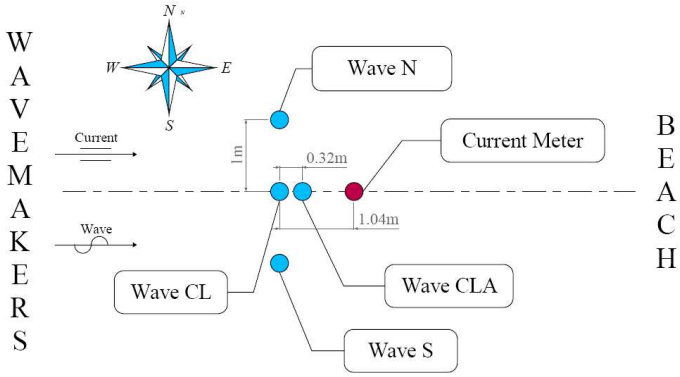


Figure 6.4: Arrangement of the probes

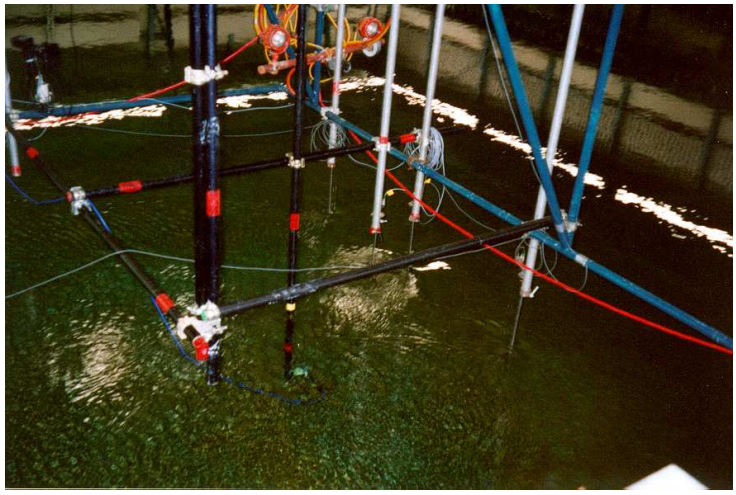

Figure 6.5: Photograph of the probes.

For all tests, the ratio between the wave length and the water depth is smaller than 0.5. This means that the experiment was executed with deep-water wave conditions. In other words, direct bottom effects on the waves can be neglected.

### 6.2.2 Measuring devices

The waves probes used in this experiment are electronic wave probes. The wave elevation is determined from the measured change of conductivity, which is proportional to the immersion depth.

To measure the flow velocities, an electro-magnetic current meter was used. This device allows us to measure two velocity components simultaneously. We chose to measure the horizontal (downstream) and the vertical velocity components. An electro-magnetic current meter measures velocities using Faraday's Law, which states that a conductor (water) moving in a magnetic field (generated by the probe) produces a voltage that varies linearly with the flow velocity. Electrodes in the probe detect the voltages generated by the flowing water. Performance of electro-magnetic current meters depends on the shape of the probe, location of the electrodes on the probe, and its electronics. MARIN reports that their current meter is accurate up to $2.5\,\mathrm{mm}\,/\,\mathrm{s}$ [44].

### 6.2.3 Proposed tests

Properties of the current-free waves in the experiment are:

- wave A: $T = 0.965\,\mathrm{s}$, $\omega = 6.51\mathrm{rad}/\,\mathrm{s}$, $a = 0.04\,\mathrm{m}$, $\lambda = 1.45\,\mathrm{m}$
- wave B: $T = 0.965\,\mathrm{s}$, $\omega = 6.51\mathrm{rad}/\,\mathrm{s}$, $a = 0.02\,\mathrm{m}$, $\lambda = 1.45\,\mathrm{m}$,

and of the wave-free current:

- Uniform current $U = 0.3\,\mathrm{m}\,/\,\mathrm{s}$.

Here $T$ is the wave period, $\omega$ is the wave frequency $(2\pi/T)$, $a$ is the wave amplitude, and $\lambda$ is the wave length.

All tests were sampled at 50 Hz. Table 6.1 shows all tests that were executed with the corresponding test conditions. Six tests were assigned for each wave-current condition in order to measure the flow velocities at six different elevations.

### 6.2.4 Test procedures

#### 6.2.4.1 Calibration of the wave conditions (tests no. 204∗ and 207∗)

Without current, the wavemakers were adjusted until the desired current-free wave was obtained. The waves were recorded for $175 - 270$ seconds at both locations, 17 m and 2 m from the wavemakers (see Figure 6.2). Information given to the wavemakers was stored and used again when we did experiments with current.

| Test | Condition | Position (m) | $a$ (m) | Carriage Speed |
|---|---|---|---|---|
| 101002 | Current only | $x = 17$, $z = -0.10$ | 0 | 0 |
| 101003 | Current only | $x = 17$, $z = -0.25$ | 0 | 0 |
| 101004 | Current only | $x = 17$, $z = -0.50$ | 0 | 0 |
| 101005 | Current only | $x = 17$, $z = -0.70$ | 0 | 0 |
| 101006 | Current only | $x = 17$, $z = -0.90$ | 0 | 0 |
| 204002 | Wave only | $x = 17$ | 0.04 | 0 |
| 204003 | Wave only | $x = 2$ | 0.04 | 0 |
| 207001 | Wave only | $x = 17$ | 0.02 | 0 |
| 207002 | Wave only | $x = 2$ | 0.02 | 0 |
| 304002 | Wave+Current | $x = 17 \dots 2$, $z = -0.08$ | 0.04 | 0.23 m / s |
| 304003 | Wave+Current | $x = 17 \dots 2$, $z = -0.17$ | 0.04 | 0.23 m / s |
| 304004 | Wave+Current | $x = 17 \dots 2$, $z = -0.32$ | 0.04 | 0.23 m / s |
| 304005 | Wave+Current | $x = 17 \dots 2$, $z = -0.10$ | 0.04 | 0.02 m / s |
| 304007 | Wave+Current | $x = 17 \dots 2$, $z = -0.20$ | 0.04 | 0.02 m / s |
| 304009 | Wave+Current | $x = 17 \dots 2$, $z = -0.50$ | 0.04 | 0.02 m / s |
| 307001 | Wave+Current | $x = 17 \dots 2$, $z = -0.08$ | 0.02 | 0.23 m / s |
| 307003 | Wave+Current | $x = 17 \dots 2$, $z = -0.17$ | 0.02 | 0.23 m / s |
| 307004 | Wave+Current | $x = 17 \dots 2$, $z = -0.32$ | 0.02 | 0.23 m / s |
| 307006 | Wave+Current | $x = 17 \dots 2$, $z = -0.10$ | 0.02 | 0.02 m / s |
| 307008 | Wave+Current | $x = 17 \dots 2$, $z = -0.20$ | 0.02 | 0.02 m / s |
| 307009 | Wave+Current | $x = 17 \dots 2$, $z = -0.50$ | 0.02 | 0.02 m / s |

Table 6.1: Description of all tests

#### 6.2.4.2 Calibration of the current conditions (tests no. 101∗)

Having done all tests for both wave A and wave B in the current-free environment, we switched-off the wavemakers and generated the proposed wave-free current. The current was adjusted until the current profile is nicely uniform from the still water level to the depth $z = -0.5$ m. In this experiment, the current was measured at the middle location (i.e. 17m after the wavemakers) and at 5 different depths: $-0.1$ m, $-0.25$ m, $-0.50$ m, $-0.70$ m, and $-0.90$ m.

#### 6.2.4.3 Wave and current (tests no. 304∗ and 307∗)

After calibrating the current conditions, we continued with experiments on wave and current. In these experiments, the current was running continuously - while the wavemakers were switched-on and off. Recorded data were: surface elevations recorded by 4 wave probes, the horizontal and the vertical velocities recorded together by one current-meter, and the speed of the carriage. Figure 6.4 illustrates the arrangement of the wave probes and the current meter.

The experiment was designed as follows:

1. The carriage was placed such that the central wave probe (i.e. probe CL) was located at $x = 17\,\mathrm{m}$ (see Figure 6.2). At this location data was recorded for 100 seconds in the absence of waves.

2. Still recording data, we switched on the wavemakers and continued recording for another 100 seconds at that location.

3. Then we run the carriage forward (toward the wavemakers). Data was still recorded.

4. The carriage stopped when it reached the position $x = 2\,\mathrm{m}$ (See Figure 6.2). Still operating the wavemakers, at this position the data was still recorded for 100 seconds.

5. Then we stopped the wavemakers but keep on recording data for some more time.

## 6.3 Predicted Values and Expected Dynamics

### 6.3.1 Wave condition A

The model predicts that the uniform current $U$ will decrease to $0.2979\,\mathrm{m/s}$, the wave amplitude $a$ will decrease to $0.0293\,\mathrm{m}$ and the wave length $\lambda = \frac{2\pi}{k}$ will increase to $1.985\,\mathrm{m}$. The mean free surface elevation is predicted to decrease $0.0000563\,\mathrm{m}$. The distance of adaptation $L$ is predicted to be $0.1677\,\mathrm{m}$. During the adaptation, the wave amplitude and the wave length are related in such a way that the 'wave volume' (the wave amplitude times the wave length) is conserved.

### 6.3.2 Wave condition B

In the presence of this wave, the uniform current will decrease to $U = 0.2994\,\mathrm{m/s}$. The wave amplitude $a$ will decrease to $0.0146\,\mathrm{m}$ and the wave length $\lambda = \frac{2\pi}{k}$ will increase to $1.988\,\mathrm{m}$. The mean free surface elevation $\eta_0$ is predicted to decrease $0.0000013\,\mathrm{cm}$. The distance of adaptation $L$ is predicted to be $0.1713\,\mathrm{m}$.

## 6.4 Results and Data Analysis

All results are documented in Report 17710-1-OB, in which they are presented using Froude scale 50. This means that lengths are scaled with a factor 50, while times and velocities are scaled with a factor $\sqrt{50}$. Results reported in this dissertation take the original (unscaled) values.

### 6.4.1 Wave-only conditions

Tests no. 204∗ and 207∗ were designed for calibrating the wavemakers. Time series of the surface elevation recorded at fixed positions, near the wavemaker and in the middle of the basin, are presented in Figure 6.6 and 6.7.

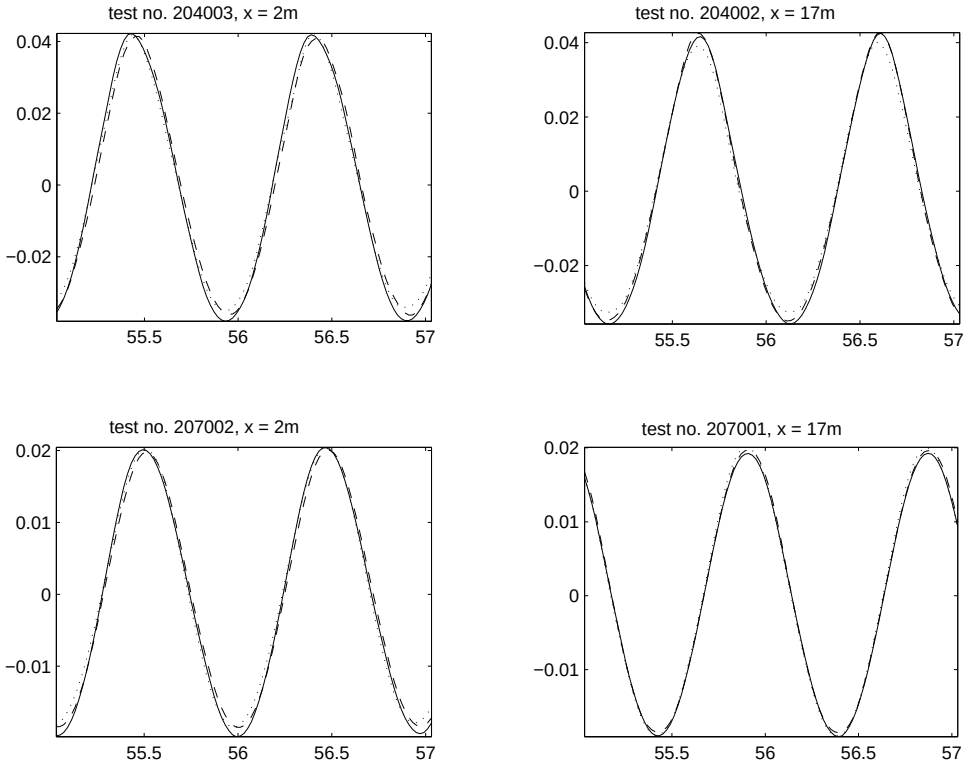


Figure 6.6: Part of the records of the surface elevation from probes N (dashed line), CL (solid line), and S (dotted line). The horizontal axis refers to time (seconds) and the vertical axis refers to the recorded surface elevation (in meter). Figures at the left refer to measurements at $x = 2\,\mathrm{m}$, and the ones at the right refer to measurements at $x = 17\,\mathrm{m}$.

To analyze the results of these measurements quantitatively, we present harmonic analysis on the part of the time series from $t = 40\,\mathrm{s}$ to $t = 90\,\mathrm{s}$ in Table 6.2. The considered time interval is free from waves reflected by the beach.

**Remark 6.4.1.1** *The wavelength predicted by the linear theory is* $1.45\,\mathrm{m}$.

From Table 6.2 we can calculate the difference between the wave amplitude measured at each position and the average amplitude. We found that the amplitude

| Test no. | Wave Amplitude (m) | | | | | | wavelength (m) |
|---|---|---|---|---|---|---|---|
| | S | CL | N | CLA | Average | STD | |
| 204002 | 0.0380 | 0.0358 | 0.0378 | 0.0362 | 0.0382 | 0.00131 | 1.38 |
| 204003 | 0.0398 | 0.0372 | 0.0382 | 0.0362 | 0.0388 | 0.00152 | 1.24 |
| 207001 | 0.0192 | 0.0196 | 0.0192 | 0.0196 | 0.0195 | 0.00029 | 1.45 |
| 207002 | 0.0200 | 0.0192 | 0.0192 | 0.0188 | 0.0195 | 0.00055 | 1.41 |

Table 6.2: Harmonic analysis of tests no. 204002-207002

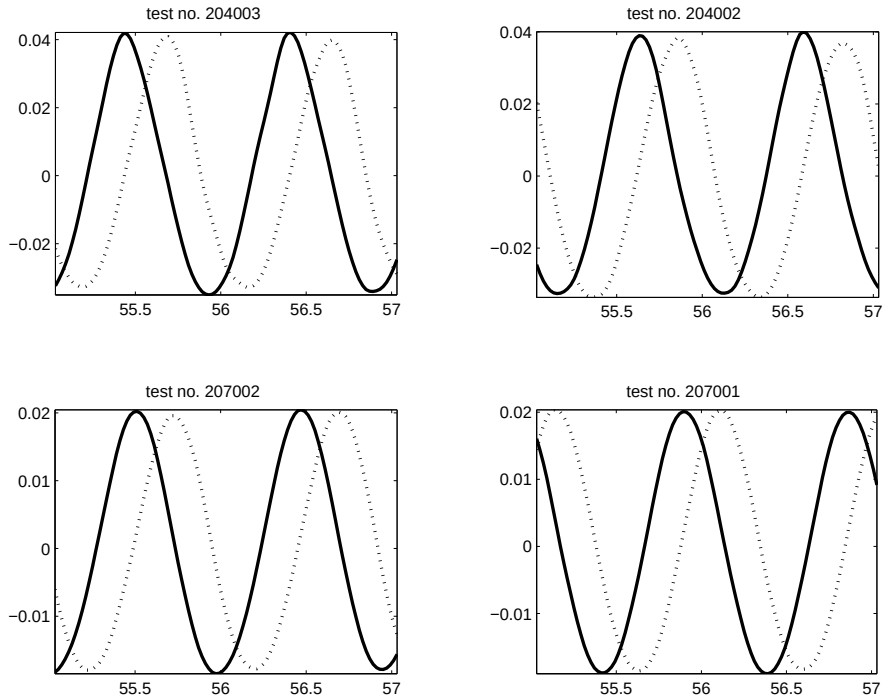


Figure 6.7: As Figure 6.6, but for probes CL (solid line) and CLA (dotted line).

modulation for the large wave is around 6% in the $y$ direction (S-CL-N), and 3% in the $x$ direction (CL-CLA); and for the small wave it is around 4% in the $y$ direction and 2% in the $x$ direction. In Table 6.2 (and throughout this chapter) "STD" stands for the standard deviation. We conclude that the generated waves are good enough: long crested and having the expected properties.

### 6.4.2 Current-only condition

This condition is analyzed from the results of tests no. 101∗, and also from the first part and the last part of tests no. 304∗ and 307∗ (i.e. the horizontal velocity recorded during the time when the wavemakers were switched off).

In Figure 6.8 we present the horizontal velocity $u$ (solid line, above) and the vertical velocity $w$ (dotted line, below) from test no. 101002, measured at $z = -0.1\,\mathrm{m}$ and plotted from time 100 second to 500 second. From this figure we see that the velocities were not steady, due to turbulence. Average values for $u$ and $w$ are presented in Table 6.3, 6.4, and 6.5. In Table 6.3, STD stands for the standard deviation and CI stands for 95% confidence interval of $U$. Assuming that these average values represent the values of the current, we observe that in the absence of waves the established current profile was quite uniform: from half of the water depth to the free surface the variation is not larger than 7%.

Notice that near the water surface, the (average) horizontal velocity at 2 m from the wavemakers was much smaller than the expected strength of the current (i.e., $0.3\,\mathrm{m/s}$). This means that at $x = 2\,\mathrm{m}$, the injected currents had not yet fully developed.

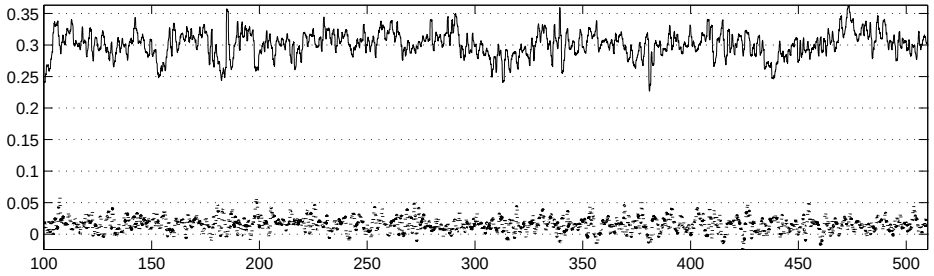


Figure 6.8: The horizontal velocity $U$ (above) and the vertical velocity $W$ (below) recorded during test no. 101002. The current meter was placed at $z = -0.1\,\mathrm{m}$. The horizontal axis refers to time (seconds) and the vertical axis refers to the velocity $(\mathrm{m/s^2})$

### 6.4.3 Combined wave-current conditions

After calibrating the waves and the current separately, their interaction was investigated using the procedure explained in the previous section. We measured the horizontal and vertical velocities, the surface elevations, and the speed of the carriage. Data recorded from tests no. 304∗ and 307∗ consists of five parts. For consistency, these parts are denoted as follows

I Data measured at $x = 17\,\mathrm{m}$, recorded in the absence of waves.

| Test no. | $z$ (m) | $U$ (m / s) | $W$ (m / s) | STD for $U$ | STD for $W$ | CI of $U$ |
|---|---|---|---|---|---|---|
| 101002 | −0.10 | 0.302 | 0.016 | 0.01958 | 0.01131 | 0.00349 |
| 101003 | −0.25 | 0.294 | 0.010 | 0.02112 | 0.01474 | 0.00354 |
| 101004 | −0.50 | 0.279 | 0.023 | 0.02268 | 0.01616 | 0.00380 |
| 101005 | −0.70 | 0.259 | 0.021 | 0.02487 | 0.01641 | 0.00417 |
| 101006 | −0.90 | 0.247 | 0.016 | 0.02335 | 0.01503 | 0.00392 |

Table 6.3: The average horizontal velocity $U$ and the average vertical velocity $W$ from tests no. 101∗. The velocities were measured at 17 m from the wavemakers

| Test No. | Position $z$ | $U$ (m / s) | $W$ (m / s) | Test No. | Position $z$ | $U$ (m / s) | $W$ (m / s) |
|---|---|---|---|---|---|---|---|
| 304002 | −0.08 m | 0.303 | 0.019 | 307001 | −0.08 m | 0.306 | 0.020 |
| 304005 | −0.10 m | 0.301 | 0.014 | 307006 | −0.10 m | 0.306 | −0.029 |
| 304003 | −0.17 m | 0.300 | 0.015 | 307003 | −0.17 m | 0.299 | 0.019 |
| 304007 | −0.20 m | 0.311 | −0.056 | 307008 | −0.20 m | 0.309 | −0.021 |
| 304004 | −0.32 m | 0.296 | −0.018 | 307004 | −0.32 m | 0.283 | 0.018 |
| 304009 | −0.50 m | 0.285 | −0.053 | 307009 | −0.50 m | 0.286 | −0.063 |

Table 6.4: As Table 6.3, for tests no. 304∗ and 307∗. Values in the table are extracted from records of the velocities measured at $x = 17$ m during the time when the wavemakers were switched off.

| Test No. | Position $z$ | $U$ (m / s) | $W$ (m / s) | Test No. | Position $z$ | $U$ (m / s) | $W$ (m / s) |
|---|---|---|---|---|---|---|---|
| 304002 | −0.08 m | 0.087 | 0.074 | 307001 | −0.08 m | 0.035 | −0.096 |
| 304005 | −0.10 m | 0.065 | −0.026 | 307006 | −0.10 m | 0.060 | −0.032 |
| 304003 | −0.17 m | 0.094 | −0.067 | 307003 | −0.17 m | 0.050 | 0.042 |
| 304007 | −0.20 m | 0.166 | 0.066 | 307008 | −0.20 m | 0.212 | 0.067 |
| 304004 | −0.32 m | 0.202 | −0.072 | 307004 | −0.32 m | 0.080 | 0.017 |
| 304009 | −0.50 m | 0.246 | −0.001 | 307009 | −0.50 m | 0.327 | 0.028 |

Table 6.5: As Table 6.4, for velocities measured at $x = 2$ m

II Data measured at $x = 17$ m, recorded in the presence of waves.

III Data recorded in the presence of waves during the time interval when the carriage was moving from $x = 17$ m to $x = 2$ m.

IV Data measured at $x = 2$ m, recorded in the presence of waves.

V Data measured at $x = 2$ m, recorded in the absence of waves.

In Figure 6.9 these parts are identified by plotting together the speed of the carriage with one of the records of the surface elevation. The free surface elevation $\eta$ recorded by the four probes, CL, CLA, N, and S, are presented in Figure 6.10 (test no. 307001) and Figure 6.11 (test no. 307008), also denoting Parts II, III, and IV.

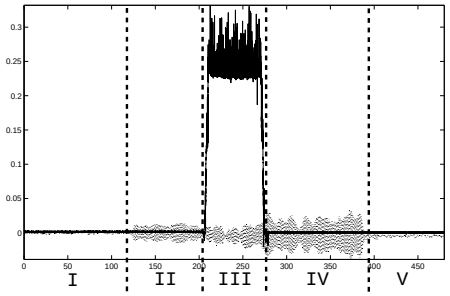


Figure 6.9: One of the records of the surface elevation, captured by a moving probe. The whole signal consists of five parts, as indicated in this figure.

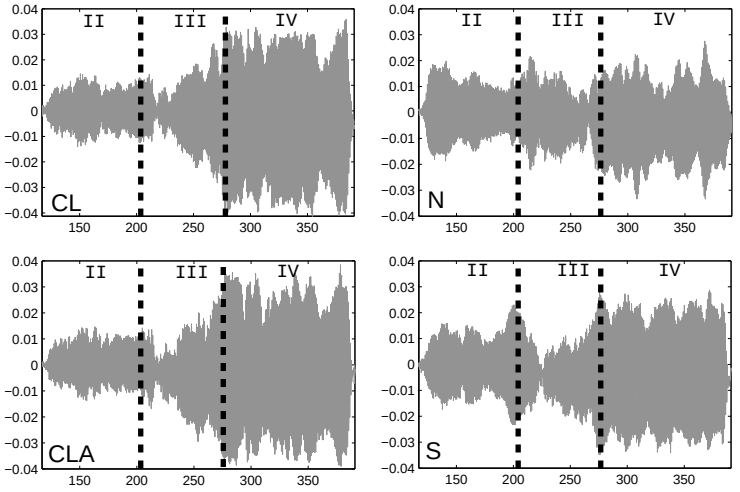


Figure 6.10: Results from test. no. 307001. The free surface elevation $\eta$ recorded by the four probes CL, CLA, N, and S. Parts II, III, and IV are denoted in this figure.

It is surprising to see that the regularity of the wave was destroyed by the presence of current. In the presence of current the surface elevation measured by probes CL, N, and S were different from each other, even when measured at fixed positions (see parts II and IV of time-series presented in Figure 6.10 and 6.11).

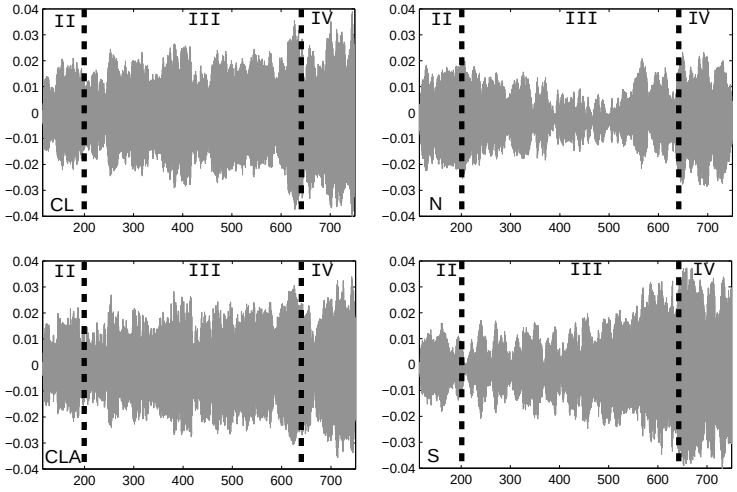


Figure 6.11: As Figure 6.10, for test no. 307008.

Analysis on possible causes of time-space modulation of the waves are reported in [39] and [75]. From these reports, we conclude that the observed modulation is not due to:

1. Waves reflected by the beach. The time which is needed by the wave energy to reach a certain position in the basin, go to the beach and come back to that position (neglecting the possible delay at the beach) is approximately

$$t_{\text{reflection}} = t_0 + \frac{L_A}{c_g^{\text{inc}}} + \frac{L_B}{c_g^{\text{inc}}} + \frac{L_B}{c_g^{\text{ref}}},$$

where $t_0$ is the time when the wavemaker was switched on ($t_0 = 100\,\text{s}$), $L_A$ is the distance to the wavemakers, $L_B$ is the distance to the beach, $c_g^{\text{inc}}$ is the group velocity of the incoming wave:

$$c_g^{\text{inc}} = \frac{d}{dk}\left(\sqrt{gk_{\text{inc}}\tanh\left(k_{\text{inc}}h\right)} + k_{\text{inc}}U\right),$$

and $c_g^{\text{ref}}$ is the group velocity of the reflected wave:

$$c_g^{\text{ref}} = \frac{d}{dk}\left(\sqrt{gk_{\text{ref}}\tanh\left(k_{\text{ref}}h\right)} - k_{\text{ref}}U\right),$$

$k_{\text{inc}}$ and $k_{\text{ref}}$ are the wave number of the incoming wave and the reflected wave (assuming that the frequency of both waves are the same). Approximately, by taking $U = 0.3\,\text{m}/\,\text{s}$, $t_{\text{reflection}}$ for $x = 17\,\text{m}$ and $x = 2\,\text{m}$ is given by $t_{\text{reflection}} = 228\,\text{s}$ and $t_{\text{reflection}} = 288\,\text{s}$, respectively. This means that the part of the signal

related to measurement at $x = 17\,\mathrm{m}$ (i.e. part II) does not contain reflected waves. Therefore the wave-amplitude modulation observed at this part of the signal is not due to the reflected waves.

2. Geometry of the basin floor. Lengths of both current-free wave and current-effected wave, which are given in Table 6.6-6.9, are smaller than twice of the water depth. This means that theoretically, we have deep water condition. In other words we assume that the bottom of the basin does not have significant influences on the wave at the free surface.

We found that the observed modulation is due probably to:

1. Unsteady current. Figure 6.8 shows one record of the velocities measured at a fixed position at $x = 17\,\mathrm{m}$, in the absence of waves. The recorded current fluctuates in time. If a wave enters a region with an unsteady current, the wave frequency tends to be unsteady as well. Even more, the current field might also be spatially fluctuating, e.g. by large eddies moving through the basin.

2. Walls separating neighbouring segments of the current inlets. As shown in Figure 1.4, along the side where the current is injected, all layers of the inlets are segmented by thin walls. Each segment is 3.6 m long. Therefore the current must have a variation in the transversal ($y$) direction, as illustrated in Figure 6.12. This idea was confirmed by de Wilde [79] who made an experiment on the characteristics of currents in the offshore basin of MARIN. Voluer [75] reconstructed the local representation of the free surface elevation, using data of calculated significant wave heights from parts of records related to fixed-probes measurement at $x = 17\,\mathrm{m}$ given in Table 6.6 and 6.8. The free surface elevation was approximated like

$$\eta = a\cos\left(\omega t - kx + \phi_0\cos\left(\frac{2\pi}{L_0}\,(y - y_0)\right)\right),$$

where $a$, $\phi_0$, $L$, and $y_0$ are approximated from the measurements. He found that the best value for the length $L_0$ is about $4\,\mathrm{m}$. This finding and the fact that near the inlets the current has a transversal variation of length that is equal to the length of the segments (i.e., 3.6 m) strengthen the claim that transversal modulation suffered by initially-regular waves must be due to the transversal variation of the current.

In Table 6.6, 6.7, 6.8, and 6.9 we present the significant wave height (divided by two) and the wavelength for different measurements. The significant wave height is given by the average height of the highest one-third of the waves. The wavelength is calculated from parts II and IV of the records measured at probes CL and CLA. Precision of the calculated wavelength is about 0.1 m, so the accuracy is approximately 95%.

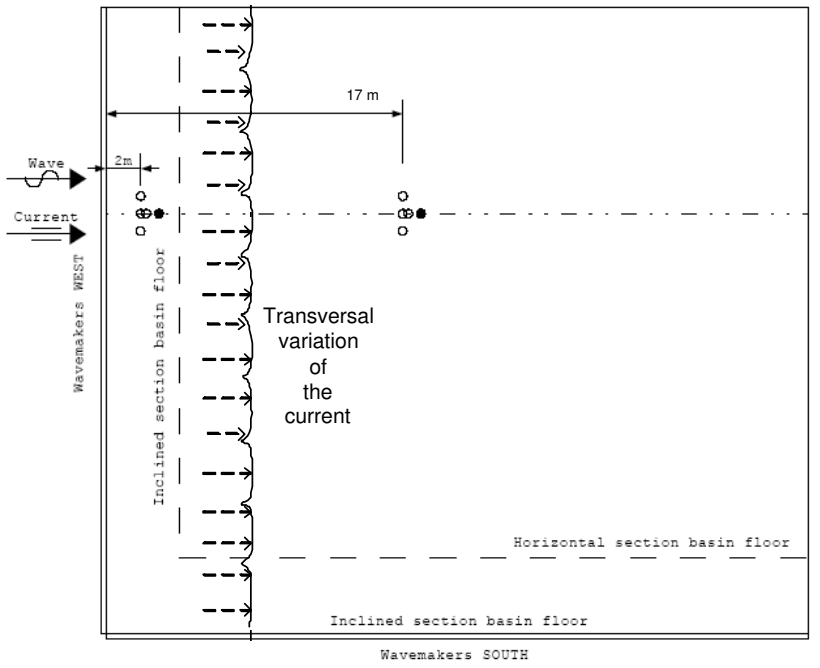


Figure 6.12: Illustration of the transversal variation of the current near the inlets

In Table 6.10 and 6.11 we present ensemble-average and standard deviation of the significant wave heights and wave length (for wave A and wave B, respectively) presented in Table 6.6-6.9. As shown in these Table, the ensemble average values are compared to the amplitudes of both wave A and wave B measured in the absence of current. For each wave, the ensemble average gives the average values of wave properties measured at different time and positions.

Remember that the probes started at $x = 17\,\mathrm{m}$ and stopped at $x = 2\,\mathrm{m}$. Data logged at $x = 17\,\mathrm{m}$ does not contains reflected waves, while the one logged at $x = 2\,\mathrm{m}$ contains waves reflected from both the beach and the wavemakers plus waves with evanescent modes. Assuming that those waves give 10% contribution to the wave height, then at $x = 2\,\mathrm{m}$ the height of the real incoming wave must be about 10% less than what was measured.

Changes on wave and current predicted by the QHA model are given in Section 6.3 of this Chapter. Assuming that the ensemble-average values presented in Table 6.10

| Test no. | $\frac{1}{2}$(significant wave height) at $x = 17\,\mathrm{m}$ | | | | Wave |
|---|---|---|---|---|---|
| | Wave N | Wave CL | Wave S | Wave CLA | length |
| 307001 | 0.016030 | 0.011579 | 0.015051 | 0.011812 | 1.9346 |
| 307003 | 0.014260 | 0.011125 | 0.013362 | 0.012230 | 2.1629 |
| 307004 | 0.016554 | 0.015136 | 0.013992 | 0.016101 | 1.9940 |
| 307006 | 0.015678 | 0.011967 | 0.014112 | 0.012888 | 2.0016 |
| 307008 | 0.018901 | 0.019735 | 0.013409 | 0.018071 | 1.9841 |
| 307009 | 0.020277 | 0.015644 | 0.014512 | 0.013134 | 1.9754 |
| | | | | Average wave length (±5% error) | 2.0088 |

Table 6.6: Significant wave height and wave length for wave B, measured in the presence of current at $x = 17\,\mathrm{m}$.

| Test no. | $\frac{1}{2}$(significant wave height) at $x = 2\,\mathrm{m}$ | | | | Wave |
|---|---|---|---|---|---|
| | Wave N | Wave CL | Wave S | Wave CLA | length |
| 307001 | 0.021789 | 0.033415 | 0.028013 | 0.034332 | 1.2916 |
| 307003 | 0.023214 | 0.037340 | 0.027111 | 0.034719 | 1.3153 |
| 307004 | 0.021236 | 0.034788 | 0.027945 | 0.034211 | 1.2831 |
| 307006 | 0.019680 | 0.034874 | 0.027385 | 0.034421 | 1.3175 |
| 307008 | 0.023632 | 0.029378 | 0.035012 | 0.024872 | 1.2404 |
| 307009 | 0.022020 | 0.031488 | 0.027195 | 0.030680 | 1.2847 |
| | | | | Average wave length (±5% error) | 1.2888 |

Table 6.7: As Table 6.6, for data measured at $x = 2\,\mathrm{m}$.

| Test no. | $\frac{1}{2}$(significant wave height) at $x = 17\,\mathrm{m}$ | | | | Wave |
|---|---|---|---|---|---|
| | Wave N | Wave CL | Wave S | Wave CLA | length |
| 304002 | 0.029366 | 0.026897 | 0.034002 | 0.028663 | 2.0143 |
| 304003 | 0.029140 | 0.028856 | 0.032430 | 0.028838 | 2.0017 |
| 304004 | 0.031933 | 0.029830 | 0.029959 | 0.030547 | 2.0454 |
| 304005 | 0.031188 | 0.032079 | 0.029857 | 0.034058 | 2.1698 |
| 304007 | 0.034050 | 0.032749 | 0.026320 | 0.032640 | 2.0986 |
| 304009 | 0.039273 | 0.031507 | 0.021599 | 0.032832 | 2.0956 |
| | | | | Average wave length (±5% error) | 2.0709 |

Table 6.8: As Table 6.6, for wave A.

| Test no. | $\frac{1}{2}$(significant wave height) at $x = 2\,\mathrm{m}$ | | | | Wave |
|---|---|---|---|---|---|
| | Wave N | Wave CL | Wave S | Wave CLA | length |
| 304002 | 0.050214 | 0.058879 | 0.061805 | 0.058322 | 1.3317 |
| 304003 | 0.043780 | 0.053144 | 0.066249 | 0.049375 | 1.3571 |
| 304004 | 0.045962 | 0.059323 | 0.062874 | 0.061733 | 1.3653 |
| 304005 | 0.050278 | 0.066744 | 0.057250 | 0.061347 | 1.4010 |
| 304007 | 0.042875 | 0.049518 | 0.067834 | 0.044893 | 1.5049 |
| 304009 | 0.050427 | 0.045282 | 0.066957 | 0.048738 | 1.4419 |
| Average wave length (±5% error) | | | | | 1.4003 |

Table 6.9: As Table 6.6, for wave A measured at $x = 2\,\mathrm{m}$.

| $x$ | Assemble-average; properties of wave A | | | | |
|---|---|---|---|---|---|
| | Amplitude (m) | | | Length (m) | |
| | Without current | With current | | Without current | With current |
| | | Mean | STD | | |
| 2 m | 0.03785 | 0.055158 | 0.008174 | 1.3788 | 1.4003 |
| 17 m | 0.03695 | 0.030776 | 0.003364 | 1.2399 | 2.0709 |

Table 6.10: Global properties of wave A.

| $x$ | Assemble-average; properties of wave B | | | | |
|---|---|---|---|---|---|
| | Amplitude (m) | | | Length (m) | |
| | Without current | With current | | Without current | With current |
| | | Mean | STD | | |
| 2 m | 0.0193 | 0.029115 | 0.005351 | 1.4539 | 1.2888 |
| 17 m | 0.0194 | 0.014773 | 0.002470 | 1.4111 | 2.0088 |

Table 6.11: Global properties of wave B.

and 6.11 represent the amplitudes and the lengths of wave A and wave B, in Table 5.6 we compare these values with the prediction from the QHA model. Changes of the wave properties are predicted well by the model. This agreement indicates that although time-space modulation is unavoidable because of the structure of the basin, global properties of the wave field are predicted well by the QHA model.

Part III of the time-series presented in Figure 6.10 and 6.11 gives the data recorded during the time when the probes move slowly from $x = 17\,\mathrm{m}$ to $x = 2\,\mathrm{m}$. Because of the time-space modulation, it is difficult to extract information on the wave amplitude and the wave number as functions of $x$. Therefore from results of this experiment we cannot verify the expected dynamics, e.g. the $a - k$ relation (4.41) or the distance of adaptation. Nevertheless, we still can compare the difference of the 'wave volume', $a\lambda$, at $x = 2\,\mathrm{m}$ and at $x = 17\,\mathrm{m}$. As discussed in Chapter 5.3.3, the difference is 2.2% for wave B and 9.7% for wave A. In the QHA model, the wave volume conservation is derived from the linear theory. The amplitude of wave B is smaller than A, then the nature of wave B is more linear than wave A. So, due to nonlinearity, error in the conservation of wave volume must also be larger for wave A than wave B.

Now we take a look at the current. In Table 6.12 we compare the mean horizontal velocity measured at six different depths in wave-free condition and wave-affected condition.

| Position $z$ (m) | $U$ (m / s) | |
|---|---|---|
| | without wave | with wave |
| −0.08 | 0.3030 | 0.2983 |
| −0.1 | 0.3011 | 0.3086 |
| −0.17 | 0.3002 | 0.2957 |
| −0.2 | 0.3109 | 0.3003 |
| −0.32 | 0.2958 | 0.2893 |
| −0.50 | 0.2849 | 0.2727 |

Table 6.12: Results from Test no. 304∗. Comparison of the mean horizontal velocity, with and without waves. CI stands for 95% confidence interval for $U$ measured in the absence of waves.

To get an idea of the current profile, values presented in Table 6.12 are picturized in Figure 6.13. We conclude that globally the current decreases in the presence of waves, in agreement with the prediction from the model.

## 6.5 Conclusions

Although it is more difficult to establish steady currents in a large basin (as the one at MARIN) than in a flume, for testing models of large ocean structures or ships this kind of basin cannot be replaced by flumes. Therefore it is worthwhile to find

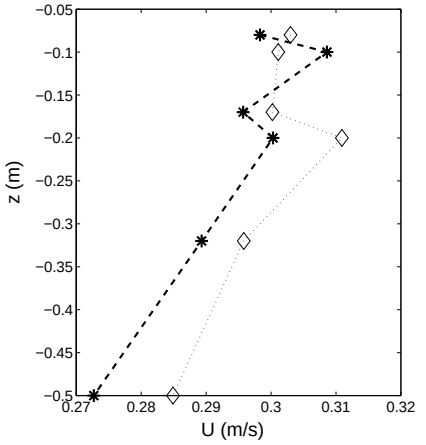


Figure 6.13: As Table 6.12, presented in a figure. The mean horizontal velocity without wave is given by diamonds (◊), and the one affected by wave A is given by asterisks (∗).

a model that can be used for designing a methodological way to accurately generate waves and currents.

In Chapter 5, we show that results from the QHA model agrees with results from various flume measurements. With the experiment reported in this chapter, we wanted to study the behaviour of current and wave in the basin of MARIN and to verify the applicability of the QHA model in pre-adjusting wave and current in that basin

From this experiment we observe that the regularity of waves are destroyed by the presence of fluctuations in the currents. The wave is not longcrested anymore. The time-space modulation is due to the unsteadiness of the current and the non uniformity of the current in the transversal direction.

We defined two variables that represent the global properties of the surface elevation, i.e. the ensemble (time-space) averages of the significant wave height and the wave length. We found that the values of these two variables measured in the middle of the basin agree very well with the prediction from the model, while the ones measured near the wavemaker are close to the properties of the current-free wave. From this observation, we conclude that it is promising to apply the model for pre-adjusting wave and current in the basin of MARIN.

# Chapter 7

# Recommendations for Further Investigations

Using the model discussed in the previous chapters, we are able to predict the properties of wave and current after the adaptation. In this chapter we present a discussion on the inverse problem and give some hints and directions for further developments in dealing with irregular waves and for extending the model to get more flexibility in describing the deformation of the current profile.

## 7.1 The inverse problem

In the introduction to this dissertation we mentioned that the objective of this research is to find a model that can be used for designing a method to generate waves and currents in the offshore basin of MARIN. As an important step to reach this objective, we designed a model that describes the adaptation process that is started when a wave enters a region with current. Using this model, properties of wave and current after the adaptation can be predicted by solving the algebraic equations (3.9), (4.32), (4.33), and (4.41), giving the (approximate) dispersion relation, conservations of mass and momentum density fluxes, and conservation of the wave volume. After obtaining the steady state properties, the spatial dynamics connecting the initial and the steady states is calculated from the conservation of energy-density flux. This spatial dynamics describes the adaptation process. The proposed model therefore solves the direct problem. For the interest of the wave-current generation, the inverse problem has to be considered.

When starting with a uniform current, the inverse problem (i.e. predicting the properties of wave and current before the adaptation) can be solved easily if we assume that the current profile remains uniform. For this case, equations derived from the proposed model are given in Chapter 5.3. Given the expected wave amplitude, wave frequency, and the desired uniform current, the corresponding wave-free uniform current can be calculated directly from the conservation of mass-density flux, while changes of the wave properties are calculated from the algebraic equations resulting

from the conservation of momentum-density flux, the dispersion relation, and the kinematic boundary condition.

When dealing with depth-dependent current, the inverse problem cannot be solved directly because the equations resulting from the conservation laws involve depth-integration of the unknown initial current $U_c(z)$. Nevertheless, the derived model shows monotonicity results for the direct problem. Base on that, the inverse problem may be found in an iterative way: take an initial guess for the wave-free current and the current-free wave, calculate the changes of wave and current, calculate the differences between the predicted and the desired wave and current, and then use this information to adapt the guess for the current-free wave and the wave-free current.

## 7.2 Dealing with irregular waves

The model presented in the dissertation is based on the assumption that the wave is monochromatic (regular). We have shown that the model gives good agreements when compared to various experiments with regular waves. In practice, models of ocean structures/ships must also be tested in random waves environments, because in reality ocean waves are irregular. The sea surface is composed of (infinitely) many regular waves with different lengths and frequencies. The concept of power spectrum, which can be found in many books on signal analysis or oceanography such as Bendat and Piersol [7] [8] or Stewart [61], is one way to describe this irregularity. The power spectrum gives the distribution of wave energy among different wave frequencies or wave-lengths. For random waves, it is given by a continuous function of the wave frequency. Examples of well-known idealized spectra for ocean waves are the Pierson-Moskowitz spectrum and the JONSWAP spectrum.

Formulating a reasonable method for dealing with irregular waves is of laboratory's interest. In a previous work by Margaretha [38] a model that describes the interaction of irregular waves and a uniform current is given. Using the conservation of mass, uniform current resulted from the interaction is predicted by assuming that the change of the current is equal to the wave-induced mass-transport velocity given by $E/c\rho h$, where $E$ = area below the spectrum and $c = \omega/k$, i.e. the phase velocity. The power spectrum $S(\omega)$ is divided into a finite number of bands of width $\Delta\omega$. Each band is related to a regular wave with amplitude $a_n$ evaluated from the approximation:

$$a_n = \sqrt{2S(\omega_n)\,\Delta\omega},\ n = 1, 2, \ldots N. \tag{7.1}$$

For each band, the change of the corresponding wave amplitude is predicted using the conservation of energy-density flux. Different from the model proposed in this dissertation, in [38] this conservation results to an algebraic equation. In fact, using the model given in [38] we can only predict the equilibrium state of the interaction but we cannot predict the length of the adaptation region.

It is interesting to formulate a method for describing the interaction of currents and irregular waves using the QHA model proposed in this dissertation, because then

we will be able to make predictions also for cases with depth dependent currents. The wave spectrum can be treated in the same way as above, i.e. by dividing it into a finite number of bands; each band is related to a regular wave with amplitude $a_n$ given by (7.1). If for each of these regular waves we apply the QHA model, changes of the wave amplitudes give the deformation of the wave spectrum. But if we do this, we will get $N$ predictions for the change of the current profile, and also for the change of the mean free surface elevation and for the distance of adaptation. We have to formulate a good averaging model to determine these three global quantities.

Another alternative for dealing with irregular waves is given as follows. Take a regular wave that has the same energy as the irregular waves. This means that the amplitude of the regular wave is related to the power spectrum $S(\omega)$ by

$$a_{\mathrm{R}} = \sqrt{2 \int_0^\infty S(\omega)\, d\omega},$$

and the period is equal to the peak period of the irregular waves. Then we calculate the changes of the current profile and the mean free surface elevation, the change of the constructed regular wave above, and the distance of adaptation using the QHA model proposed in Chapter 4. Afterward, using the current profile and the mean free surface elevation predicted in the previous step, we calculate the deformation of the wave spectrum as follows. We divide the spectrum into a finite number of bands, and apply the conservation of wave volume (4.41) and the dispersion relation (3.9) to calculate the changes of the amplitude and the wave number of each regular wave. Finally, using the prediction for the amplitude of the corresponding regular waves, the deformation of the wave spectrum can be calculated from (7.1).

## 7.3 Extension of the model

At its present stage, the QHA model proposed in this dissertation can only take four parameters, one of which describes changes in the vertical dependence of the current. To increase the flexibility in describing the deformation of the current profile we need to take additional parameters, but this implies that we need more equations. These additional equations can be constructed from the two alternatives below.

### 7.3.1 Vorticity-related conservation laws

Besides mass, momentum, and energy conservations, for the case that the velocity field satisfies the continuity equation and the bottom boundary condition exactly, we also have a balance law for the vorticity. In fact, for any continuous function $G(\gamma)$ it holds that

$$\partial_t \int_{-1}^{\eta} G(\gamma)\, dz + \partial_x \int_{-1}^{\eta} uG(\gamma)\, dz = \int_{-1}^{\eta} \frac{dG}{d\gamma} \left(\partial_z \mathcal{R}^{\mathrm{E}_1} - \partial_x \mathcal{R}^{\mathrm{E}_2}\right) + G(\gamma)|_{z=\eta}\, \mathcal{R}^{\mathrm{kbc}}, \tag{7.2}$$

where $\gamma$ is the vorticity:

$$\gamma = \partial_z u - \partial_x w.$$

If $\eta$, $u$, $w$, $p$ are exact solutions, then the right-hand side of (7.2) vanishes. This means that every continuous function of vorticity $G(\gamma)$ is conserved. For periodic solutions, time-averaging of (7.2) with respect to the period leads to

$$\left\langle \int_{-1}^{\eta} uG(\gamma)\, dz \right\rangle = G^{\infty} = \text{constant}, \tag{7.3}$$

where the angle brackets denotes the time-average.

Additional equations can be constructed from (7.3). Although in principle, (7.3) holds for any continuous function $G(\gamma)$, it is important to investigate which functions $G(\gamma)$ lead to physically meaningful quantities. For example, taking $G(\gamma) =$ constant leads to conservation of mass-density flux; taking $G(\gamma) = \gamma$ leads to conservation of vorticity-density flux; and taking $G(\gamma) = \gamma^2$ leads to conservation of enstrophy-density flux.

In Chapter 4 of the dissertation we show that the Green-Naghdi method leads to conservations of mass, momentum, and energy. However, in the GN method, the projection does not lead to conservation of vorticity-related quantities (7.3).

We have to investigate the relevance of the vorticity-related conservations to the problem we are dealing with. For dealing with depth-dependent currents (especially with sheared currents) it might be physically relevant.

In Chapter 5 we show that the curvature of the current profile influences the solution of the Rayleigh equation. This is the reason why we take a parabolic function to describe the deformation of the current profile. By having additional equations, we will have more flexibility to model the deformation of the current profile. Depth-dependent functions describing this deformation still have to be carefully chosen. It is interesting to investigate whether these functions can be chosen independently from the choice we take for $G(\gamma)$.

### 7.3.2 Numerical codes based on the Green-Naghdi Method

A brief description of the Green-Naghdi method is given in Section 4.4.3. With the GN method, the problem is reduced to 1D time-dependent problem. In principal, with the GN method we can take any finite set of functions to describe changes in the vertical dependence of the current. The wave nonlinearity can also be modelled by the GN method; for irrotational flows, Kim et.al. [31] apply the GN method to calculate the spatial evolution of nonlinear free surface waves.

When applying the GN method, base functions describing the vertical dependence of the wave part of the velocity have to be chosen carefully. In [21], [22], [31] the base functions are given by $\sinh(nk(z+h))$, $n = 1, 2, \ldots N$ or, for deep water, $\exp(nkz)$, $n = 1, 2, \ldots N$. In practice, usually $N$ is not larger than 4 or 5. For the problem

of hydrodynamic laboratories, the wave number $k$ varies spatially. For this case an example of a set of base functions is given in Section 4.4.3.

In principal, the GN method offers a lot of flexibility in modelling hydrodynamic problems. However, the most difficult problem encountered when applying the GN method is to solve the resulting set of equations (which is as large as $2N+2$). Studies on possible simplifications and numerical methods for calculating the solutions are interesting topics for further research.

# Appendices

# Appendix A

## Exact Solutions and the Dispersion Relation for the Homogeneous Problem with Piecewise-Linear Currents

The approach based on the piecewise linear current velocity approximation (e.g. [18], [20]) reduces the problem to a set of algebraic equations. By solving these algebraic equations, we get the exact solution of the Rayleigh equation; thus we get the exact dispersion relation. Although as said by Shrira [57] that the convergency of these solution to the solution of the corresponding smooth problem as the number of vorticity jumps tends to infinity is not yet rigorously proven, this approach is simple and practical.

Let $\Delta\hat{w}_k = \lim_{z\to z_k^+} \hat{w}(z) - \lim_{z\to z_k^-} \hat{w}(z)$ denote the 'jump' in $\hat{w}$ at $z = z_k$, $k = 1, 2, \ldots N$. When a current profile is approximated by a piecewise linear function (3.17), where $U(z)$ is continous at each kink, it is known that exact analytical solutions can be derived by satisfying $2N$ matching conditions (see the book of Drazin and Reid [18] and the paper of Gertsenshtein [20]):

$$\Delta\left[(U-c)\,\hat{w}^{'} - U'\hat{w}\right]_k = 0,\ k = 1, 2, \ldots N, \tag{A.1}$$

and (when $[U-c]_{z=z_k} \neq 0$)

$$\Delta\left(\frac{\hat{w}}{U-c}\right)_k = 0,\ k = 1, 2, \ldots N, \tag{A.2}$$

where $c = \frac{\omega}{k}$. As explained in [18], the first matching condition means that the pressure (2.20) is continuous across the interfaces, and the second matching condition means that the normal velocity of the fluid is continuous at the interfaces. Taking

$$\hat{w}(z) = \begin{cases} C_0 \sinh\left(k\left(z-z_1\right)\right) + D_0 \cosh\left(k\left(z-z_1\right)\right), & z_1 < z \leq \eta_0, \\ C_1 \sinh\left(k\left(z-z_2\right)\right) + D_1 \cosh\left(k\left(z-z_2\right)\right), & z_2 < z \leq z_1, \\ \vdots & \vdots \\ C_{N-1} \sinh\left(k\left(z-z_N\right)\right) + D_{N-1} \cosh\left(k\left(z-z_N\right)\right), & z_{N-1} < z \leq z_N, \\ C_N \sinh k\left(z+1\right), & -1 \leq z \leq z_N, \end{cases} \tag{A.3}$$

as the solution of the Rayleigh equation, the coefficients $C_k$ and $D_k$ are determined from (2.27), (A.1) and (A.2).

When the current profile is given by a piecewise-linear function consisting of two linear functions (bilinear current, i.e. $N = 1$), the solution of the boundary value problem is given by (A.3) where $N = 1$. The parameters $C_0$, $C_1$, and $D_0$ are derived from (2.27), and (A.1)-(A.2). After substituting the solution $\hat{w}$ into (2.25), the dispersion relation is found:

$$\begin{aligned} k\tilde{C}_0 \cosh k\left(\eta_0 - z_1\right) + k\tilde{D}_0 \sinh k\left(\eta_0 - z_1\right) = \\ \beta\left\{\tilde{C}_0 \sinh k\left(\eta_0 - z_1\right) + \tilde{D}_0 \cosh k\left(\eta_0 - z_1\right)\right\} = 0, \end{aligned} \tag{A.4}$$

where $\beta$ is given by (2.26) and

$$\begin{aligned} \widetilde{C}_0 &= \left(\frac{\left(s_0 - s_1\right)\sinh\left(k\left(z_1+1\right)\right) + k\left(U_1 - c\right)\cosh\left(k\left(z_1+1\right)\right)}{k\left(z_1 - \eta_0\right) + \left(U_0 - c\right)}\right), \\ \widetilde{D}_0 &= \sinh k\left(z_1 + 1\right). \end{aligned}$$

Observe that the dispersion relation is not affected by the amplitude of $\hat{w}$ (2.27). As $N$ increases, the expression for the dispersion relation inevitably becomes more and more intricate and lengthy.

# Appendix B

# Numerical Methods for Calculating the Eigenvalues and Solutions of the Rayleigh Equation

## B.1 Transformation to a second-order initial value problem

This discussion follows the method presented by Fenton [19] and Thomas [69]. Define $\varphi(z)$ as follow

$$\varphi(z) = \phi(z) / \frac{d\phi}{dz}(-1),$$

and substitute into (2.22), (2.6), and (2.25). The Rayleigh equation becomes

$$\varphi''(z) - f(z)\varphi(z) = 0, \tag{B.1}$$

with initial conditions

$$\begin{aligned} \varphi(-1) &= 0 \\ \frac{d\varphi}{dz}(-1) &= 1. \end{aligned} \tag{B.2}$$

The surface condition corresponding to the dispersion relation is

$$Q(k) = 0, \tag{B.3}$$

where

$$Q(k) = \varphi'(0) - \beta\varphi(0). \tag{B.4}$$

The known quantities are $\omega$ and $U(z)$. We regard the system (B.1)-(B.2) as one with an unknown function $\varphi$ and an unknown quantity $k$ related by (B.3).

Suppose the value $k = k_1$ is fixed *a priori*. With this value of $k$ equation (B.1) subject to initial conditions (B.2) is readily solved by a standard computer library Runge-Kutta routine and $Q(k_1)$ is then obtained from (B.4). If another value $k = k_2$ is chosen, $Q(k_2)$ can be found similarly. By choosing $k_1$ and $k_2$ such that $Q(k_1)\,Q(k_2) < 0$ the solution to $Q(k) = 0$ can be found iteratively using any root-bracketing method.

In general when $U(z)$ is sign-definite, we can find the physically-meaningful root when the initial guess for $k_1$ and $k_2$ are given by

$$\omega^2 = k_1 \tanh k_1$$
$$\left(\omega \mp k_2 \max_{z\in[-1,0]} |U(z)|\right)^2 = k_2 \tanh k_2,$$

in which we take the minus sign if $U(z) > 0$ (favourable current) and the plus sign if $U(z) < 0$ (adverse current). The value $k_1$ corresponds to the zero-current wave number, and $k_2$ is the analoguous wave number for waves running on a favourable/adverse uniform current $\pm U_{\max} = \pm \max_{z\in[-1,0]} |U(z)|$. The choice of $k_1$ and $k_2$ was deduced from wavelength consideration which suggest $k_1 < k < k_2$ if the wave runs on an adverse current, and $k_2 < k < k_1$ if the wave runs on a favourable current.

## B.2 Transformation to a Riccati Equation

Define $\varphi(z)$ as follow

$$\varphi(z) = \phi(z) / \frac{d\phi}{dz}(z).$$

Observe that the following equation holds provided that the Rayleigh equation is satisfied

$$\varphi' = 1 - f(z)\varphi^2, \quad -1 \le z \le 0. \tag{B.5}$$

The initial condition is given by

$$\varphi(-1) = 0. \tag{B.6}$$

The surface condition corresponding to the dispersion relation is transformed into

$$Q(k) = 1 - \beta\varphi(0) = 0. \tag{B.7}$$

Equation (B.5) has the form of a Ricatti equation, which is a nonlinear first-order ODE. Solutions for $\varphi(z)$ and $k$ are obtained iteratively in the same way as the previous method.

## B.3 Finite Element Method

### B.3.1 Transformation to a linear eigenvalue problem ($c = \omega/k$ is given)

We restrict the functional to a finite dimensional subspace given by

$$N = \left\{ \sum_{i=0}^{N} a_i \xi_i(z) \,\middle|\, a_i, i = 0..N \right\},$$

in which $\xi_i$ 's are base functions. Then the restricted functional is given by

$$\hat{\mathcal{L}}\left(a_0, a_1, \ldots a_N\right) = \frac{1}{2}\int_{-1}^{0}\left[\left(\sum_{i=0}^{N} a_i \xi_i'\left(z\right)\right)^2 + f\left(z\right)\left(\sum_{i=0}^{N} a_i \xi_i\left(z\right)\right)^2\right] dz - \frac{1}{2}\beta\left(\sum_{i=0}^{N} a_i \xi_i\left(0\right)\right)^2. \tag{B.8}$$

We can take for instance linear spline functions as a simplest choice. This finite dimensional representation of the functional must satisfy

$$\frac{d\hat{\mathcal{L}}}{da_i}\left(a_0, a_1, \ldots a_N\right) = 0 \text{ for all } a_i. \tag{B.9}$$

When $f\left(z\right)$ and $\beta$ are written using the phase speed $c = \omega/k$ like

$$f\left(z\right) = k^2 + \frac{U''\left(z\right)}{U\left(z\right) - c}, \tag{B.10}$$

$$\beta = \frac{1}{\left(U\left(0\right) - c\right)^2} + \frac{U'\left(0\right)}{\left(U\left(0\right) - c\right)}, \tag{B.11}$$

then for a given $c$ the linear eigenvalue problem for $\lambda = -k^2$ reads

$$A\overline{a} = -k^2 B\overline{a}, \tag{B.12}$$

in which

$$\overline{a} = \left(a_0, a_1, \ldots a_{N-1}\right)^T,$$

and $A$ and $B$ are $N \times N$ three-diagonal matrices, the non-zero components of which are given by

$$A_{ij} = \begin{cases} \int_{z_1}^{z_0}\left\{\xi_{j-1}'\xi_{i-1}' + H\left(z\right)\xi_{j-1}\xi_{i-1}\right\}dz - \beta, i = j = 1 \\ \int_{l_1}^{l_2}\left\{\xi_{j-1}'\xi_{i-1}' + H\left(z\right)\xi_{j-1}\xi_{i-1}\right\}dz, j = i \neq 1 \text{ or } j = i \pm 1 \end{cases}, \tag{B.13}$$

$$B_{ij} = \begin{cases} \int_{z_1}^{z_0}\xi_{j-1}\xi_{i-1}dz, & j = i = 1 \\ \int_{l_1}^{l_2}\xi_{j-1}\xi_{i-1}dz, & j = i \neq 1 \text{ or } j = i \pm 1 \end{cases}. \tag{B.14}$$

Here

$$H\left(z\right) = \frac{U''\left(z\right)}{U\left(z\right) - c},$$

and the integration boundaries in (B.13) and (B.14) are given by

$$l_1 = z_i,\ l_2 = z_{i-2},\ \text{for } j = i \neq 1, \tag{B.15}$$

$$l_1 = z_j,\ l_2 = z_{j-1},\ \text{for } j = i - 1, \tag{B.16}$$

$$l_1 = z_{j-1},\ l_2 = z_{j-2},\ \text{for } j = i + 1, \tag{B.17}$$

Solutions for both $k$ and $\overline{a}$ are obtained by solving the eigenvalue problem (B.12). Notice that the task of finding $k$ is decoupled from that of finding $\overline{a}$.

The wavenumber $k$ is calculated from the smallest negative eigenvalue of the matrix $A$ (B.13).

### B.3.2 Transformation to a quadratic eigenvalue problem ($k$ is given)

When $k$ is given instead of $c$ (or $\omega$), we can transform the problem into a quadratic eigenvalue problem by first of all defining

$$\varphi(z) = \frac{\hat{w}(z)}{(kU(z) - \omega)}. \tag{B.18}$$

Substuting (B.18) into (3.1) and applying some partial derivatives gives the following functional for $\varphi$

$$G(\varphi) = \frac{1}{2}\int_{-1}^{0} (kU(z) - \omega)^2 \left\{(\varphi')^2 + k^2\varphi^2\right\} dz - \frac{1}{2}k^2\varphi(0)^2.$$

This variational formulation is already given in (Miles [46]) (assuming that $U'(0) = 0$). Notice that this formulation actually holds also for cases in which $U'(0) \neq 0$.

When $\varphi(z)$ is given by

$$\varphi(z) = \sum_{i=0}^{N-1} b_i \xi_i(z),$$

in which $\xi_i(z)$ 's are the base functions for the finite element method, observe that the resulting matrix equation is given by

$$\left(P + \omega Q + \omega^2 R\right)\overline{b} = 0,$$

where $\overline{b} = (b_0, b_1, \ldots, b_{N-1})^T$ and $P$, $Q$, and $R$ are $N \times N$ three-diagonal matrices which have non-zero elements:

$$P_{ij} = \begin{cases} \int_{z_1}^{z_0} k^2 U(z)^2 \left\{\xi'_{j-1}\xi'_{i-1} + k^2\xi_{j-1}\xi_{i-1}\right\} dz - k^2, & i = j = 1 \\ \int_{l_1}^{l_2} k^2 U(z)^2 \left\{\xi'_{j-1}\xi'_{i-1} + k^2\xi_{j-1}\xi_{i-1}\right\} dz, & j = i \neq 1 \text{ or } j = i \pm 1 \end{cases},$$

$$Q_{ij} = \begin{cases} -2\int_{z_1}^{z_0} kU(z) \left\{\xi'_{j-1}\xi'_{i-1} + k^2\xi_{j-1}\xi_{i-1}\right\} dz, & i = j = 1 \\ -2\int_{l_1}^{l_2} kU(z) \left\{\xi'_{j-1}\xi'_{i-1} + k^2\xi_{j-1}\xi_{i-1}\right\} dz, & j = i \neq 1 \text{ or } j = i \pm 1 \end{cases},$$

$$R_{ij} = \begin{cases} \int_{z_1}^{z_0} \left\{\xi'_{j-1}\xi'_{i-1} + k^2\xi_{j-1}\xi_{i-1}\right\} dz, & i = j = 1 \\ \int_{l_1}^{l_2} \left\{\xi'_{j-1}\xi'_{i-1} + k^2\xi_{j-1}\xi_{i-1}\right\} dz, & j = i \neq 1 \text{ or } j = i \pm 1 \end{cases},$$

where the integration boundaries are given by (B.15)-(B.17).

A method to solve the quadratic eigenvalue problem is given by Tisseur [72].

# Bibliography


[1] Abramowitz, M. & Stegun, I.A. 1972 *Handbook of Mathematical Functions with Formulas, Graphs, and Mathematical Tables*, **10**th pr. John Wiley, New York.

[2] Andrews, D. G. & McIntyre, M. E. 1978 An exact theory of nonlinear waves on a Lagrangian mean flow. *J. Fluid Mech.* **89**, 609-646.

[3] Baddour, R.E. & Song, S. 1990 On the interaction between waves and currents. *Ocean Eng.* **17** (1/2), pp. 1-21.

[4] Baddour, R.E. & Song, S. 1998 The rotational flow of finite amplitude periodic water waves on shear currents. *Appl. Ocean Res.* **20**, pp. 163-171.

[5] Bakker, W. T. & Van Doorn, T. 1978 Near-bottom velocities in waves with a current. *In Proc. 16th Conf. on Coastal Eng., Hamburg, Germany,* pp. 1394-1413. ASCE.

[6] Battjes, J.A. 1982 A case study of wave height variation due to currents in a tidal entrance. *Coastal Eng.* **6**, pp. 47-57.

[7] Bendat, J.S. & Piersol, A.G. 1966 *Measurement and Analysis of Random Data.* John Wiley & Sons, New York.

[8] Bendat, J.S. & Piersol, A.G. 1993 *Engineering Applications of Correlation and Spectral Analysis* **2**nd ed. John Wiley & Sons, New York.

[9] Brand. L. 1966 *Differential and Difference Equations.* John Wiley, New York.

[10] Brevik, I. 1976 The stopping of linear gravity waves in currents of uniform vorticity. *Phys. Norvegica* **8**, pp. 157-162.

[11] Chen, Q., Madsen, P.A., Schäffer, H.A., & Basco, D.R. 1998 Wave-current interaction based on an enhanced Boussinesq approach, *Coastal Eng.* **33**(1), pp. l-39.

[12] Dalrymple, R.A. 1973 Water wave models and wave forces with shear currents. *Coastal Ocean Eng. Lab., Univ. Florida Tech. Rep.* no. **20**.

[13] Dalrymple, R.A. 1977 A numerical model for periodic finite amplitude wave on a rotational fluid. *J. Computational Phys.* **24**, pp. 29-42.

[14] Dean & Dalrymple, R.A. 1984 *Water Wave Mechanics for Engineers and Scientists.* Prentice Hall, Inc. Reprinted in 1991 by World Scientific, Singapore, as Vol. **2** of Adv. Series on Ocean Eng.

[15] VAN DIJK, R.R.T., VOOGT, A., FOURCHY, P. & MIRZA, S. 2003 The effect of mooring system and sheared currents on vortex induced motions of truss spars. *Proceedings of 22nd Intl. Conf. on Offshore Mech. and Artic Eng. (OMAE03),* pp. 1-8.

[16] DINGEMANS, M. W., VAN KESTER, J. A. TH. M., RADDER, A. C. & UITTENBOGAARD, R. E. 1996 The effect of the CL-vortex force in 3D wave-current interaction. *In Proc. 25th Intl Conf. on Coastal Eng., Orlando*, pp. 4821-4832. ASCE.

[17] DINGEMANS, M.W. 1997 *Water Wave Propagation over Uneven Bottoms - Part 1: Linear Wave Propagation.* Adv. Series on Ocean Eng., Vol. **13**, Word Scientific.

[18] DRAZIN, P.G. & REID, W.H. 1981 *Hydrodynamic Stability.* Cambridge Univ. Press.

[19] FENTON, J.D. 1973 Some results for surface gravity waves on shear flows. *J. Inst. Math. Appl.* **12**, pp. 1-20.

[20] GERTSENSHTEIN, S.Y., ROMASHOVA, N.B., & CHERNYAVSKI, V.M. 1988 On the generation and development of wind waves. *Izv. Akad Nauk SSSR Mech. Zhid i Gaza* **3**, pp. 163-169.

[21] GREEN, A.E. & NAGHDI, P.M. 1986 A nonlinear theory of water waves for finite and infinite depths. *Phil. Trans. R. Soc. Lond.* A **320**, pp. 37-70.

[22] GREEN, A.E. 1995 On gravity waves in channels. *Z. angew Math. Phys.* **46** Special Issue, pp. S525-S565.

[23] GROENEWEG, J. & KLOPMAN, G. 1998 Changes of the mean velocity profiles in the combined wave-current motion in a GLM formulation. *J. Fluid Mech.* **370**, 271-296.

[24] GROENEWEG, J. & BATTJES, J.A. 2003 Three-dimensional wave effects on a steady current. *J. Fluid Mech.* **478**, pp. 325-343.

[25] VAN GROESEN, E. 1998 WKB- and SVEA-approximative methods for slowly varying on n-linear dielectric media. *Optical and Quantum Electronics* **30**, pp. 467-474.

[26] HAVELOCK, T.H. 1929 Forced surface waves on water. *Phil. Magazine* **8**, pp. 569-576.

[27] HEDGES, T.S. & LEE, B.W. 1992 The equivalent uniform current in wave-current computation. *Coastal Eng.* **16**, pp. 301-311.

[28] JONSSON, I.G. 1990 Wave-current interactions, In: *The Sea*, Ed. B. Le Mehaute and D.M. Hanes, *Ocean Eng. Sc.*, Vol. **9**(A). Wiley (New York), pp. 65-120.

[29] KEMP, P.H. & SIMONS, R.R. 1982 The interaction between waves and a turbulent current: waves propagating with the current. *J. Fluid Mech.* **116**, pp. 227-250.

[30] KEMP, P.H. & SIMONS, R.R. 1983 The interaction between waves and a turbulent current: waves propagating against the current. *J. Fluid Mech.* **130**, pp. 73-89.

[31] KIM, J.W., BAI, K.J., ERTEKIN, R.C. & WEBSTER, W.C. 2001 A derivation of the Green-Naghdi equations for irrotational flows. *J. Eng. Math.* **40**(1), 17-34.

[32] Kirby, J.T. & Chen, T-M. 1989 Surface waves on vertically sheared flows: approximate dispersion relations. *J. Geophys. Res.* **94**(C1), pp. 1013-1027.

[33] Klopman, G. 1994 *Vertical Structure of the Flow Due to Waves and Currents*. WL |delft hydraulics, report **H840.30**, Part II.

[34] Kyung, D.S., Woo, S.P., & Beom S.P. 2001 Separation of incident and reflected waves in wave-current flumes. *Coastal Eng.* **43**(3-4), pp. 149-159.

[35] Lighthill, M.J. 1978 *Waves in Fluids*. Camb. Univ. Press.

[36] Longuet-Higgins, M.S. & Stewart, R.W. 1960 Changes in the form of short gravity waves on long waves and tidal currents. *J. Fluid Mech.* **8**, pp. 565-583.

[37] Longuet-Higgins, M.S. & Stewart, R.W. 1961 Changes in the form of short gravity waves on steady non-uniform currents. *J. Fluid Mech.* **10**, pp. 529-549.

[38] Margaretha, H. 1999 *Wave-current interaction in hydrodynamic laboratories*. MSc Thesis, University of Twente, The Netherlands.

[39] Margaretha, H. 2003 *Report on the Experiment on Wave-Current Interaction*. Internal report, University of Twente, The Netherlands.

[40] Margaretha, H., van Groesen, E., & Klopman, G. 2004 Variational characterization of the dispersion relation for linear waves on arbitrary currents. Submitted for publication in *Ocean Eng.*

[41] Margaretha, H., van Groesen, E., & Klopman, G. 2005 A low-dimensional model for the spatial adaptation of wave and current - Part 1: theory. Submitted for publication in *Wave Motion*.

[42] Margaretha, H., van Groesen, E., & Klopman, G. 2005 A low-dimensional model for the spatial adaptation of wave and current - Part 2: case studies and comparison with experiments. Submitted for publication in *Wave Motion*.

[43] *MARIN's website*. www.marin.nl

[44] *REPORT* (MARIN's newsletter) no. **70** 2000.

[45] Mei, C. C., Liu, P. L-.F. & Carter, T. G. 1972 Mass transport in water waves. *MIT Rep.* Ralph M. Parsons Lab. Water Resources Hydrodynamics, no. **146**.

[46] Miles, J.W. 2001a Gravity waves on shear flows. *J. Fluid Mech.* **443**, pp. 293-299.

[47] Miles, J.W. 2001b A note on surface waves generated by shear-flow instability. *J. Fluid Mech.* **447**, pp. 173-177.

[48] Nielsen, P. & You, Z.-J. 1996 Eulerian-mean velocities under non-breaking waves on horizontal bottoms. *In Proc. 25th Intl Conf. on Coastal Eng., Orlando*, pp. 4066-4078. ASCE.

[49] PEARSON, C.E. 1983 *Handbook of Applied Mathematics*, **2**nd ed., Van Nostrand Reinhold.

[50] PEREGRINE, D.H. 1976 Interaction of water waves and currents. *Adv. Appl. Mech.* **16**, pp. 9-117.

[51] PEREGRINE, D.H. & JONSSON, I.G. 1983 Interaction of waves and currents. *Misc. Report U.S. Army, Corps of Engineers* No. **83-6**, Coastal Eng. Res. Center, Fort Belvoir, Va.

[52] RUSSELL, R. C. H. & OSORIO, J. D. C. 1957 An experimental investigation of drift profiles in closed channels. *In Proc. 6th Conf. on Coastal Eng., Miami,* pp. 171-193. ASCE.

[53] RUSSELL, J.M. 1994 A survey of exact solutions of inviscid field equations in the theory of shear flow instability. *Appl. Sci. Res.* **53**(1-2), pp. 163-186.

[54] SCHÄFFER, H.A. 1996 Second-order wavemaker theory for irregular waves. *Ocean Eng.* **23**, pp. 47-88.

[55] SCHÄFFER, H.A. & KLOPMAN, G. 2000 Review of multidirectional active wave absorption methods. *J. Waterway, Port, Coastal, and Ocean Eng.* **126**(2), pp. 88-97.

[56] SCHÄFFER, H.A. & STEENBERG, C.M. 2003 Second-order wave maker theory for multi directional waves. *Ocean Eng.* **30**, pp. 1203-1231.

[57] SHRIRA, V.I. 1993 Surface waves on shear currents: solution of the boundary-value problem. *J. Fluid Mech.* **252**, pp. 565-584.

[58] SIMMEN, J.A. & SAFFMAN, P.G. 1985 Steady deep water waves on a linear shear currents. *Stud. Appl. Maths.* **73**, pp. 35-57.

[59] SKOP, R.A. 1987 Approximate dispersion relation for wave-current interactions. *J. Waterway, Port, Coastal and Ocean Eng.* **113**(2), pp. 187-195.

[60] STEWART, R.H. & JOY, J.W. 1974 HF radio measurements of surface currents. *Deep Sea Res.* **21**, pp. 1039-1049.

[61] STEWART, R.H. 2005 *Introduction to Physical Oceanography*, online textbook, Texas A&M University, http://oceanworld.tamu.edu/resources/ocng_textbook/contents.html

[62] SUASTIKA, I.K., DE JONG, M.P.C., & BATTJES, J.A. 2000 Experimental study of wave blocking. *Proc. 27th Int. Conf. Coastal Eng., Sydney*, Vol.**1**, pp. 227-240. ASCE.

[63] SUASTIKA, I.K. 2004 *Wave Blocking.* PhD Thesis, Technische Universiteit Delft, The Netherlands.

[64] SURYANTO, A. 1999 *Model for Reflection Properties of Hydrodynamic Beaches.* MSc Thesis, University of Twente, The Netherlands.

[65] Swan, C. 1990 An experimental study of waves on a strongly sheared current profile. *Proc. 22nd Conf. on Coastal Eng. Delft*, pp. 489-502. ASCE.

[66] Swan, C. & James, R.L. 2001 A simple analytical model for surface water waves on a depth-varying current. *Appl. Ocean Res.* **22**, pp. 331-347.

[67] Swan, C., Cummins, I.P., & James, R.L. 2001 An experimental study of two-dimensional surface water waves propagating on depth-varying currents (Part 1. Regular waves). *J. Fluid Mech.* **428**, pp. 273-304.

[68] Taylor, G.I. 1955 The action of a surface current used as a breakwater. *Proc. Roy. Soc.* A **231**, pp. 466-478.

[69] Thomas, G.P. 1981 Wave-current interactions: An experimental and numerical study - Part 1: Linear waves. *J. Fluid Mech.* **110**, pp. 457-474.

[70] Thomas, G.P. & Klopman, G. 1996. Wave-current interactions in the nearshore region. In: Gravity waves in water of finite depth, Ed. J.N. Hunt, *Adv. in Fluid Mech.*, Vol. **10**, Comp. Mech. Pub., Southampton, U.K., Chapter 7, pp. 255-319.

[71] Thompson, P.D. 1949 The propagation of small surface disturbance through rotational flow. *Ann. N.Y. Acad. Sci.* **51**, pp. 463-474.

[72] Tisseur, J. & Meerbergen, K. 2001 The quadratic eigenvalue problem. *SIAM Review* **43**, pp. 235-286.

[73] Tsao, S. 1957 Behaviour of surface waves on linearly varying currents. *J. Geophys. Res.* **79**, pp. 4498-4508.

[74] Vainberg, B.R. 1989 *Asymptotic Method in Equations of Mathematical Physics*. Gordon & Breach Science Publishers, New York.

[75] Voluer, B. 2003 *Wave-Current Interaction in the Hydrodynamic Laboratory - Experiment Analysis and Numerical Modelling*. Final project report, Ecole Centrale de Nantes, France.

[76] Westhuis, J.H. 2001 *The Numerical Simulation of Nonlinear Waves in a Hydrodynamic Model Test Basin*. PhD Thesis, University of Twente, The Netherlands.

[77] Whitham, G.B. 1974 *Linear and Nonlinear Waves*. Wiley, New York

[78] Whitham, G.B. 1962 Mass, momentum and energy flux in water waves. *J. Fluid Mech.* **12**, pp. 135-147.

[79] de Wilde, J.J. 2003 *Internal report on Project no.* **18446**, MARIN.

# Samenvatting

Dit proefschrift betreft de studie van oppervlaktegolven op een laag vloeistof waarin een stroming aanwezig is. In het bijzonder leiden we een model af dat het aanpassingsproces beschrijft als een gegeven oppervlaktegolf op een zekere plaats een stroming ontmoet. Dan zullen zowel de golf als de stroming beginnen te veranderen om zich aan te passen om een stabiele toestand te bereiken. Voor de gebruikelijke taak voor een hydrodynamisch laboratorium om een gewenste golf boven een gegeven stroming te genereren, kan dit model helpen bij de praktische generatie door de eigenschappen van de golven en stroming vr de aanpassing te bepalen.

We zullen ons beperken tot golven met kleine amplitudes; daarvoor geldt dan dat voor elk stromingsprofiel een harmonische golf met gegeven frequentie aan de stroming is aangepast als aan de dispersierelatie wordt voldaan. Deze dispersierelatie is algemeen bekend in de afwezigheid van stromingen, maar is tamelijk ingewikkeld in de aanwezigheid van diepte-afhankelijke niet-lineaire stromingen. Om in die gevallen de dispersierelatie te vinden moet de vergelijking voor de verticale snelheid van de vloeistof in de laag, de zogenoemde Rayleigh-vergelijking die afhangt van de gegeven stroming, opgelost worden. In het algemeen kan geen analytische oplossingen gevonden worden en moet de oplossing benaderd worden, hetgeen leidt tot een benaderde dispersierelatie. In dit proefschrift wordt de benadering verkregen door een variationele karakterisering van de dispersierelatie te gebruiken. Het substitueren van benaderde oplossingen van de Rayleigh-vergelijking in de relevante functionaal leidt dan tot de benaderde dispersierelatie. We laten zien dat het gebruik van de WKB benaderingen voor oplossingen van de Rayleigh-vergelijking leidt tot een goede benadering van de dispersierelatie voor stromingen met niet-lineaire profielen.

Nu we op deze manier de steady states van monochromatische golven op willekeurige stromingen hebben geformuleerd, bekijken we het probleem wanneer een golf en een stroming elkaar op een bepaalde plaats ontmoeten. Op die positie wordt dan niet voldaan aan de dispersierelatie, en een aanpassingsproces begint. Er wordt een model ontworpen dat een quasi-homogene ruimtelijke ontwikkeling beschrijft naar een asymptotische toestand waarin de veranderde golf en stroming weer steady zijn.

Om fysisch begrip van het adaptatieproces te krijgen, hebben we een laagdimensionaal model ontworpen dat gebruik maakt van duidelijk interpreteerbare variabelen. De natuurlijke variabelen die de golf beschrijven zijn de golffrequentie, de

golflengte, de golfamplitude en de gemiddelde vrije oppervlakte verhoging. Om veranderingen in de stroming te beschrijven hebben we er voor gekozen om benaderde, geparameteriseerde, profielen te gebruiken; veranderingen in de stroming worden dan beschreven door veranderingen in de parameters. Het adaptatiemodel wordt dan verkregen door te eisen dat aan verschillende natuurlijke behoudseigenschappen wordt voldaan. Meer specifiek zullen we er voor zorgen dat op elke positie exact wordt voldaan aan de continuteitsvergelijking en de kinematische randvoorwaarde. Bovendien eisen we dat de tijdgemiddelde flux van massa, impuls en energie worden behouden. Deze voorwaarden maken het mogelijk om de ruimtelijke veranderingen van de parameters van het model te definiren, en de waarden van de asymptotische toestand te voorspellen. Het afgeleide quasi-homogene proces is slechts een benaderde beschrijving, maar we onderzoeken a-priori schattingen en laten zien dat de fouten klein zijn. Om het model te valideren hebben we modelresultaten vergeleken met laboratorium experimenten die in de literatuur gevonden kunnen worden. Daarnaast werd een serie testen ontworpen en uitgevoerd in het offshore basin van MARIN, het Maritime Research Institute Netherlands, Wageningen. Vergelijking met resultaten van alle beschikbare experimenten in flumes en basins, toont in alle gevallen dat het model de kwalitatieve resultaten van het interactieproces correct voorspelt, en dat voor veel experimenten, inclusief die bij het MARIN, de voorspellingen ook kwantitatief correct zijn.